Infrared Spectroelectrochemical Study of the Oxidation of Substituted Phenols of relevance to the Surface Oxidation of Polystyrene

Mohamed Diallo

University College London

Thesis submitted for the degree of Doctor of Philosophy

January 2019

I, Mohamed Diallo confirm that the work presented in this thesis is my own. Where information has been derived from other sources, I confirm that this has been indicated in this thesis.

Mohamed Diallo

Abstract

This work explores the changes in chemical structure to polystyrene upon treatment with oxidising agents and to monitor the oxidation in situ on addition of these agents using FTIR spectroscopy technique in order to understand the oxidation mechanisms. The electrochemical oxidation of TBP, unsubstituted phenol and o,m,p-cresols presented as defect sites in surface microstructure of the polystyrene was first studied using cyclic voltammetry and a combined technique of chronoamperometry and in situ ATR-FTIR spectroscopy. The results obtained showed that the oxidation of TBP involves a one electron per proton transfer, leading to the formation of 2,4,6-tri-tert-butylphenoxy radical. Additionally, enhanced electron-transfer kinetics was observed at the EPPG in comparison to the GC and BDD electrodes and this was attributed to the presence of the edge sites in the surface microstructure of the EPPG. The electrochemical oxidation of the unsubstituted phenol studied under the same experimental conditions as the TBP reveals that the oxidation proceeds by a one electron transfer, leading to the phenoxy radical then to polymeric, dimer link through O−O and quinone as oxidation products. The oxidation reaction was found to be dependent of the experimental conditions. The results obtained from the electrochemical oxidation of the cresols indicate that the oxidation is influencing by the substitution pattern in the phenyl ring and this was confirmed by the different oxidation products obtained for each cresol. While polymeric, dimer link through O−O and quinone products oxidation products were obtained for o-cresol, the oxidation of m-cresol produces polymeric and dimer link through O−O as oxidation products. Only dimer link through O−O oxidation product was obtained for p-cresol. The formation of quinoid compound was not observed in both the m-cresol and p-cresol and this was probably due the fact that the molecule being too sterically crowded.

The electrochemical oxidation of these phenolic compounds was monitored using a combined technique of chronoamperometry and in situ ATR-FTIR spectroscopy in order to confirm the mechanism proposed for these phenolic compounds. IR peaks consistent with the vibration stretch of the oxidations product resulting from the oxidation of these phenolic compounds were identified.

The changes to polystyrene structure after chemical treatments using oxidising agents such as iridium (IV) tetrachloride, iridium (IV) hexachloride and hydrogen peroxides were investigated. Carbonyl and hydroxyl groups were observed on the surface of the polystyrene and this is indicative of oxidation. These oxygen containing groups were also observed in the in situ study of the PS in water on addition of Iridium (IV) hexachloride in oxygen and oxygen free environment. This shows that polystyrene can be oxidised in situ on addition of mild oxidation agent such as Iridium (IV) hexachloride regardless of the presence or not of oxygen.

Impact Statement

Polystyrene (PS) due to its attractive properties (low cost, durability, appearance, etc.) is one of the most used polymers in the manufacturing industry. However, the accumulation of polymer waste in the environment has become a great source of concern, leading to a long term environmental waste management problem. Therefore, it is essential to understand the oxidative degradation chemistry of PS to understand how it persists in the natural environment and to assist in preventing or reducing environmental pollution.

The first part of our project was focussed onto the electrochemical oxidation of unsubstituted and substituted phenols such as phenol, TPB and cresols that were presented as a defect site in the polystyrene structure, therefore understanding the oxidation of these phenolic compounds will allow us to determine at what potential PS is more susceptible to undergo oxidation. This study has shown that these compounds can be successfully detected using cyclic voltammetry in solution and this can have a positive impact in waste water treatment where phenols are present.

In the second part of this project, in situ experiments were designed to monitor the oxidation mechanism of these compounds in order to confirm the oxidation mechanism proposed for the different phenols previously. This study showed that FTIR can be successfully used to detect oxidation product and to confirm the oxidation mechanism of these compounds at one hand and at the other hand phenol of concentration lower than 20 mM can be detect with this technique and this was not shown before.

In the third and final part of our work, the chemical oxidation of polystyrene was investigated. In this work oxidation mechanisms were proposed for polystyrene treated with oxidising agents such as H_2O_2, iridium (IV) tetrachloride and iridium (IV) hexachloride.

Acknowledgements

I would like to take this opportunity to thank the variety of people who have contributed significantly to this thesis and made it a success. First of all, I would like to thank my Supervisor, Pr Katherine Holt whose expert guidance has led to the realization of this thesis.

I would like to thank my second supervisor Dr Hugo Bronstein and all my friends and colleagues past and present in the UCL Electrochemistry Group for all the memorable moments in the past 3 years; in particular, Dr Daren Caruana, Dr Siti Zakaria, Dr Mailis Lounasvuori, Dr Meetal Hirani, Dr Matin Lopez, Bell Taylor and Maria. Words cannot express my gratitude for all their help and advice.
I would then like to extend my heartfelt gratitude to my all family, in particular to my wife, parent and wonderful sister Alimatu Sesay for being my source of inspiration.

The research council, EPSRC, is also acknowledged for their funding of this research.

Table of Contents

List of Symbols

Symbol	Meaning	Unit
O	Oxidised species; used as subscript to denote quantities pertaining to O	
R	Reduced species; used as subscript to denote quantities pertaining to R	
ν	scan rate	Vs^{-1}
t	time	s
θ	Angle of incidence	
v	Volume	L
i_p	Current	A
A	Area	cm^2
D	Diffusion coefficient	cm^2 /s
C	Concentration of the analyte	M
d_p	Penetration depth	
λ	Refractive index	
E_p	Binding energy	J
E_k	Kinetic energy	J
h	Planck constant	
$\propto$	Proportional	
%	Percentage	
E_p^{ox}	Oxidation potential	V
E_p^{red}	Reduction potential	V
i_p^{ox}	Oxidation current	A
i_p^{red}	Reduction current	A
F	Faraday constant	C / mol

List of Abbreviations

ATR	Attenuated total reflectance
BDD	Boron doped diamond
CV	Cyclic Voltammetry
EPPG	Edge plane pyrolytic graphite
FTIR	Fourier transform infrared
GC	Glassy carbon
GNF	Graphene nanoflask
IR	Infrared
m-	meta
NMR	Nuclear magnetic resonance
o-	ortho
p-	para
PBS	Potassium buffer solution
PE	Polyethylene
PS	Polystyrene
SWCNT	Single walled carbon nanotube
TBP	2,4,6-tri-tert-butylphenol
XPS	X-ray Photoelectron Spectroscopy

List of Figures

List of Schemes

Chapter 1
Introduction

Polystyrene (PS) due to its special properties (thermal stability, low cost, durability, etc.) is one of the most used thermoplastics in the manufacturing industry. PS is employed in various applications ranging from food packaging, electronic, construction, automobile and medical ware [1]. However, the inadequate disposal of the polystyrene waste in environment had led to serious pollution problem [2]. Polystyrene material persists in the nature without decomposition for a long period a time owing it to its exclusive properties and this had caused serious problem to marine life and ecosystems. As the waste plastic materials has become a great source of concern, recycling appears as one of the solution to prevent or reducing environmental pollution [1], [2].

Polystyrene degradation has been the subject of intensive researches over the years and it has been reported that the polymer undergoes degradation under the effect of environmental factors such as light, high temperature, tensile stress, chemical reagents (acids, base, oxidizing reagents) [3]. All these modes of degradation have been reported to be very similar since they all involve chemical reactions that lead to bond scission and depolymerisation (decrease in molecular weight), which lead to the deterioration in physical properties of the polymer [3].

In the past studies on polystyrene degradation thermal analysis techniques such as Differential Scanning Calorimetry (DSC) and Thermo Gravimetric Analysis (TGA) were widely used to monitor the degradation process [4]. However, some advanced techniques such as nuclear magnetic resonance (NMR), High performance liquid chromatography (HPLC) and Fourier Transform Infrared spectroscopy (FTIR) were also used to successfully monitor the degradation process [4].

From this study, we wish to gain more insight into the degradation of polystyrene to understand how it persists in the environment. The better understand of the degradation will facilitate the better use of the alternative waste disposal strategies.

1.1 Polystyrene

Polystyrene is a long chain hydrocarbon belonging to the group of standard thermoplastics that also includes polypropylene (PP), polyethylene (PE) and polyvinyl chloride (PVC). Polystyrene due to its desirable properties is widely used in the manufacturing industry. Polystyrene is produced via the polymerization of the monomer styrene with the most popular being free radical polymerisation of the styrene.

1.1.1 Free Radical Polymerization of Styrene

Free radical polymerization is often the preferred mechanism for forming polystyrene due to its economical and practical advantages over other forms of polymerization (such as anionic polymerization, etc.). However, one of often cited problems is the range of undefined defect structures and other form of structure irregularity that may be present in polystyrene prepared by this mechanism. Free radical polymerization mechanism requires the presence of an initiator, such as a peroxide compound that can react with the monomer to produce reactive compounds which begins the polymerisation process [5]. The most commonly used peroxide initiator, benzoyl peroxide, can initiate the process by firstly producing a pair of benzoyloxy radicals in the presence of heat by cleaving the oxygen- oxygen bond (scheme 1.1). The benzoyl radical thus formed can then react with the monomer to produce a reactive radical which can start the linking process [5]. There is also a possibility that the benzoyloxy radical formed might decompose to give a phenyl radical and carbon dioxide. This phenyl radical might also initiate the polymerisation process. Once the polymer chain reaches a desirable length or molecular weight, the polymerization is terminated. The mechanism of free radical polymerisation of styrene using benzoyl peroxide as initiator is shown below [5]. This reaction mechanism is divided into three important stages describing the initiation (scheme 1.2), the propagation (scheme 1.3) and termination steps (schemes 1.4 and 1.5).

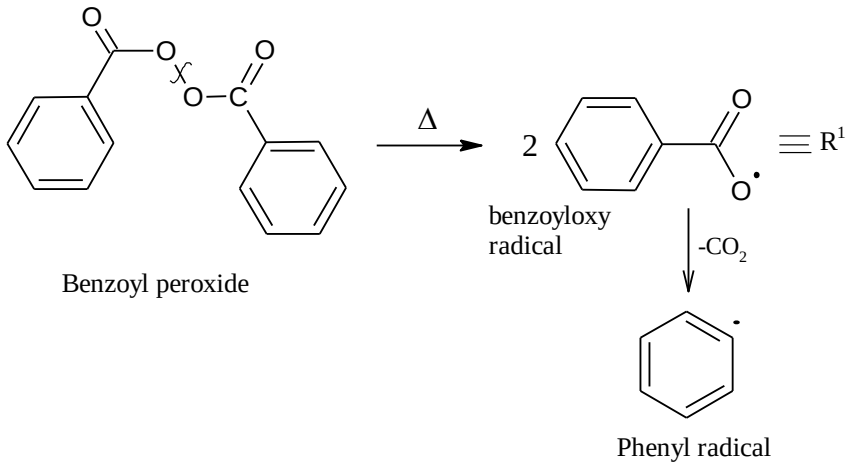

Scheme 1.1 Mechanism showing the formation of the radical initiator

The polymerisation reaction starts by the initiation steps where the benzoyloxy radical formed reacts with the monomer styrene to produced radicals R^2, R^3 and R^4 as shown in scheme (1.2).

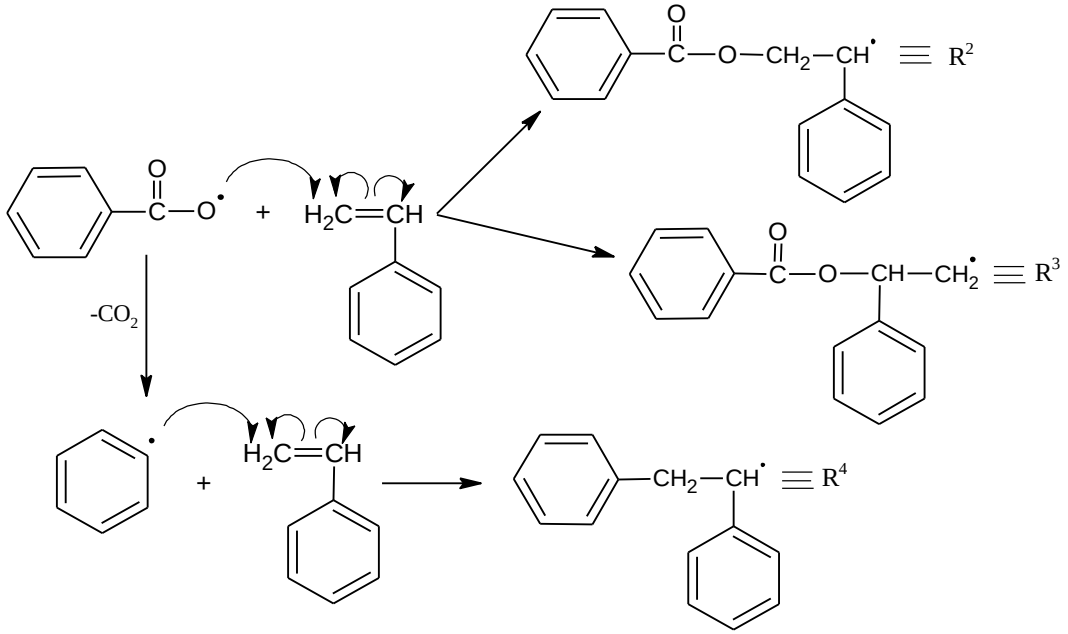

Scheme 1.2 Initiation step of polymerisation of styrene

All these three radicals (R^2, R^3, R^4) can start the linking process following the same pathways, therefore the linkage of radical R^2 will be shown as an example for the others. This linkage process is characterised by the reaction of the radical R^2 with the monomer styrene to form a long molecular weight radical and the reaction proceeds until the

polymer reaches a desirable molecular weight. This process called propagation step is shown is scheme 1.3.

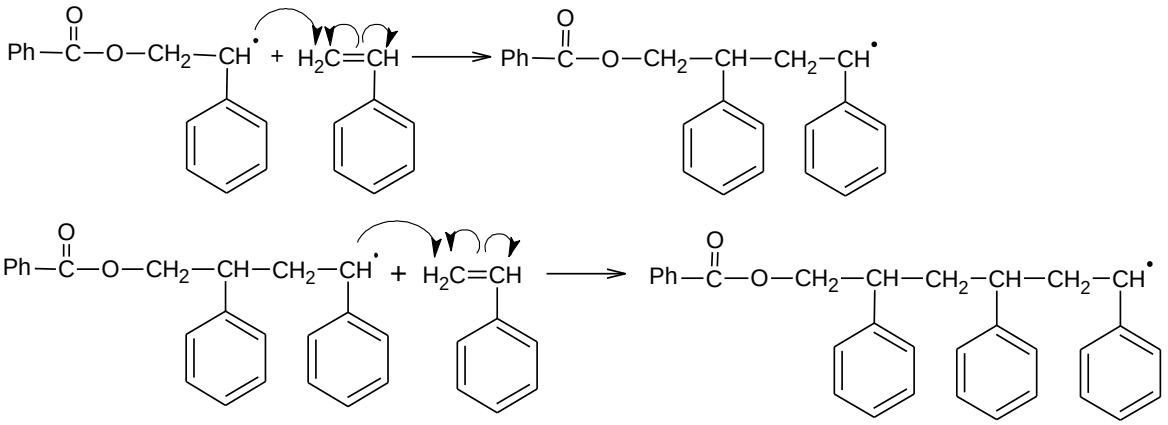

Scheme 1.3 Propagation step of polymerisation of styrene

After the polymer reaches a desirable length, the polymerisation process is terminated, and this step is shown in schemes (1.4 and 1.5). In this step, either two $2R^2$ (scheme 1.4) or R^1 and R^2 (scheme 1.5) radicals can combine and terminate the reaction. The ester functionalities formed by both mechanisms may be present as impurities at the polymer surface and can therefore be involved in later degradation mechanisms.

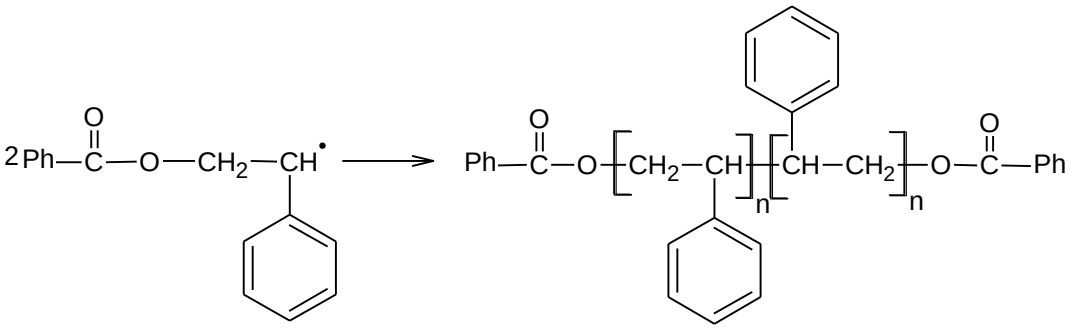

Scheme 1.4 Recombination of two R^2

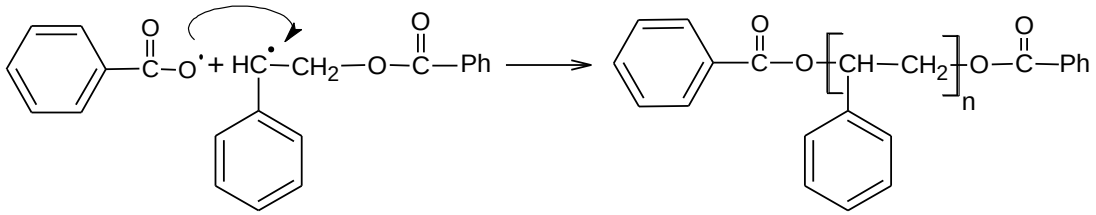

Scheme 1.5 Recombination of R^1 and R^2

The ether linkage observed at the chain end of the polystyrene is presented as defects site in the polystyrene structure and this will be review below.

1.1.2 Defect Structures in Polystyrene

There is substantial literature on photochemical and thermal degradation of polystyrene and it is well established that polystyrene properties are sensitive to the manner in which a particular sample is prepared. For example, it has been reported that polystyrene prepared by anionic polymerisation shows better stability with respect to that prepared by free radical polymerisation [5]. This has generally been associated with the presence of 'weak links' in the latter polymer. In some cases, the 'weak links' may be peroxidic linkages. Such groups may become incorporated in the polymer formed by radical polymerisation through copolymerisation of adventitious oxygen. These groups may either be at the chain ends or they may be part of the backbone (as a consequence of initiation, termination by combination or impurities). Head- to- head linkages, such as those formed by termination by combination (see scheme 1.4 above), have been proposed as a source of thermal instability [5]. However, there is also evidence that thermal behaviour depends on the particular radical initiator or reaction conditions (temperature, solvent, etc.,) used in the polymer preparation.

It also appears that in some cases the thermal degradation of radical polystyrene can be interpreted in terms of initiation by random chain scission facilitated by processes initiated at weak links. As discussed above benzoyl peroxide is commonly used as an initiator and it has been reported that its use can lead to yellowing and impaired stability in polystyrene [5].

Nuclear magnetic resonance (NMR) studies on polymers prepared with ^{13}C-labelled benzoyl peroxide have shown that the primary benzoyloxy and phenyl end group formed by tail addition to styrene monomer are thermally stable under conditions where the polymer degrades. Thus, these groups are unlikely to be directly responsible for the poor thermal stability of polystyrene prepared with benzoyl peroxide as initiator. On the other hand, the secondary benzoate end groups formed by head addition appear extremely labile under these conditions (scheme 1.5).

Studies with model compounds such as 2-phenyl butane show that secondary benzoate esters eliminate benzoic acid to form unsaturated chain ends which have long been

thought to be also a ‘weak link’ in polystyrene [5]. It has been found that for benzoyl peroxide styrene polymerization at high conversion most chain termination may be by way of primary radical termination. Therefore, if these groups are responsible for initiating the chain degradation process, it provides a good explanation for high conversion polystyrene formed with benzoyl peroxide initiator being less thermally stable than either a similar low conversion polymer or a polymer prepared with different initiator.

1.1.3 Polystyrene Degradation

Polystyrene degradation is characterised by the changes in the polymer properties due to physical, chemical and biological reactions, leading to the rupture on the long hydrocarbon chain [6]. Different modes of polystyrene degradation exist depending on the nature of the factors involved, but in this work, we will be interested in the chemical degradation induced by chemical reagents.

1.1.3.1 Factors Affecting Polymer Degradation

Certain parameters such molecular weight, crystallinity and heteroatom incorporation are known to affect the rate of degradation of polystyrene. The presence only of the long carbon chains in the polymers makes them resistant to degradation by microorganisms. However, when oxygen is incorporated into the structure it becomes more hydrophilic and susceptible to biodegradation. The presence of heteroatoms such as oxygen in the polymer chain influences the strength of the neighbouring C−H bonds and encourages carbanion formation in the presence of base [7]. Additionally, crystalline areas of polystyrene have been reported to be less susceptible to thermal oxidation than the amorphous region due to their low permeability to oxygen.

Environments factors such as temperature, moisture and microorganisms can affect degradation. High temperature and high humidity generally enhance hydrolytic degradation of polystyrene materials [7]. Moisture promotes photodegradation due to the fact that under high humidity soluble photo-stabilizers might leach out of the polymer matrix resulting to its degradation. However, the impacts of these factors are not very clear.

Among the different mode of polystyrene degradation, photodegradation is the most widely studied and more understood; therefore, it will be discussed here as a model for the other types of degradation.

1.1.3.2 Chemical Oxidation of Polymer Surface

The earliest (and still accepted) surface treatments of polymer were exposure to oxidising chemicals such as nitric acid, potassium permanganate or chromic acid. In most cases, these treatments were applied to polymers such as polyethylene, polypropylene and polyester, leading to general oxidation with formation of hydroxyl, carbonyl and carboxylic acid groups on the polymers surface. The incorporation of these oxygen containing functional groups increase the polarity and the potential for hydrogen bonding, which in turn improves adhesion and wettability. The surface hydrophilicity of substrates is known to strongly influence the adhesion of proteins. Therefore, hydrophobic substrates such as polystyrene (PS) have been modified with a view to improve their biocompatibility.

Arayik and co-workers [8] have conducted a similar study by reacting polystyrene with sodium with sodium hydroxide (NaOH) in a water-methanol solution at 50^{o}C for 15 h. Ten samples of PS (disks of PS films) were immersed into a solution of NaOH (4 N; 100 mL) in water: methanol (4:1, v/v), and heated at 50^{o}C for 15 h, under air atmosphere. The samples were then taken off and washed for 1 h with an aqueous solution of citric acid (10%; 50 mL), drained over filter paper and dried under nitrogen flow. The resulting samples of PS analysed by XPS showed incorporation of hydroxyl and carbonyl groups. Other studies have also shown similar surface functionalisation of polystyrene when treated with chemical reagents.

Varley and co-workers [9] in their study of the surface redox chemistry and mechanochemistry of insulating polystyrene have shown that polystyrene undergoes oxidative degradation when subjected to chemical treatment using Iridium hexachloride (IV) solution. This was confirmed by the presence of oxygen containing groups at the surface of the polymer detected by XPS analysis.

An interesting feature of oxidised polymer surfaces is that they are higher in free energy than the original non-oxidised surface and may experience a phenomenon called surface reconstruction. This is characterised by the reorientation and diffusion of the polar

oxygen groups away from the surface and into the bulk, leaving lower-free energy and hydrophobic segment exposed [10],[11]. In the case of polystyrene, it has been reported that the polymer has a high dynamic surface and tend to rearrange in response to change to hydrophobicity/ hydrophilicity of the interface conditions. When exposed to water, the oxygen containing groups are more likely to migrate from the bulk to the surface to interact with the water and reduce the free energy at the interface. Inversely, in a hydrophobic environment (e.g. in a nitrogen atmosphere) the polar groups are pulled from the surface to the bulk of the polymer [9]–[11].

Although the surface oxidation of polystyrene using chemical agents has been well investigated and this shows the formation of carbonyl (−C=O) and hydroxyl (−OH) groups which can be easily detected by infrared and XPS techniques, the reaction mechanisms are not well understood. The formation of the intermediate hydroperoxides which lead to the formation of carbonyl and hydroxyl groups is general accepted, but there is little agreement on the initiation steps. This may be because different oxidising agents initiate the oxidation by different mechanisms. Alternatively, the polystyrene under study may contain different concentrations of impurities and defects, such as double bonds and oxygen functionalities. This will have an effect on the mechanism and rate of further oxidation and degradation.

1.1.3.3 Photodegradation Mechanisms of Polystyrene

Among the different mode of polystyrene degradation, the degradation mechanism of photodegradation is the most studied and well understood, therefore will be used as an example for the other type of degradation as the only difference between the mechanisms is known to be the initiation steps [12]–[14]. The photodegradation process was proposed on the basis of the IR spectrum of the photoirradiated film. This indicates the formation of peroxy radical and hydroperoxide intermediate. The photochemical reactions cause the dissociation of a polystyryl radical by creating an electronically excited state. The polystyryl radical is converted to peroxy radicals by reacting with oxygen. The peroxy radical undergoes chain scission and formation of carbonyl compound. Although, this mechanism of photodegradation is general accepted, there still ambiguities on the initiation steps and the photoproducts formed. A generalised proposed mechanism for photodegradation is shown in Scheme 1.6.

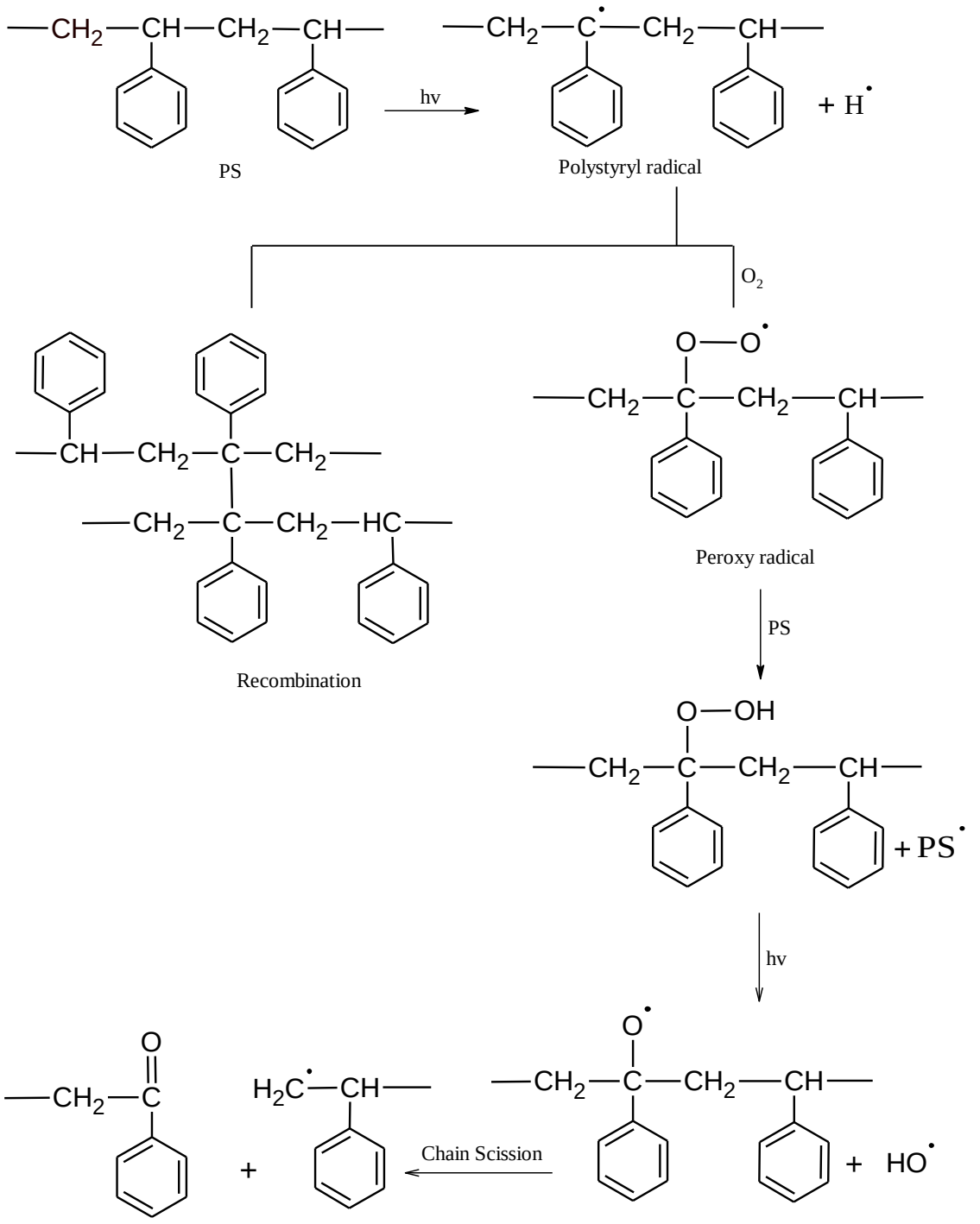

Scheme 1.6 Proposed Mechanism of Photodegradation [15].

In this general mechanism, the hydroperoxy groups are assumed to be formed along the polystyrene main chains. However, the oxidation of phenyl groups in polystyrene with formation of hydroxyl groups in ortho position following similar mechanism was also proposed by other authors [16]. These mechanisms are presented in schemes 1.7 and 1.8.

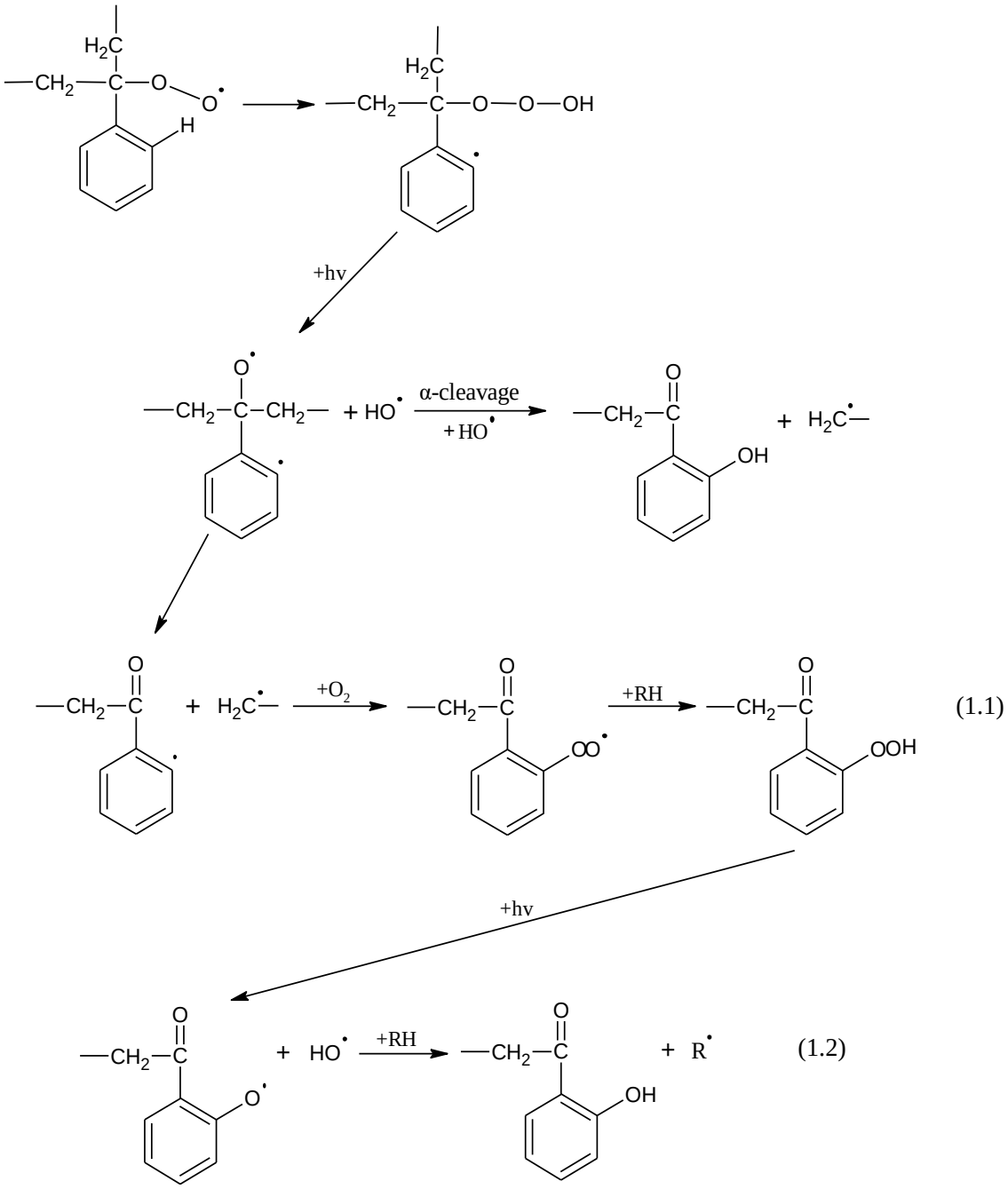

Scheme 1.7 Peroxy radical reaction by intermediate ring mechanism

In scheme 1.7, reactions (1.1) and (1.2) are two alternatives of peroxy radical reactions by intermediate ring mechanisms. Both these reactions lead to chain scission and formation of the same ortho-substituted acetophenone end group and free radical. The intermediate steps are known and accepted in photo-initiated oxidation of hydrocarbons. Another mechanism that was suggested was the ring opening reaction occurring by a five-membered ring mechanism between an alkyl peroxy radical and an adjacent excited

phenyl group (scheme 1.8). This reaction led to the formation of an aldehyde and a ketone groups and occurs without polystyrene chain scission. Other ring opening reactions with formation of ketolactone groups and formation of polyene compounds were also reported for polystyrene based on model compound (2-phenyl-butane) studies but this will not be considered here.

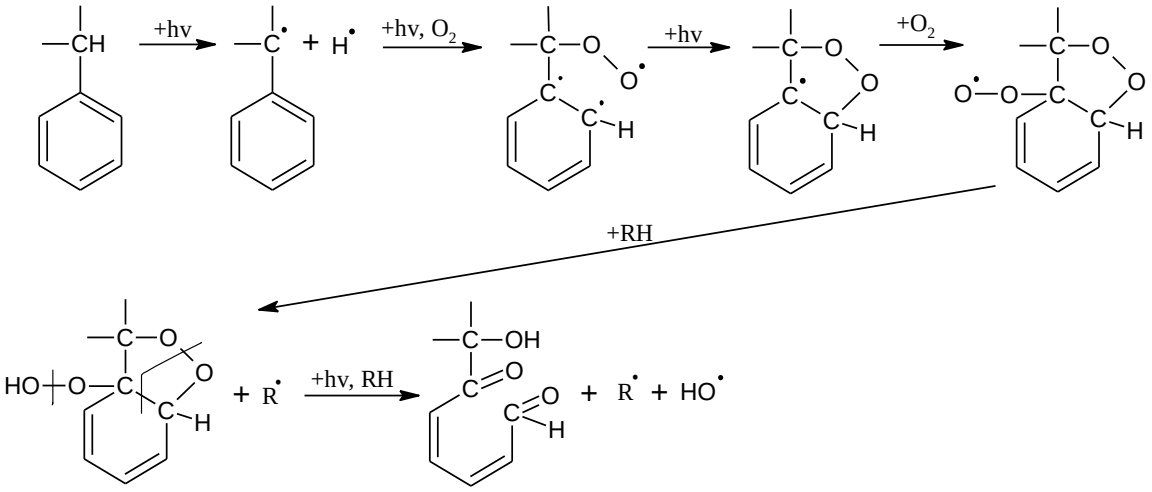

Scheme 1.8 Ring opening reaction by five-membered ring

1.1.3.4 Fourier Transform Infrared Spectroscopy (FTIR) Study of Polymer Degradation

IR spectroscopy has been well known as a powerful tool to study polymer degradation quantitatively. The high sensitivity towards the chemical changes and controlled probing depth of the technique are important functionalities to elucidate the degradation mechanisms of polymers by identifying and quantifying the degradation products.

IR technique has been extensively used in the past to investigate the photo-oxidation and thermo-oxidation mechanisms of polymers. Such mechanisms have shown the formation of carbonyl and hydroxyl compounds, which may be identified by examination of the 1800 − 1600 cm^{-1} and 3600 − 3100 cm^{-1} regions, respectively, in the infrared spectra. Given that there may be a complex mixture of oxidation products; this will result in a complex infrared absorption band [17]. However, the degradation products may be identified by treating the oxidised polymer samples with a reactive gas, such as SF_4 or NH_4. Such a derivatization process selectively converts the oxidation products and there will be subsequent modification of the overlapped infrared bands. Many aldehydes and

ketones are converted to gem-difluoro compounds with sulfur tetrafluoride (SF_4). Esters and carboxylic acids also give trifluororides and 1,1,1-trifluorides respectively [17].

The role of infrared spectroscopy in polymer degradation is illustrated by its application to thermo-and photo-oxidised polyethylene (PE). During the thermal-oxidation process of PE, a range of carbonyl-containing compounds is formed. These decomposition products give rise to a broad C=O stretching band at about 1725 cm^{-1}, consisting of a number of overlapping component bands. When the oxidised samples are treated with an alkali, a shoulder at 1715 cm^{-1} disappears and is replaced by a distinctive peak near 1610 cm^{-1}. This band is due to C=O stretching of the COO^- ion of salt, indicating that the shoulder at 1715 cm^{-1} is characteristic of saturated carboxylic acids. Another shoulder at 1735 cm^{-1} is characteristic of a saturated aldehyde which does not change on addition of base but becomes more defined once the 1715 cm^{-1} shoulder due to carboxylic acid is removed. However, the major contribution to the carbonyl band is due to the presence of saturated ketones (at 1690 cm^{-1}). The broad C=O stretching band is also present in the infrared spectrum of photo-oxidised PE samples, which also show additional bands at 990 cm^{-1} and 910 cm^{-1}. The latter bands are characteristic of vinyl groups and their presence show that chain-terminating unsaturated groups are being formed, most likely as a result of chain scission.

Although Attenuated total reflectance - Fourier transform infrared spectroscopy (ATR-FTIR) technique gives valuable information on the surface functionalization of polymers, there are some inherent challenges. One of the biggest challenges is the correct subtraction of the contribution of water. Water is known to show two intense absorption bands at 3280 cm^{-1} and 1645 cm^{-1} coming from the solution phase which can make the signals from other species ($-OH$ groups resulting from degradation) completely unobservable [17], [18].Therefore, in all the analysis a blank subtraction is carried out. However, this can lead to spectral artifacts arising from instrumental drifts and thermal fluctuations. Especially for those requiring data acquisition for a long period of time this can pose significant impact. Performing the analysis in D_2O can help in resolving the issue but if there is proton exchange with D_2O as in the case of acids the challenge can persist.

1.2 Phenol Chemistry

1.2.1 Overview

Phenol belongs to the group of organic compounds having a hydroxyl group (−OH) attached to a carbon atom that is part of an aromatic ring. These compounds can be synthetized either by hydrolysis of chlorobenzene following the Dow process or oxidation of isopropylbenzene and similar compounds. An example of the first process is described in scheme1.9 below [19]:

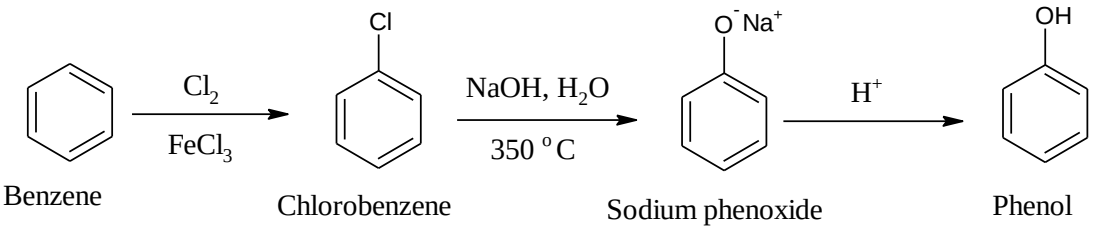

Scheme 1.9 Synthesis of phenol by hydrolysis of chlorobenzene [19].

In this process a molecule of benzene is converted onto chlorobenzene in the presence of chlorine in iron (III) chloride solution. The chlorobenzene formed undergoes hydrolysis in the presence of a strong base such as sodium hydroxide at high temperature to give a phenoxide salt, which is then acidified to phenol.

Phenols are known to be highly reactive towards electrophilic aromatic substitution due the presence of the lone pair electrons on the oxygen, which stabilizes the intermediate cation [20]. This stabilization effect is more effective for attack at the ortho or para position of the ring and, this effect is shown in the example below in scheme 1.10.

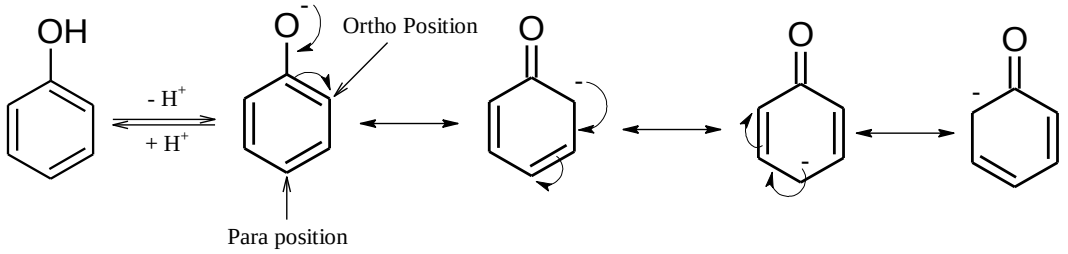

Scheme 1.10 Resonance structure of phenol phenoxide [20].

Phenols and derivatives are present in effluent from food industries, chemical industries, the production of resin and pesticides to name only a few. Phenol with a pKa of approximately equal to 10 is presented as a slightly acidic compound. However, this

acidity character is influenced by the presence of substitution in the phenol ring. For example, for substituted phenols such as methylphenols (o,m,p-cresols), the methyl group produces a positive inductive effect (+I) which increases the negative charge around the phenolate oxygen. This is the reason why these cresols are less acidic than the phenol [20]. In addition, meta-cresol compounds are found to be more acidic than para and ortho-cresol respectively due to the resonance structures, which show a negative charge in ortho and para, but not in meta- position.

1.2.2 Electrochemical Oxidation of Phenolic Compounds

1.2.2.1 Overview

Several studies have been carried out and published on the electrochemical oxidation and detection of phenolic compounds. Different electrode materials were used including platinum, gold, glassy carbon, boron-doped diamond and others. Mathiyarasu et al [21] studied the electrochemical detection of phenol in aqueous solution using cyclic voltammetry and differential pulse voltammetry at glassy carbon electrode. The effect of pH, scan rate and concentration on the cyclic voltammetry response were investigated and they found that the peak potentials were distinct for each pH value and a linear relationship was observed between the peak current and the concentration ranging from micro-to milli-molar levels. However, a significant decrease in the peak current during the second cycle was noticed and this was reported to be due to the blocking of the electrode surface with the phenolic oxidation products. These findings were also reported by Nady et al [22] in their study of electrochemical oxidation behaviour of some hazardous phenolic compounds in acidic solution. In their study, the cyclic voltammetry response of phenol, resorcinol and pyrogallol at different concentrations in the presence of sulphuric acid on platinum electrode were investigated using cyclic voltammetry. The blocking of the electrode surface was also reported, and some reaction mechanisms proposed.

The electrochemical behaviour of compounds such as o-cresol in acidic medium on a platinum electrode was also investigated by Taleb and coworkers using cyclic voltammetry and in situ FTIR spectroscopy techniques. The authors reported that the electrochemical oxidation of o-cresol also leads to the formation of polymeric film on the electrode surface that prevents further oxidation of the molecule [23].

Although, different studies are associated with the electrochemical oxidation of phenol and substituted phenols, the electro-oxidation mechanism is still not well known. The electrochemical oxidation of phenol is notoriously complex as it can give a mixture of product in addition to the fact that the same phenol can also yield different product mixture with different oxidants.

1.2.2.2 Electrochemical Oxidation Mechanism

In most published works on electrochemical oxidation of phenol, the mechanism proposed includes formation of intermediate phenoxy radicals that undergo further oxidation and lead to monomeric quinones as oxidation products. One of the issues faced is that these intermediate phenoxy radicals are highly reactive species and can undergo diverse chemical reactions, leading to different final products. Therefore, the oxidation of substituted phenols such as 2,4,6-tri-tert-butylphenol (TBP) producing a stable radical was viewed as a logical starting point for a series of studies whose aim was to paint a good picture of phenol electrochemistry [24].

1.2.2.2.1 Electrochemical Oxidation Mechanism of TBP

The electrochemical oxidation of TBP involves the formation of a stable phenoxy radical through a one reversible electron transfer. This radical can then react with other species in solution to give a final product. Other investigations have suggested that the radical is further oxidised to give a phenoxide cation which can undergo further reaction to produce final products such as quinones or cyclohexadienone depending on the experimental conditions. Jeffrey and coworkers [24] have reported this type of mechanism (Scheme 1.11) on their work on electrochemical oxidation of 2,4,6-tri-tert-butylphenol in both acetonitrile and ethanol/ water solvent. In this mechanism the TBP molecule (Ia) is deprotonated to give a phenoxide anion (Ib), which is oxidised to the stable phenoxy radical (Ic) through a one electron transfer reaction. This radical is then oxidised further to produce a phenoxonium ion (Id) which is attacked by water leading to a final product such as 2,4,6-tri-tert-butyl-4-hydroxy-2,5-cyclohexadienone. An alternative reaction pathway is a concerted two electrons two protons transfer oxidation of the phenol (Ia) to form the phenoxonium ion, leading to the final product through hydrolysis. It is important to mention that in the ethanol / water solvent, the oxidation reaction is dependent greatly

on the pH of the solution. The phenol / phenoxy radical couple is noted to be irreversible in a solution of pH<10, while reversible in solution of pH ≥ 10. Although the oxidation pathway leading to the formation of the phenoxy radical (product Ic) is well established, there are ambiguities on the alternative oxidation mechanism pathways leading to the formation of compound II as the oxidation products will depend greatly to the experimental conditions.

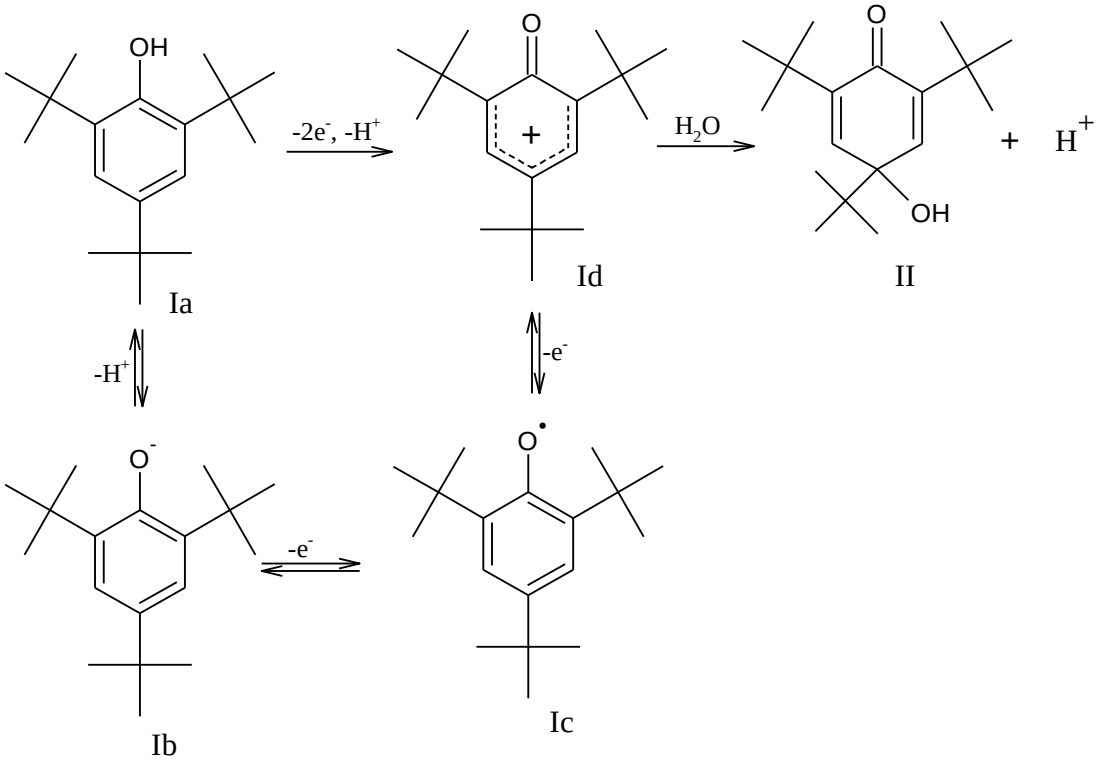

Scheme 1.11 Proposed oxidation mechanism of TBP [24].

1.2.2.2.2 Electrochemical Oxidation Mechanism of Unsubstituted Phenol

The oxidation of unsubstituted phenol is extensively studied but there are still ambiguities in the oxidation products due to the reasons mention above. Several oxidations mechanism were proposed in the literature but here the oxidation mechanism proposed by William et al [25] in their study on the mechanism of one-electron oxidation of phenol will be discussed as the mechanism proposed in this paper covers the mechanism reported by several authors. In this work Williams and Coworkers have used the Fieser's critical (E_{crit}) which defines as the potential at which the rate of phenol oxidation become first detectable to predict the one electron oxidation potential of phenol, but the equation for this critical potential is pH dependent [25]. Therefore, the

graph potential (E) against pH was plotted below (graph 1.1), where line (1) and (2) represent the oxidation reaction (1.3) and (1.4) of phenols presented below:

$$ArOH \rightarrow ArO^{\bullet} + H^{+} + e^{-} \quad (1.3)$$

$$ArO\bullet \rightarrow ArO^{+} + e^{-} \quad (1.4)$$

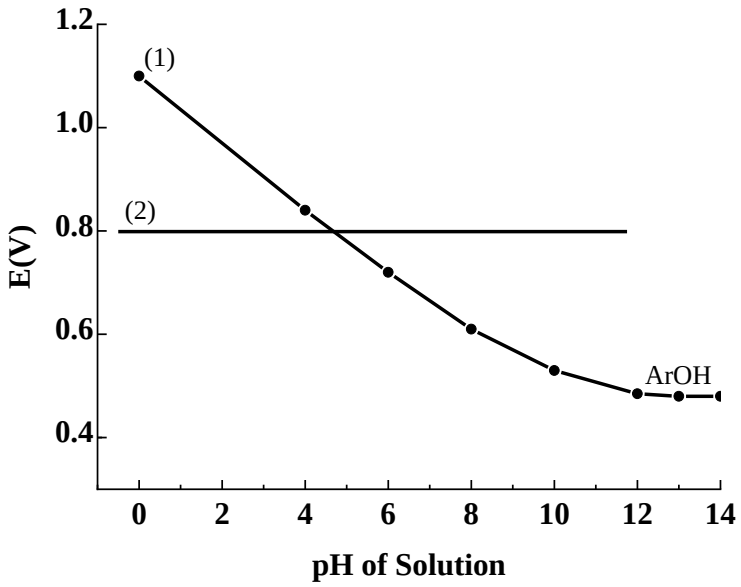

Figure 2.1: Plot of E (V) vs pH (taken from [25])

According to this prediction, for solution of pH < 4 both reaction (1.3) and (1.4) can take place consecutively at the same potential, leading to the formation of the phenoxy radical ($ArO^{\bullet}$) and phenoxide cation (ArO^{+}), while under condition where the potential is below the critical potential (for solution of pH > 4), the ArO• is metastable and therefore can undergo further oxidation to give ArO^{+} [25].

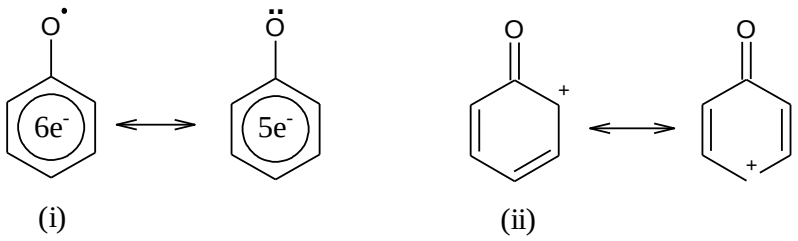

On account of this, dimerization of radicals (i) can occur through C-O-C coupling leading to the formation of a compound (vi) that undergoes one electron oxidation to produce product (v) and then the polymeric product (vi) as shown in scheme 1.12.

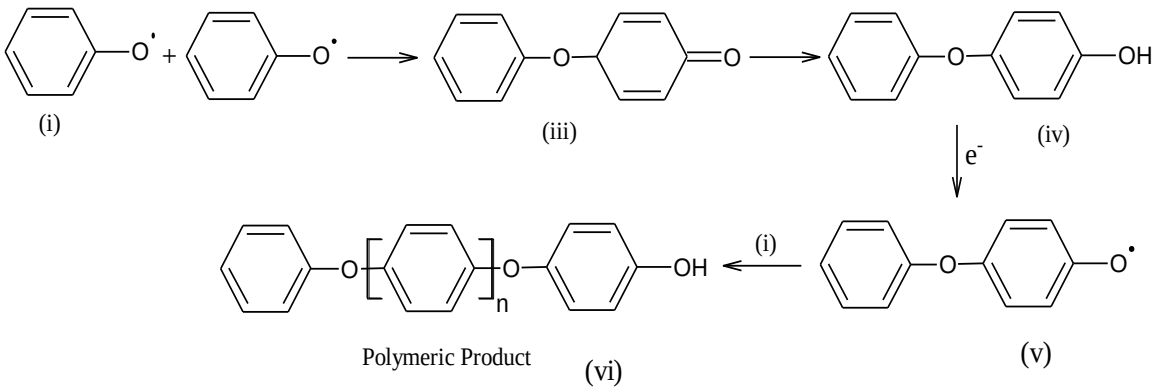

Scheme 1.12 Oxidation mechanism leading to dimers and polymeric products [25].

An alternative pathway is the electrophilic substitution between cation (ii) and the initial phenol to give the dimer (vii) that undergo one electron oxidation to give product (viii) and then the dipheno-quinone (ix) (scheme 1.15). Concurrently, the cation (ii) can react with water to yield compound (X) that then the monomeric quinone (xi) after oxidation. However, published evidence has indicated that the monomeric quinones (xi) and the dipheno-quinones but not dimer (iv) or polymer (vi) are obtained in acid solution or with reagents of high potential, while the formation of polymer (vi) is favoured in alkaline solution. The complexity of this reaction mechanism results in the fact that different radicals of (i) type can be obtained due to the delocalisation of the electrons in the ring, resulting in radicals in ortho and para-position. All these radical can undergo different reaction mechanisms and coupling leading to the formation of several dimers.

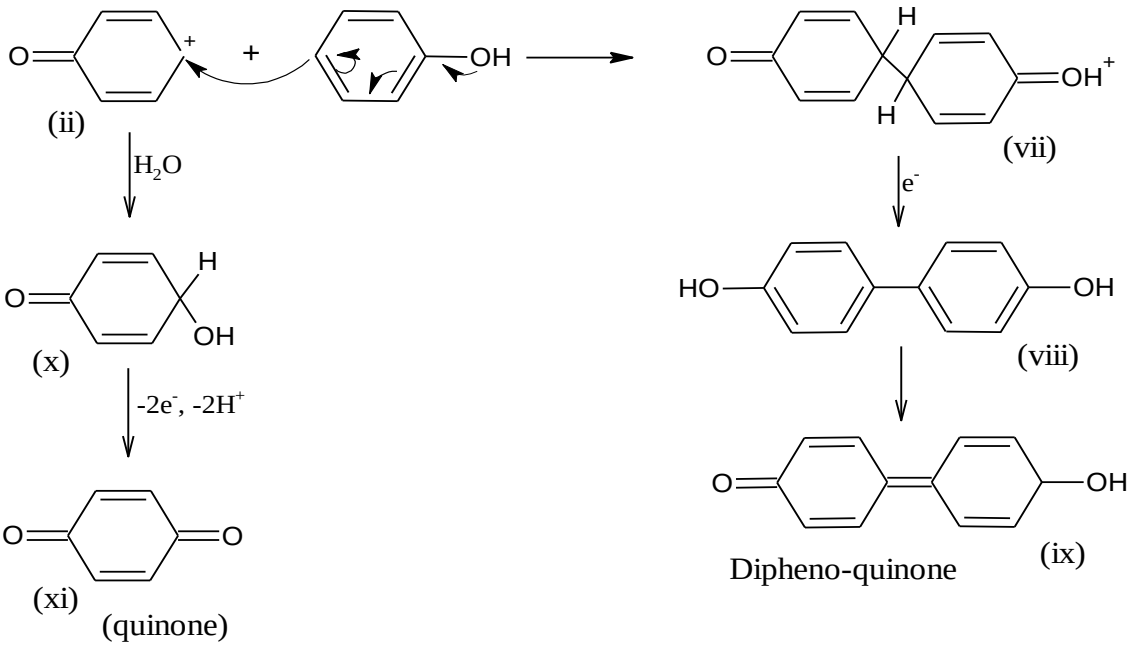

Scheme 1.13 Oxidation mechanism leading to quinones [25].

1.2.3 In Situ FITR Spectroscopy Study of Phenolic Compounds

FTIR spectroscopy has been widely used in the past to detect the oxidation products of phenolic compounds. This technique combined with cyclic voltammetry was commonly used to successfully study the electrochemical behaviour of phenolic compounds. Webster and co-workers have used this technique to monitor the one electron oxidation of 2,4,6-tri-tert-butylphenolate in CH_3CN. From their results, the authors identified several IR absorption bands notably in the 1592 −1573 cm^{-1} and 1509 −1505 cm^{-1} ranges which were assigned to C_oC_m (carbon in the ortho-and meta-position) ring and C−O• stretching vibration of 2,4,6-tri-tert-butylphenoxyl respectively [26]. Other authors such as Haracio and co-workers have also reported the use of this technique to detect the oxidation products for para-, meta-, and ortho-aminophenols while studying the electrochemical oxidation of aminophenols on platinum electrode in acid medium. In their study, the authors observed that the three isomers of aminophenols showed different behaviour with the platinum electrode, leading to different oxidation products. While meta- and para-aminophenol give polymeric compounds, quinone and CO_2 as oxidation products, electroactive dimers were observed as the oxidation product for ortho-aminophenols and these active dimers can polymerize to form an electroactive layer on the electrode surface [27].

Taleb and Co-workers have also used this technique to detect the oxidation products from the electrochemical oxidation of o-cresol in their study on electrochemical and in situ study of o-cresol on platinum electrode in acid medium. The results obtained from the in situ spectroscopy show CO_2 and methyl-p-benzoquinone as the oxidation products [27].

1.3 Thesis Objectives and Structure

The overall aim of this thesis is to explore the changes in chemical structure to polystyrene upon treatment with oxidising agents and to monitor the oxidation in situ on addition of these agents using FTIR spectroscopy technique. This will enable us to get more insight into the oxidation mechanism of PS which is not well understood especially in chemical oxidation. As phenolic defect sites in the PS structure are indicated as potential sites of oxidation, this thesis first explores the oxidation chemistry of substituted phenol compounds using cyclic voltammetry and in situ spectroscopy.

In this thesis, the techniques used such as cyclic voltammetry and ATR-FTIR are described in chapter 2. Cyclic voltammetry was used to study the electrochemical oxidation of molecules with structures similar to proposed defects sites (such as phenols) in the polystyrene. This allows us to determine at what potential they undergo oxidation in order to identify the sites at which the polystyrene is most susceptible to oxidation especially upon treatment with mild oxidising such as iridium (IV) hexachloride that has a potential of 0.75 V (vs Ag / AgCl) which is below 2V (vs. Ag / AgCl) the minimum potential required to oxidise the benzene ring but enough to oxidise the defect sites.

Chapter 3 present the results obtained for the electrochemical oxidation of phenols and substituted phenols at EPPG electrodes. In this chapter the electrochemical oxidation of phenols and substituted phenols such as o-cresol (2-methylphenol), m-cresol (3-methylphenol), p-cresol (4-methylphenol) and TBP (2, 4, 6-tri-tert-butylphenol) at edge plane pyrolytic graphite (EPPG) electrode is monitored using cyclic voltammetry. The pH, concentration and scan rate dependence on the electrochemical responses of these phenolic compounds are investigated. The activity of various carbon electrodes towards the electrochemical oxidation of TBP is examined and compared to each other.

More importantly, a reaction mechanism is proposed for each phenolic compound and then compared to each other in order to determine how the different substitutions affect the reaction mechanism pathways.

In order to confirm the mechanisms proposed for the different phenolic compounds, a combined technique of chronoamperometry and in situ ATR-FTIR spectroscopy was designed and the results obtained are presented in chapter 4. Chapter 4 studies the electrochemical oxidation of the unsubstituted phenols, TBP and cresols in situ using FTIR spectroscopy techniques. These allows us to identify IR peaks that were assigned to the oxidation products proposed for the different phenolic compounds that can be compared to the CV results in Chapter 3.

The chemical oxidation of polystyrene was studied using FTIR techniques and the results are given in chapter 5. In this chapter, PS non- treated and treated with iridium (IV) tetrachloride, iridium (IV) hexachloride and hydrogen peroxide were characterised first using FTIR spectroscopy technique. The resulting spectra obtained were analysing and a reaction mechanism was proposed for each of these oxidising agents. In addition, the broad band reported in several FTIR studies usually observed in the $3600 - 3200\ cm^{-1}$ region was investigated in the presence and absence of O_2 and water. The effect of immersion in water on the spectra of the non-oxidised and oxidised PS was also investigated. Additionally, the effect of oxidizing agents on the non-oxidised polystyrene surface in situ with and without the presence of oxygen was also studied in order to investigate the effect of oxygen on the oxidation mechanism of the PS.

Finally, in Chapter 6 the conclusions are summarised and the implications for understanding the oxidation mechanisms of PS discussed. Future research directions are identified.

References for Chapter 1

[1] A. Naima, "Biodegradability of Synthetic Plastics Polystyrene and Styrofoam by Fungal Isolates," Qaid-i-Azam University, Islamabad, 2011.

[2] L. Cole, *Polystyrene: Synthesis, Characteristics and Applications*. Nova Science Publishers, Inc. New York, 2014.

[3] E. Yousif and R. Haddad, "Photodegradation and Photostabilization of Polymers, Especially Polystyrene: Review," *Springerplus*, vol. 2, no. 1, pp. 1–32, 2013.

[4] K. Chen and S. Vyazovkin, "Mechanistic Differences in Degradation of Polystyrene and Polystyrene-Clay Nanocomposite: Thermal and Thermo-Oxidative Degradation," *Macromol. Chem. Phys.*, vol. 207, pp. 587–595, 2006.

[5] M. Graeme and S. David, H, *The Chemistry of Radical Polymerization*, 2nd ed. Australia: Elsevier Ltd, 2006.

[6] J. Propil, Z. Horak, Z. Krulis, and S. Nespurek, "The Origin and Role of Structural Inhomogeneities and Impurities in Material Recycling of Plastics," *Macromol. Symp.*, vol. 135, no. 1, pp. 127–263, 1998.

[7] B. Dickens and J. Marchal, "Oxidation of Polystyrene in Solution," *Polym. Degrad. Stab.*, vol. 6, no. 4, pp. 211–241, 1984.

[8] S. Biltresse, Y. Dufrêne, and J. Marchand-Brynaert, "An Unprecedented Surface Oxidation of Polystyrene Substrates by Wet Chemistry under Basic Conditions.," *J. Colloid Interface Sci.*, vol. 252, no. 2, pp. 443–9, 2002.

[9] T. S. Varley, M. Rosillo-lopez, S. Sehmi, N. Hollingsworth, and K. B. Holt, "Surface Redox Chemistry and Mechanochemistry of Insulating Polystyrene Nanospheres," *Phys. Chem. Chem. Phys.*, vol. 17, no. 3, pp. 1837–1846, 2015.

[10] M. Inutsuka, H. Tanoue, N. L. Yamada, K. Ito, and H. Yokoyama, "Dynamic Contact Angle on a Reconstructive Polymer Surface by Segregation," *RSC Adv.*, vol. 7, no. 28, pp. 17202–17207, 2017.

[11] T. Murakami, S. Kuroda, and Z. Osawa, "Dynamics of Polymeric Solid Surfaces Treated with Oxygen Plasma: Effect of Aging Media after Plasma Treatment," *J. Colloid Interface Sci.*, vol. 202, no. 202, pp. 37–44, 1998.

[12] B. Mailhot, S. Morlat, and J. L. Gardette, "Photooxidation of Blends of Polystyrene and Poly(vinyl methyl ether): FTIR and AFM Studies," *Polymer (Guildf).*, vol. 41, pp. 1981–1988, 2000.

[13] J. L. Gardette, B. Mailhot, and J. Lemaire, "Photooxidation Mechanisms of Styrenic Polymers," *Polym. Degrad. Stab.*, vol. 48, no. 3, pp. 457–470, Jan. 1995.

[14] J. Gardette and M. Benedicte, "Polystyrene Photooxidation. 1. Identification of the IR-Absorbing Photoproducts formed at short and long wavelenghts," *Macromolecules*, vol. 25, no. 16, pp. 4119–4126, 1992.

[15] H. Raghad, A. Dina, S, A. Ahmed, M. Salam, and Y. Emad, "Detection of Degradation of PS Thin Films Containg Triazole Complexes by FTIR Technique," *Orient. J. Phys. Sci.*, vol. 3, no. 1, pp. 53–57, 2018.

[16] B. Ranby and J. Lucki, "New Aspects of Photodegradation and Photooxidation of Polystyrene," *Pure Appl. Chem.*, vol. 52, no. 2, pp. 295–303, 1980.

[17] B. Stuart, *Infrared Spectroscopy : Fundamentals and Applications*, 1st ed. Chichester: John Wiley & Sons, Ltd, 2014.

[18] C. Stihi, "Atr-Ftir Spectrometry Characterisation of Polymeric Materials," *Rom. reports Phys.*, vol. 66, no. 3, pp. 765–777, 2014.

[19] L. Wade, "Phenol Chemical Compound." [Online]. Available: https://www.britannica.com/science/phenol. [Accessed: 20-Dec-2018].

[20] Chemistry libretext, "Electrophilic Substitution of the Phenol Aromatic Ring," 2014. [Online]. Available: https://chem.libretexts.org/Bookshelves/organic_Chemistry. [Accessed: 20-Dec-2018].

[21] J. Mathiyarasu, J. Joseph, K. L. N. Phani, and V. Yegnaraman, "Electrochemical Detection of Phenol in Aqueous Solutions," *Indian J. Chem. Technol.*, vol. 11, no. 6, pp. 797–803, 2004.

[22] H. Nady, M. M. El-rabiei, and G. M. A. El-hafez, "Electrochemical Oxidation Behavior of Some Hazardous Phenolic Compounds in Acidic Solution," *Egypt. J. Pet.*, vol. 10, no. 9, pp. 1–10, 2016.

[23] Z. Taleb, F. Montilla, C. Quijada, E. Morallon, and S. Taleb, "Electrochemical and In Situ FTIR Study of O-Cresol on Platinum Electrode in Acid Medium," *Electrocatalysis*, vol. 5, no. 2, pp. 186–192, 2014.

[24] H. Eickhoff *et al.*, "Electrochemical Oxidation of 2,4,6-Tri-Tert-Butylphenol," *J. Chem. Soc. B Phys. Org.*, vol. 63, no. 3, pp. 858–867, 1971.

[25] W. A. Waters, "Comments on the Mechanism of One-Electron Oxidation of Phenol: A Fresh Interpretation of Oxidative Coupling Reactions of Plant Phenols," *J. Chem. Soc. B Phys. Org.*, pp. 2026–2029, 1971.

[26] R. D. Webster, "In Situ Electrochemical-ATR-FTIR Spectroscopic Studies on Solution Phase 2 , 4 , 6-tri-substituted Phenoxyl Radicals," *Electrochem. commun.*, vol. 5, pp. 6–11, 2003.

[27] H. J. Salavagione, J. Arias, P. Garcés, E. Morallón, C. Barbero, and J. L. Vázquez, "Spectroelectrochemical Study of the Oxidation of Aminophenols on Platinum Electrode in Acid Medium," *J. Electroanal. Chem.*, vol. 565, no. 2, pp. 375–383, 2004.

[28] C. Engineer, J. Parikh, and A. Raval, "Review on Hydrolytic Degradation Behavior of Biodegradable Polymers from Controlled Drug Delivery System," *Trends Biomater. Artif. Organs*, vol. 25, no. 2, pp. 79–85, 2011.

[29] M. A. Grayson, C. J. Wolf, R. L. Levy, D. B. Miller, and M. Douglas, "The Mechanical Degradation of Polystyrene Determination of Residual Volatile Compounds," *J. Polym. Sci.*, vol. 14, pp. 1601–1609, 1976.

[30] A. J. McQuillan, "Probing Solid-Solution Interfacial Chemistry with ATR-IR Spectroscopy of Particle Films," *Adv. Mater.*, vol. 13, no. 12–13, pp. 1034–1038, 2001.

[31] S. Stack, O. O'Donoghue, and C. Birkinshaw, "The Thermal Stability and Thermal Degradation of Blends of Syndiotactic Polystyrene and Polyphenylene Ecosther," *Polym. Degrad. Stab.*, vol. 79, pp. 29–36, 2003.

[32] M. Coşkun, K. Demirelli, and E. Özdemir, "Preparation, Characterization and Thermal Degradation of Poly p-(2,4-dichlorobenzyl)Styrene," *Polym. Degrad. Stab.*, vol. 47, pp. 251–256, 1995.

[33] O. Watanabe, M. Tabata, J. Sohma, and A. Lund, "Chemical Degradation of Polystyrene Induced by Chlorinated Nitrosobenzene," *Polym. Degrad. Stab.*, vol. 7, pp. 13–24, 1984.

[34] G. Chen, S. Liu, S. Chen, and Z. Qi, "FTIR Spectra, Thermal Properties, and Dispersibility of a Polystyrene/Montmorillonite Nanocomposite," *Macromol. Chem. Phys.*, vol. 202, pp. 1189–1193, 2001.

[35] G. Botelho, A. Queirós, A. Machado, P. Frangiosa, and J. Ferreira, "Enhancement of The Thermooxidative Degradability of Polystyrene by Chemical Modification," *Polym. Degrad. Stab.*, vol. 86, pp. 493–497, 2004.

[36] L. F. A. Pinto, B. E. Goi, C. C. Schmitt, and M. G. Neumann, "Photodegradation of Polystyrene Films Containing UV-Visible sensitizers," *J. Res. Updat. Polym. Sci.*, vol. 2, no. 1, pp. 39–47, 2013.

[37] F. Kanwal, S. M. Waraich, and T. Jamil, "FT-IR Analysis of Recycled Polystyrene for Food Packaging," *J.chem.Soc.Pak*, vol. 29, no. 3, pp. 239–242, 2007.

[38] G. Gryn'ova, J. L. Hodgson, and M. L. Coote, "Revising the Mechanism of Polymer Autooxidation," *Org. Biomol. Chem.*, vol. 9, no. 2, pp. 480–490, 2011.

[39] K. P. J. Williams and D. L. Gerrard, "The Degradation of Poly(vinyl chloride) Studied using Fourier Transform Raman Spectroscopy," *Eur. Polym. J.*, vol. 26, no. 12, pp. 1355–1358, 1990.

[40] F. Vilaplana, A. Ribes-Greus, and S. Karlsson, "Degradation of Recycled High-Impact Polystyrene. Simulation by Reprocessing and Thermo-Oxidation," *Polym. Degrad. Stab.*, vol. 91, pp. 2163–2170, 2006.

[41] N. Grassie and N. A. Weir, "The Photooxidation of Polymers.," *J. Appl. Polym. Sci.*, vol. 9, pp. 999–1003, 1965.

[42] G. Guerra, P. Musto, F. E. Karasz, and W. J. MacKnight, "Fourier Transform Infrared Spectroscopy of the Polymorphic Forms of Syndiotactic Polystyrene," *Makromoil . Chem*, vol. 191, pp. 2111–2119, 1990.

[43] J. López Gejo *et al.*, "Vacuum-Ultraviolet Photochemically Initiated Modification of Polystyrene Surfaces: Morphological Changes and Mechanistic IUnvestigations.," *Photochem. Photobiol. Sci.*, vol. 5, pp. 948–954, 2006.

[44] N. B. Tahar and A. Savall, "Electropolymerization of Phenol on a Vitreous Carbon Electrode in Alkaline Aqueous Solution at Different Temperatures," *Electrochem. Acta*, vol. 55, pp. 465–469, 2009.

[45] G. Grampp, S. Landgraf, and C. Mureşanu, "Redox Properties and Bond Dissociations Energies of Phenoxyl Radicals," *Electrochim. Acta*, vol. 49, no. 4, pp. 537–544, 2004.

[46] M. E. Tessensohn, H. Hirao, and R. D. Webster, "Electrochemical Properties of Phenols and Quinones in Organic Solvents are Strongly Influenced by Hydrogen-Bonding with Water," *J. Phys. Chem. C*, vol. 117, no. 2, pp. 1081–1090, 2013.

[47] D. H. Evans, P. J. Jimenez, and M. J. Kelly, "Reversible Dimerization of Phenoxyl Radicals Formed by Anodic Oxidation of Phenolates. A Quantitative Study by Cyclic Voltammetry," *J. Electroanal. Chem.*, vol. 163, pp. 145–157, 1984.

[48] P. Hapiot and J. Pinson, "Multiple Reaction Pathways for the Oxidation of 2,6- Diphenylphenolates," *J. Electroanal. Chem.*, vol. 362, pp. 257–265, 1993.

[49] S. Patai, *The Chemistry of Phenols*, 1st ed. Chichester: John Wiley & sons, Ltd, 2003.

[50] F. Wantz, C. E. Banks, and R. G. Compton, "Edge Plane Pyrolytic Graphite Electrodes for Stripping Voltammetry: A Comparison with Other Carbon Based Electrodes," *Electroanalysis*, vol. 17, no. 8, pp. 655–661, 2005.

[51] W. Yuan *et al.*, "The Edge- and Basal-Plane-Specific Electrochemistry of a Single-Layer Graphene Sheet," *Sci. Rep.*, vol. 3, pp. 1–7, 2013.

Chapter 2

Experimental Theory and Techniques

2.1 Introduction

This chapter outlines the main experimental techniques employed in this thesis. Particular emphasis is placed upon the cyclic voltammetry and ATR-FTIR spectroscopy techniques, as these were used mostly throughout the project. X-ray Photoelectron Spectroscopy (XPS) was also used to investigate the chemical composition of the polystyrene beads used in this study.

2.2 Cyclic Voltammetry

2.2.1 Theory

Cyclic voltammetry (CV) is an electrochemical technique widely used to conduct mechanistic investigations. In CV experiment the current is measured as the function of voltage and this can provide valuable mechanistic information about the electron transfer process occurring.

CV requires applying a triangular potential waveform (Figure 2.1a) and this involves sweeping the electrode potential of the working electrode between two potentials, E_1 and E_2 at a known scan rate, ν. On reaching the potential E_2 the sweep is reversed back to the initial potential E_1 to give a triangular potential cycle [1] . Figure 2.1b shows a cyclic voltammogram resulting from a single electron transfer process. Considering the following reversible reaction:

$$O + e^- \leftrightarrow R \qquad (2.1)$$

On reversing the potential back from E_2 to E_1, the species R formed at the electrode surface during the forward sweep is re-oxidised back to O. Current in the opposite sense to the forward scan is observed due to the oxidation of R to O. This oxidation current increases initially since a high concentration of R is present is the diffusion layer and the kinetics for the reconversion of R to O become more favourable as the potential becomes more positive. Gradually, all of R present in the diffusion layer is reconverted to O and the current drops to zero [2].

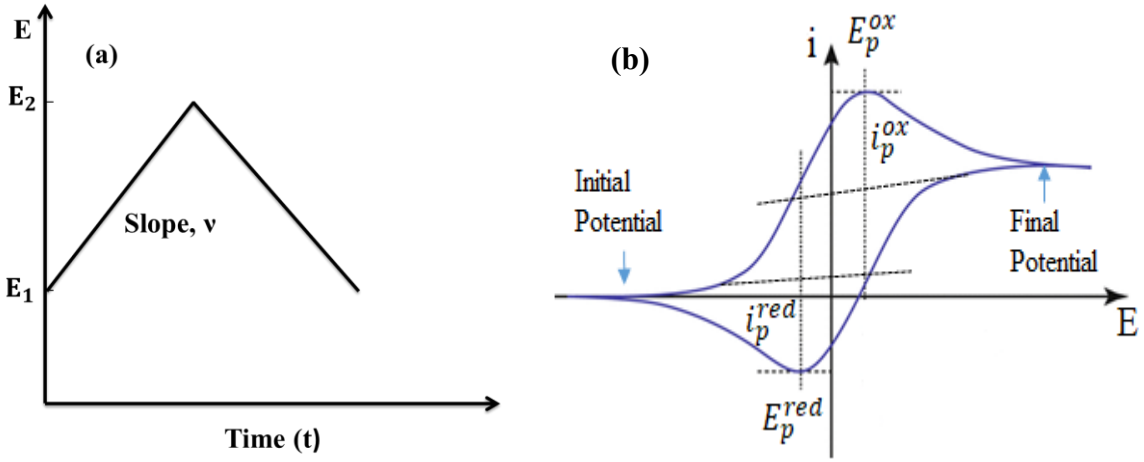

Figure 2.1: (a) Potential-time waveform for CV (adapted from [1]) and (b) A typical cyclic voltammogram for a single electron transfer. The key parameters are the peaks potentials, E_p^{ox} and E_p^{red} and the peaks currents, i_p^{ox} and i_p^{red} (adapted from [3]).

In CV experiments, a three electrodes set-up is used as presented in Figure 2.2 and this consists of working, reference and counter electrodes. The electrochemical process being investigated takes place at the working electrode. The reference electrode provides a fixed potential with which the potential of the working electrode can be measured against. The counter electrode supplies the current requires by the working electrode without in any way limiting the measured response of the cell. A potentiostat is used to control the potential at the working electrode with respect to the reference electrode or the current that flows between the working electrode and the counter electrode. Experiments can also be carried out in oxygen free environment by purging the solution with argon or nitrogen.

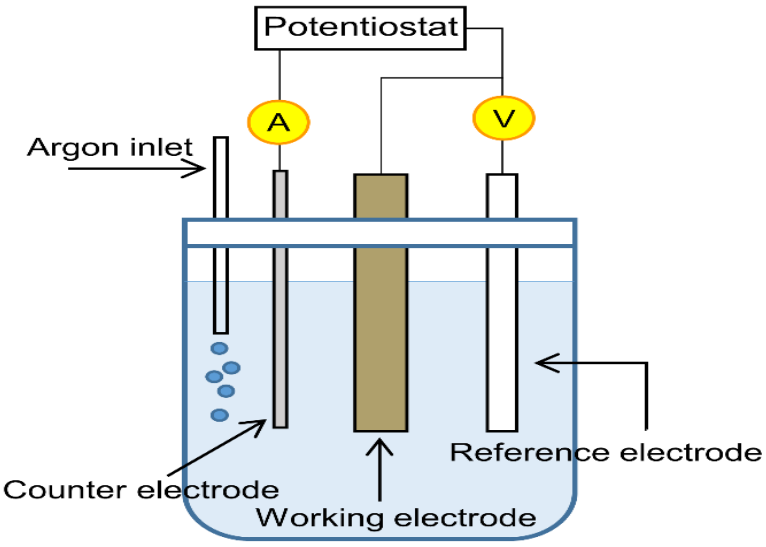

Figure 2.2: A typical three electrode cyclic voltammetry set up [4].

2.2.2 Characteristic of Cyclic Voltammograms

The shape of the voltammogram depends on the reversibility of the electrode kinetics for the redox couple O/R. For reversible couples, significant current flows at small overpotentials. The heights of the forward and reverse current peaks are equal in magnitude and are separated by a potential of 59 mV at all scan rates at 298 K (Equation 2.2).

$$\Delta E_p = \left| E_p^{ox} - E_p^{red} \right| = 2.218 \frac{RT}{nF} \qquad (2.2)$$

In the irreversible case, the peak separation ΔE_p is bigger, as a larger overpotential is required to reconvert R into O. The size of the reverse peak is much smaller relative to the forward peak and depends on the voltage scan rate. The peak separation and dependence on scan rate are therefore diagnostic of the nature of the electrode kinetics. 'Reversible' and 'irreversible' electrode kinetics refers to limiting cases of reactions but intermediate cases exist and these are called 'quasi-reversible'. In this latter case, the ratio of the backward and the forward peak current is close to unity, like reversible reactions, but the peak separation is scan rate dependent [2],[5].

For any system, reversible or not, the current i_p is directly proportional to the concentration of O and increases with scan rate. The dependence of i_p with the scan rate

is explained by the fact that i_p is dependent on the flux of material reacting at the electrode surface, which is controlled by the rate of diffusion of reactant. This is dependent on the concentration gradient near the electrode surface i.e the diffusion layer thickness. If fast scan rate is employed, relatively less time is available for the electrolysis of the reactant, so its depletion close to the electrode is lowered. This results in thinner diffusion layer and steeper concentration gradient, which leads to increased flux of reactant and higher i_p [5], [6].

The size of the peak current for a reversible reaction is given by the Randles-Sevick equation (2.3), where i_p is the current maximum (in amps); n is the number of moles of electrons transferred in the reaction; A is the area of the electrode (in cm^2); D is the diffusion coefficient (cm^2 / s); C is the electrolyte concentration (in moles cm^{-3}) and ν is the scan rates of the applied potential (in Vs^{-1}). The peak current is proportional to the concentration and to the square root of the scan rate.

$$i_p = (2.69 \times 10^5)\, n^{3/2}\, A\, D^{1/2}\, C\, \nu^{1/2} \qquad (2.3)$$

The characteristic CV features of reversible, irreversible and quasi-reversible electron transfer kinetics is summarized in table 2.1 below (adapted from [1]).

Table 2.1: Characteristic CV features of reversible, irreversible and quasi-reversible electron transfer kinetics (taken from[1])

	Reversible	Irreversible	Quasi-reversible
ΔE_p	59/n mv		> 59/n mV
$\lvert\frac{i_p^{red}}{i_p^{ox}}\rvert$	1		1
i_p	$\propto \nu^{1/2}$	$\propto \nu^{1/2}$	increase with $\nu^{1/2}$
E_p	independent of ν	dependent of ν	dependent on ν

2.3 Attenuated Total Reflectance - Fourier Transform Infrared Spectroscopy (ATR-FTIR)

Infrared spectroscopy is a technique based on the vibrations of bonds in a molecule. An infrared spectrum is commonly obtained by passing infrared radiation through a sample and determining what fraction of the incident radiation is absorbed at a particular energy. The energy at which any peak in an absorption spectrum appears corresponds to the frequency of a vibration of a part of a sample molecule. The selection rule for a molecular to show infrared absorptions is that its electric dipole must change during the vibration [7].

In an FTIR spectrometer, the radiation emerging from the source is passed through an interferometer to the sample before reaching a detector. Upon amplification of the signal, in which the high-frequency contribution has been eliminated by a filter, the data are converted to a digital form by employing an analog-to-digital converter and then sent to the computer for the Fourier transformation (tools that breaks a waveform into an alternate representation, characterize by sine and cosines) to take place [7]. The Michelson interferometer is one of the most important components of recent FTIR instruments and makes it possible to record high spectral resolution data within a larger frequency range simultaneously at short time and to also record complicated spectra of materials.

Furthermore, FTIR is proven to be useful for elucidating the physical and chemical surface structure, hydrogen bonding, degradation reactions, end group detection, crosslinking behaviour of molecules and copolymer composition both in solid and liquid form of polymers [7], [8].

The ATR method is based on the phenomenon of total internal reflection. A beam of radiation entering a crystal will undergo total reflection when the angle of incidence at the interface between the sample and the crystal is greater than the critical angle, where the latter is a function of the refractive indices of the two surfaces. The beams penetrates a fraction of a wavelength beyond the reflecting surface and when a material that selectively absorbs radiation is in close contact with the reflecting surface, the beam loses energy at the wavelength where the material absorbs [7], [9].

The resultant attenuated radiation is measured and plotted as a function of wavelength by the spectrometer and gives rise to the absorption spectral characteristics of the sample. A schematic of a typical attenuated total reflectance cell is presented in Figure 2.3.

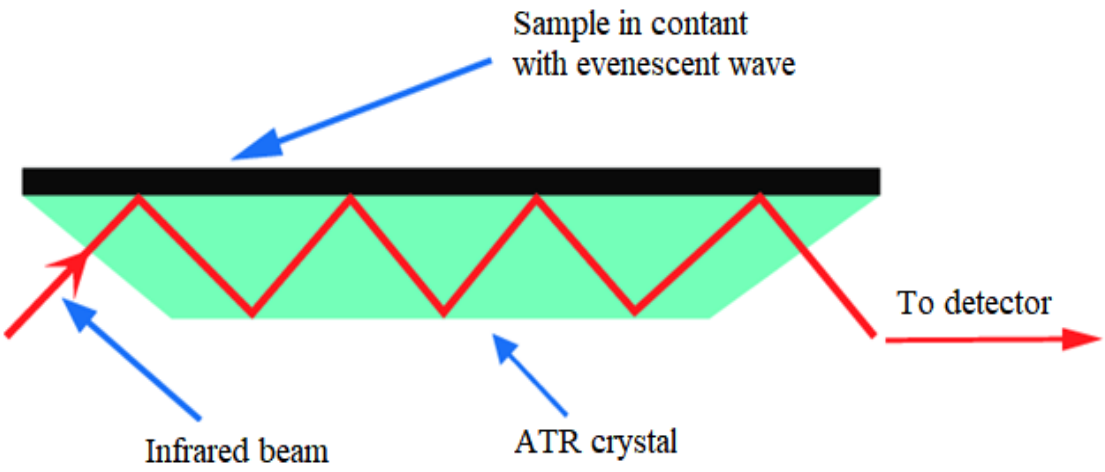

Figure 2.3: Schematic of a typical attenuated total reflectance cell (taken from [9])

The depth of penetration in ATR spectroscopy is a function of the wavelength, λ, the refractive index of the crystal, n_2, and the angle of incidence radiation, θ. The depth of penetration, d_p, for a non-absorbing medium is given by the following:

$$d_p = (\lambda / n_1) / \left\{2\pi\left[sin\theta - \left({}^{n_1}/_{n_2}\right)^2\right]^{\frac{1}{2}}\right\} \qquad (2.4)$$

where n_1 is the refractive index of the sample.

The crystals used in ATR cells are made from materials that have low solubility in water and are of a very high refractive index. Such materials include zinc selenide (ZnSe), germanium (Ge) and thallium-iodide (KRS-5) [7].

One of the key advantages of this method is the analysis of small quantities of samples and without sample preparation. Despite its numerous advantages, ATR method has a relatively low sensitivity and susceptibility to the action of environmental factors [10].

ATR-FTIR can be successfully used for the detection and quantification of specific end groups in evaluating the degree of degradation of polymeric materials.

This technique also has the advantage of recording spectra in situ in solution and in the presence of oxidizing agents.

2.4 X-ray Photoelectron Spectroscopy (XPS)

X-ray photoelectron spectroscopy (XPS) also called Electron spectroscopy for chemical analysis (ESCA) provides valuable information on the surface elemental and fundamental group compositions of polymers. In this technique, the sample is irradiated with soft X-rays, usually MgKα, and photoelectrons are emitted. These photoelectrons can arise from the core or valence levels depending of the energy of the X-ray source employed.

XPS analysis is commonly carried out in a high-vacuum chamber. When the sample is irradiated, the emitted photoelectrons are collected by a lens system and focused into an energy analyser. The latter counts the number of electrons with a given kinetic energy (E_K). The binding energies (E_B) of the photoelectrons are obtained by using the Einstein equation as follows:

$$E_B = h\upsilon - E_k - \phi \qquad (2.5)$$

where E_B is the binding energy, $h\upsilon$ the energy of the X-ray photons being used, E_k the kinetic energy of the electron as measured by the instrument and ϕ the work function dependent on both the spectrometer and the material.

2.5 Experimental Methods

2.5.1 CV Experimental Set -Up

Most of the CV experiments were carried out using a convention three-electrode system immersed in an electrolyte (consisting of 0.5 mM of the corresponding phenol in 50:50 (v:v) EtOH / PBS (pH11)). The three-electrode system is controlled by a computer-controlled potentiostat (μAutolab PGSTAT, Eco Chemie, The Netherlands) running GPES (v4.9) software, which allows the current to flow only between the working and counter electrode. This experimental set-up is shown above in section 2.2 (Figure 2.2) and the exact experimental conditions are described in the relevant chapter.

2.5.2 ATR-FTIR Spectroscopy Set-Up

This technique was used to monitor the oxidation of the phenolic compounds in order to confirm the oxidation mechanisms proposed in Chapter 3. All experiments were performed by using a combined technique of chronoamperometry and in situ ATR-FTIR spectroscopy. A three electrodes electrochemical cell was used which consists of a working electrode (EPPG coated with singlet walled carbon nanotubes (SWCNT), a reference electrode (Ag / AgCl) and a counter electrode (platinum wire) dipped in the electrolyte. The three electrodes cell system was controlled electronically by a laptop-controlled potentiostat, which allows a fixed potential to be applied to the system.

Most FTIR spectra were recorded between 4000 − 400 cm^{-1} with a spectral resolution of 4 cm^{-1} using a Bruker Tensor 27 Fourier-transform spectrometer equipped with a diamond crystal prism and having an Opus data collection program. The exact experimental conditions are described in the relevant chapter. Figure 2.4 shows a typical set-up for the combined technique measurements.

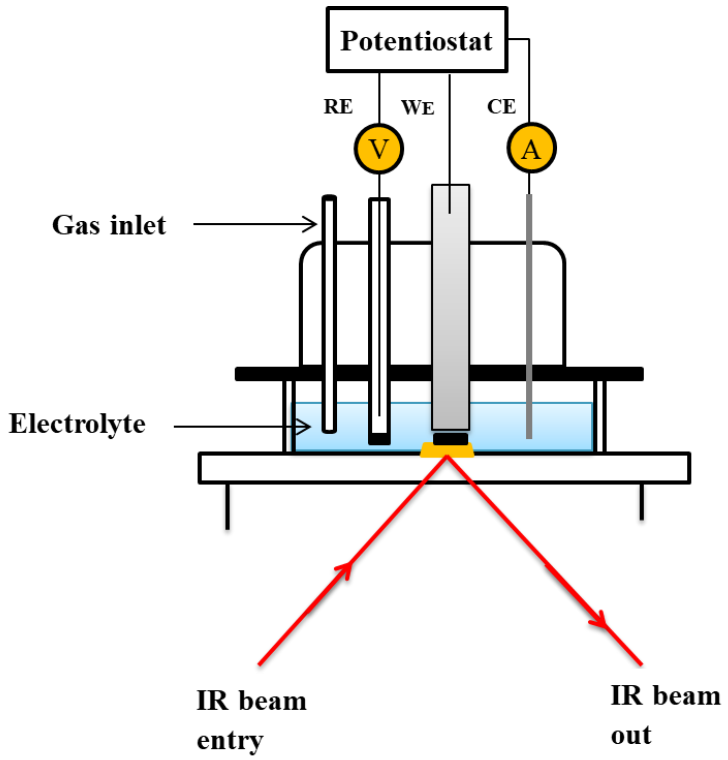

Figure 2.4: A typical set-up for the combined technique measurements.

ATR-FTIR technique was also employed to investigate the changes to the polystyrene structure in situ in the presence in solution of oxidizing agents such as iridium (IV) tetrachloride, iridium (IV) hexachloride, hydrogen peroxide and potassium ferricyanide. It was also used to characterise the unoxidised and oxidised polystyrene upon chemical treatment. All these experiments were carried out using the Bruker Tensor 27 Fourier-transform spectrometer mentioned above. The experimental set-up is presented in Figure 2.5 and the experimental conditions and procedures are described in the relevant chapter.

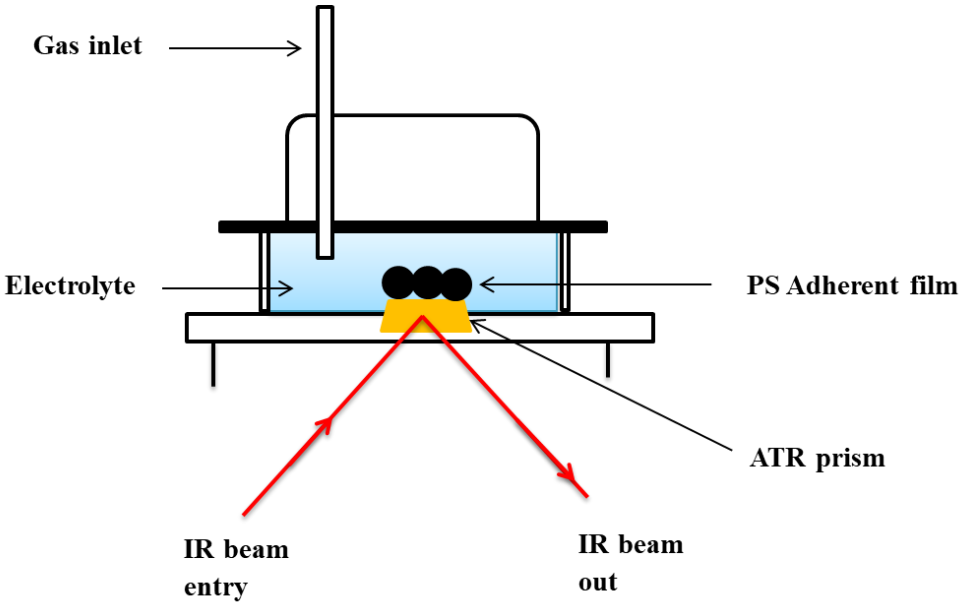

Figure 2.5: In situ FTIR spectroscopy set up

Reference for Chapter 2

[1] R. Greef, R. Peat, D. Pletcher, and J. Robinson, *Instrumental Methods in Electrochemistry*. West Susex, England: Ellis Horwood Limited, 1993.

[2] A. Fisher, C, *Electrode Dynamics*. New York: Oxford University Press InC, 1996.

[3] S. Bilal, *Encyclopedia of Applied Electrochemistry*. New York: Springer, 2014.

[4] M. Lounasvuori, "Electrochemical and Spectroscopic Studies of Graphene Nanoflakes with Functionalised Edges," University College London, 2017.

[5] K. B. Holt, "Characterisation and Applications of Boron-Doped Diamond Electrodes," University of Oxford, 2002.

[6] Pletcher, *A Fisrt Course in Electrode Process*. Romsey, England: The Electrochemical Consultancy, Ltd, 1991.

[7] B. Stuart, *Infrared Spectroscopy : Fundamentals and Applications*, 1st ed. Wliley & sons ltd, 2014.

[8] C. Stihi, "Atr-Ftir Spectrometry Characterisation of Polymeric Materials," *Rom. reports Phys.*, vol. 66, no. 3, pp. 765–777, 2014.

[9] T. S. R. Group, "Fourier Transform Infrared (FTIR)- Attenuated Total Reflection (ATR) Spectroscopy." [Online]. Available: https://sites.temple.edu/strongingroup/laboratories/atr/. [Accessed: 23-Dec-2018].

[10] C. Y. Liang and S. Krimm, "Infrared Spectra of High Polymers," *J. Mol. Spectrosc.*, vol. 3, no. 1958, pp. 554–574, 1959.

[11] I. A. Mudunkotuwa, A. Al Minshid, and V. H. Grassian, "ATR-FTIR Spectroscopy as a Tool to Probe Surface Adsorption on Nanoparticles at the Liquid-Solid Interface in Environmentally and Biologically Relevant Media.," *Analyst*, vol. 139, pp. 870–81, 2014.

[12] B. D. Hibbert, *Introduction To Electrochemistry*. London: macmillan Press, Ltd, 1993.

[13] A. J. Bard and L. R. Faulkner, *Electrochemical Methods : Fundamentals and Applications*, 2nd ed. New York: John Wiley and Sons, Inc., 1993.

Chapter 3

Electrochemical Oxidation of Phenols and Substituted Phenols at Edge Plane Pyrolytic Graphite Electrode

3.1 Introduction

Previous studies on polystyrene degradation have reported the presence of phenol and derivatives in the structure of polystyrene. These groups are considered as defects sites in the polystyrene structure and they can easily undergo oxidation. Therefore, studying the electrochemical behaviour of these compounds will allow us to determine at what potential these compounds undergo oxidation. This will allow us to identify the sites at which the polystyrene is most susceptible to oxidation.

A second motivation for this study is that, phenols and derivatives are present in effluent from food industries, chemical industries, the production of resin and pesticides to name only a few [1], [2]. However, they present toxicity and bioaccumulation problems. Therefore, the electrochemical oxidation of these species appears as a promising method for the treatment of industrial effluents and wastewater remediation.

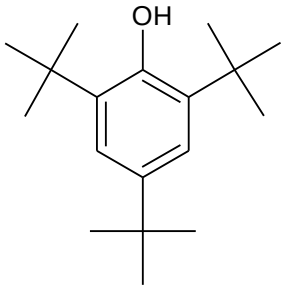

TBP

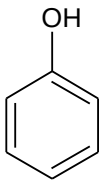

Phenol

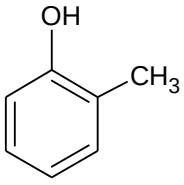

o-cresol

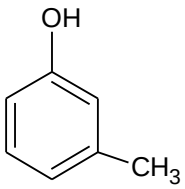

m-cresol

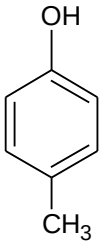

p-cresol

Many studies have been carried out and published on the electrochemical oxidation and detection of phenolic compounds. Different electrode materials were used including platinum, gold, glassy carbon (GC), boron-doped diamond (BDD) and others.

The electro-oxidation of phenolic compounds occurs through the formation of the phenoxy radical. This radical can either react with other species present in the solution (e.g. proton, water, oxygen) to generate oxidation products such as quinone species, or react with other phenol molecules to form a polymeric product. In all cases fouling of the electrode was reported and this was due to the deposition on the electrode surface of the polymeric products formed, leading to the passivation of the electrode [2]. Although, the electrochemical oxidation of phenols has been extensively studied, the electro-oxidation mechanism is still not well understood under all conditions.

The study of the electro-oxidation of phenolic compound using cyclic voltammetry is a popular method, due to its sensitivity, low cost and the requirement of only a small concentration of reactant to obtain a signal with little sample preparation. However, this technique presents some difficulties with the more common being the rapid passivation of the electrode after the first cycle using certain electrode materials such as platinum and glassy carbon.

In this chapter the electrochemical oxidation of phenols and substituted phenols such as o-cresol (2-methylphenol), m-cresol (3-methylphenol), p-cresol (4-methylphenol) and TBP (2, 4, 6-tri-tert-butylphenol) at edge plane pyrolytic graphite (EPPG) electrode will be monitored using cyclic voltammetry. The pH, concentration and scan rate dependence on the electrochemical responses of these phenolic compounds are investigated. The activity of various carbon electrodes towards the electrochemical oxidation of TBP is examined and compared to each other. More importantly, a reaction mechanism will be proposed for each phenolic compound and then compared to each other in order to determine how the different substitutions affect the reaction mechanism pathways.

3.2 Methodology

3.2.1 Chemicals and Solutions

All electrochemical experiments were carried out in solutions containing 50:50 (v:v) ethanol and potassium phosphate buffer (0.1M) consisting of potassium phosphate monobasic and potassium phosphate dibasic trihydrate (≥ 99%) in varying proportion to obtain pH of 5,6,7,8 and 9. Solution of pH 11 was obtained by adjusting the buffer using NaOH (0.1M).

All chemicals were purchased from Sigma Aldrich and used as received except the cresols, which were obtained from another research group within the department. The potassium phosphate buffers were prepared using a Millipore Milli-Q water of 18.2 MΩ cm.

3.2.2 Cyclic Voltammetry Measurements

Cyclic Voltammetry measurements were performed using a μAutolab PGSTAT potentiostat (Eco Chemie, Utrecht, Netherlands) running GPES (v4.9) software. A standard three electrode cell configuration was used, which consisted of an edge plane pyrolytic graphite (EPPG) disk (d = 3 mm) working electrode, an Ag / AgCl (sat. KCl) reference electrode (BASi, West Lafayette, America) and a platinum wire as a counter electrode. In some experiments GC and BDD were used as working electrodes. The solutions were not deoxygenated. The potential was first swept to more positive potentials (oxidation scan), followed by a reduction scan. The working electrodes were polished manually with aqueous slurry of alumina powder (0.05 μm) for few minutes on a polishing pad and thoroughly rinsed with de-ionised water and air-dried before each measurement. Three scans were performed for each experiment.

3.3 Results and Discussions

The electrochemical oxidation of TBP as mentioned in the introduction section is the most studied and well understood. The oxidation process including an intermediate phenoxy radical is well established [3], [4]. Therefore, in this study the electrochemical oxidation of TBP was investigated first using different electrode materials such as EPPG, GC and BDD. This allows us to choose the more suitable substrate for our investigations.

In the following cyclic voltammetry experiments, a mixture of PBS buffer and ethanol was used as the electrolyte. Ethanol was added to the PBS buffer to help in dissolving the tri-substituted phenol (TBP) which was insoluble in the buffer alone due to the tertbutyl groups.

3.3.1 Electrochemical Oxidation of 2, 4, 6-tri-tert-butylphenol (TBP) at Various Carbon Electrode Materials.

The electrochemical response of 0.5 mM TBP in 50:50 (v:v) EtOH / PBS (pH11) solution at EPPG, GC and BDD electrodes was characterised by cyclic voltammetry (Figure 3.1). Under these conditions, defined oxidation and reduction peaks are observed for TBP at the EPPG (E_p^{ox} = 0.246 V and E_p^{red} = 0.146 V) and GC (E_p^{ox} = 0.276 V and E_p^{red} = 0.138 V) electrodes. On the surface of the BDD electrode, the TBP response appeared weak and sluggish. Fast electrode kinetics exemplified by the small peak separation is also observed at the EPPG electrode as compared to the GC and BDD electrodes. Additionally, the magnitude of the reduction and oxidation current ($|I_p^{red}/ I_p^{ox}|$) give a peak ratio of 0.8 and 1 for the GC and EPPG electrodes respectively. This indicates a reversible or quasi-reversible process at the EPPG and quasi-reversible process at the GC electrode.

The superior electrochemical performance of the EPPG electrode is attributed to the presence of the edge plane sites in its microstructure. These sites are highly reactive, have an excellent electronic conductivity leading to high electroactive area for this electrode.

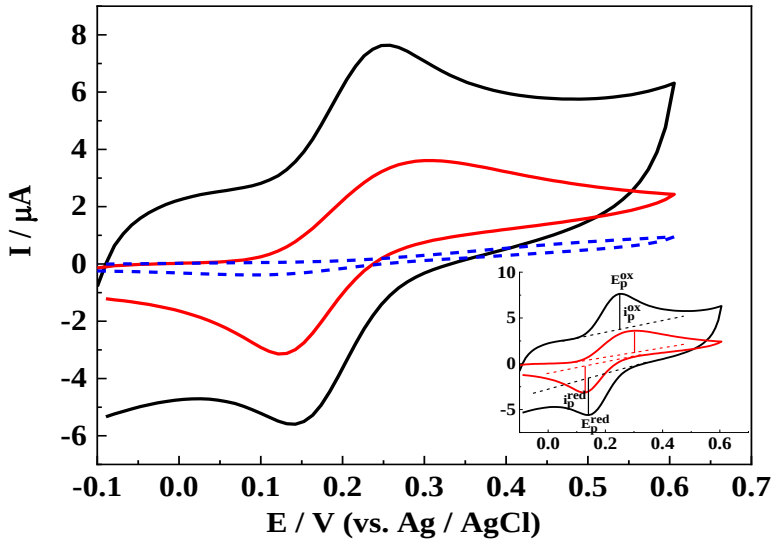

Figure 3.1: CVs of 0.5 mM TBP in 50:50(v:v) EtOH:0.1M PBS(pH11) at 0.1 Vs^{-1} scan rate using: (black solid line) EPPG; (red solid line) GC and (blue dashed line) BDD electrodes.

3.3.1.1 pH Dependence

The cyclic voltammetry of TBP at EPPG and GC electrodes was carried out at different pHs to gain more insight into the electron transfer process occurring.

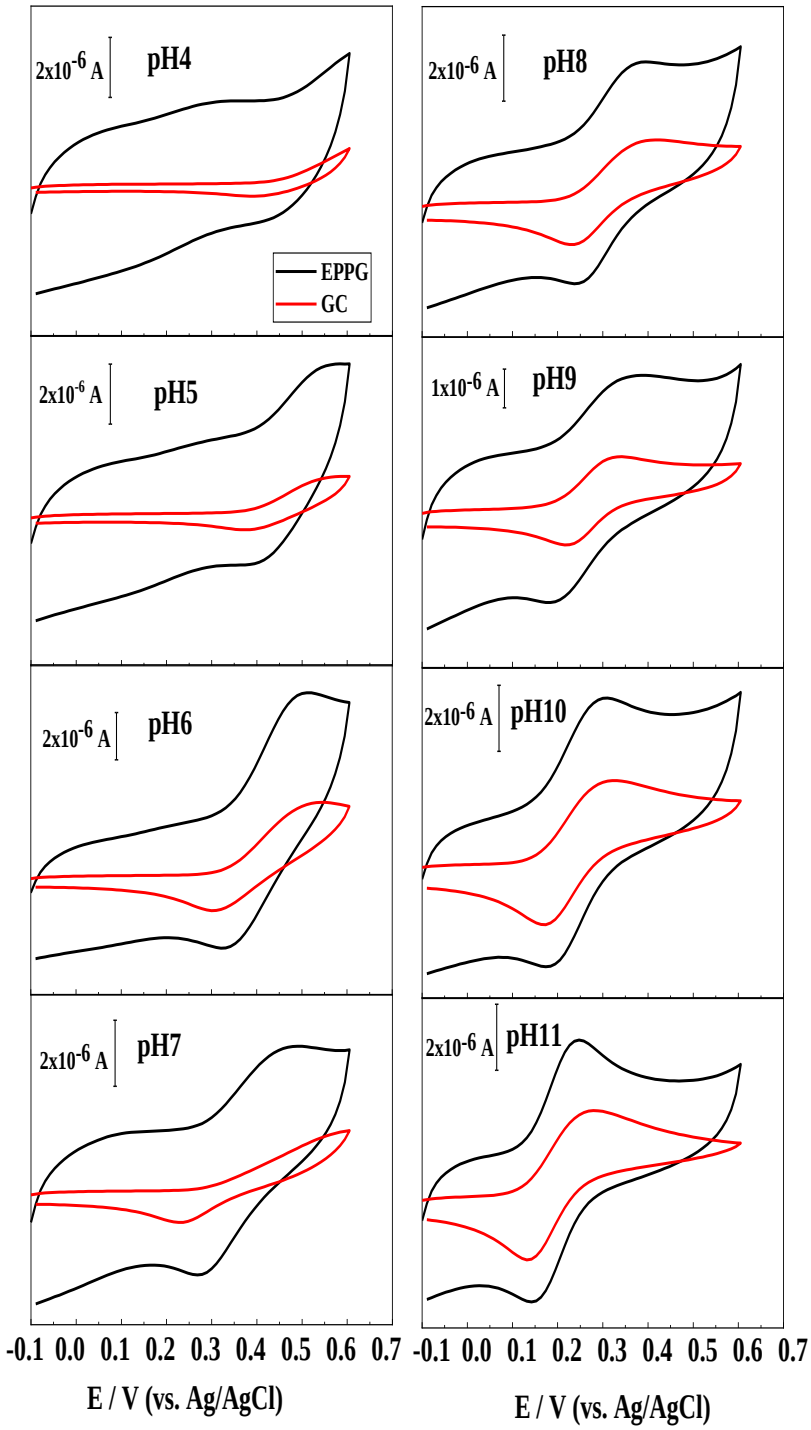

Figure 3.2: Cyclic Voltammograms of 0.5 mM TBP in 50:50(v:v) EtOH:0.1M PBS at different pHs 4 − 11 at EPPG (black) and at GC (red). The potential was scanned from -0.1 → 0.7 V vs. Ag/AgCl. ν = 200 mVs^{-1}.

Figure 3.2 shows the forward and backward sweep of the first scans for the oxidation of TBP at different pH values ranging from 4 to 11. It can be seen that the oxidation potential decreases with an increase in pH at both electrodes as predicted by the Nernst equation. At pH 5, E_p^{ox} = 0.58 V vs. Ag/AgCl, which decreases to E_p^{ox} = 0.23 V at pH 11. This relationship is shown in the plot of peak potential against pH for both electrodes in Figure 3.3. In Figure 3.3 A, it can be seen that, E_p^{ox} (A) = 0.7961− 0.0505 pH (R^2 = 0.9822). The gradient of the slope was 51 ± 2 mV per pH which is consistent with a linear Nernstian response corresponding to a one electron transfer process where theoretically at 298 K a slope of 59 mV is predicted. At the GC electrode the equation: E_p^{ox} (B) = 0.8321− 0.0526 pH (R^2 = 0.9662) is obtained (Figure 3.3B) with the gradient of the slope equal to approximatively 53 ± 4 mV per pH unit which is also consistent with a one electron / one proton transfer process. However, the value of the slopes obtained for both electrodes is smaller than the theoretically expected value and this is indicative of a possible adsorption effect at both electrodes.

The relationship between the peak potential and pH can be illustrated using the Nernst equation (3.1) and reaction (3.1).

$$Ph{-}OH \rightarrow Ph{-}O^{\bullet} + H^+ + e^- \qquad (3.1)$$

$$E = E^o - \frac{RT}{F}\ln\frac{[Ph{-}O^{\bullet}]\,[H^+]}{[Ph{-}OH]} \qquad (3.1)$$

$$E = E^o - \frac{RT}{F}\ln\frac{[Ph{-}O^{\bullet}]}{[Ph{-}OH]} + \frac{RT}{F}\ln[H^+]$$

By assuming that the term $E^o - \frac{RT}{F}\ln\frac{[Ph{-}O^{\bullet}]}{[Ph{-}OH]}$ is constant and equal to $E^{o\prime}$

Therefore,

$$E = E^{o\prime} + \frac{RT}{F}\ln[H^+] = E^{o\prime} + 2.3\frac{RT}{F}\log[H^+] \qquad \text{(with ln = 2.3log)}$$

$$E = E^{o\prime} - 2.3\frac{RT}{F}pH$$

The peak potential should shift $-2.3\frac{RT}{F}$ which is equal to 59 mV per increase in pH unit at 298K if one proton is transferred per electron transferred.

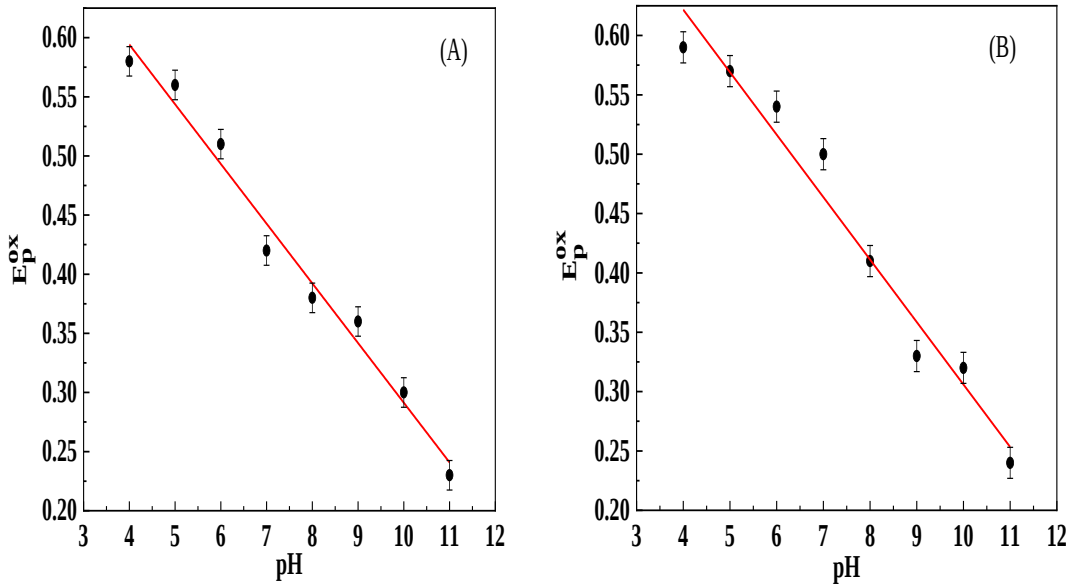

Figure 3.3: pH dependence of 0.5 mM TBP in 50:50(v:v) EtOH:0.1M PBS at pH values varying from 4 to 11 at: (A) EPPG and (B) GC electrodes.

Based on the results obtained, an oxidation mechanism is proposed for the TBP (scheme 3.1)**.** A one quasi- reversible electron transfer occurs between the TBP and the electrode to produce 2,4,6-tri-tert-butylphenoxy radical. This one electron reaction corresponds to the anodic and cathodic peaks in the cyclic voltammetry (Fig 3.1).

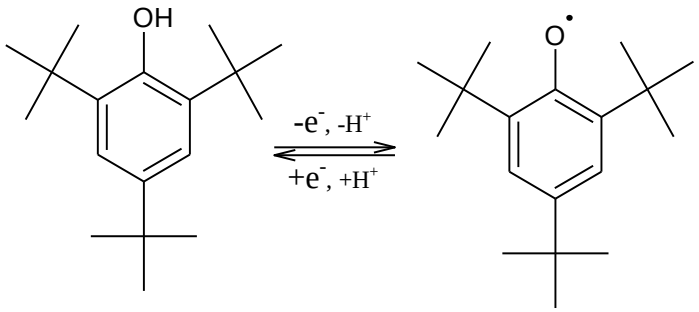

Scheme 3.1: TBP electrochemical oxidation mechanism at EPPG electrode

3.3.1.2 Effect of Scan Rates

Figure 3.4 shows the scan rate dependence of the oxidation peak current of TBP at both EPPG and GC electrodes. It can be seen that the oxidation current shows a linear relationship with the square root of scan rate at the GC electrode (Figure 3.4 B). This implies that the redox process is diffusion controlled at the GC electrode. In contrast, the oxidation current increases with the increasing scan rate at the EPPG electrode but it is

not directly proportional to square root of scan rate (Figure 3.4 A). This suggests that the process at the EPPG electrode is not controlled by diffusion alone, but by a mixture of diffusion and adsorption processes.

This relationship between the current and the square root of scan rate for a diffusion-controlled reaction is described by the Randles-Sevick equation:

$$i_p = (2.69 \times 10^5)\, n^{3/2}\, A\, D^{1/2}\, C\, \nu^{1/2} \qquad (3.2)$$

where i_p is the current maximum (in amps); n is the number of moles of electrons transferred in the reaction; A is the area of the electrode (in cm^2); D is the diffusion coefficient (cm^2 / s); C is the electrolyte concentration (in moles cm^{-3}) and ν is the scan rates of the applied potential (in Vs^{-1}). Thus, the diffusion coefficient for TBP at 298 K can be calculated from the slope of the plot i_p versus $\nu^{1/2}$ which is equal to $i_p / \nu^{1/2}$ from the equation.

Slope = $i_p / \nu^{1/2} = (2.69 \times 10^5)\, n^{3/2}\, A\, C\, D^{1/2}$, where n = 1 and A = 0.07 cm^2

A value of D = 2.291321×10^{-6} cm^2 s^{-1} and 1.625750×10^{-6} cm^2 s^{-1} were obtained for the EPPG and GC electrodes respectively after calculation. These values are consistent with the diffusion coefficient obtained for molecules of the size of TBP in aqueous solutions (i.e. D for ferrocene in aqueous ethanol is 9.78 $x10^{-6}$ $cm^2.s^{-1}$[5]).

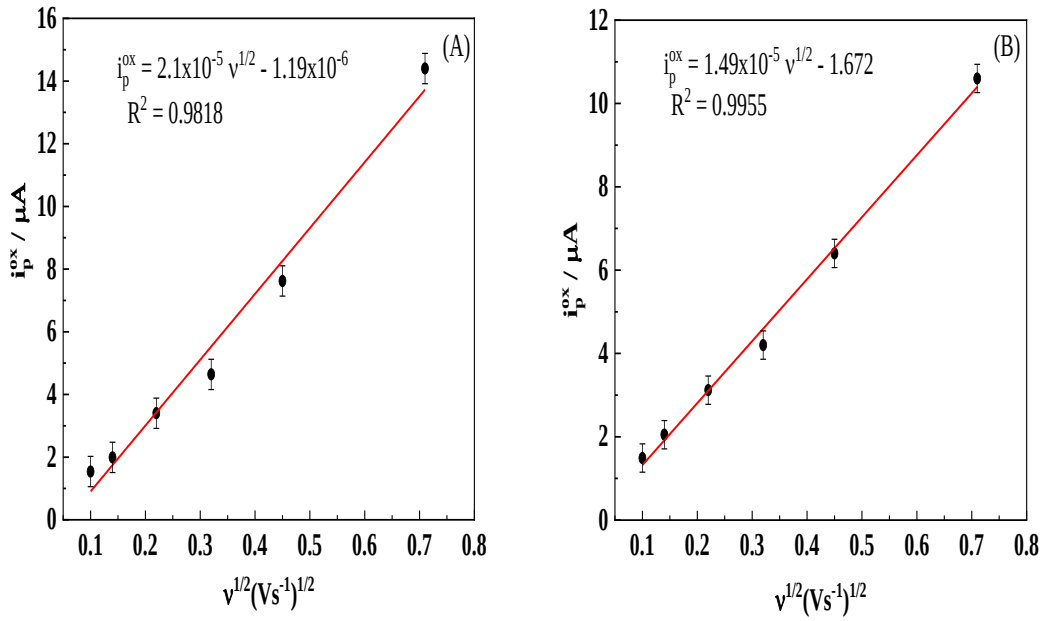

Figure 3.4: Scan rate dependence of 0.5 mM TBP in 50:50(v:v) EtOH:0.1M PBS(pH11) at: (A) EPPG and (B) GC electrodes.

The difference in electrochemical response observed between the different electrode materials could be explained by the difference in their surface microstructures. While glassy carbon comprises of highly random and disordered twisted ribbons of graphitic planes creating a tight mixture of sp^2 and sp^3 carbons domains, the surface of the EPPG electrode consists of a layer of graphite which lies perpendicularly to the surface and with interlayer spacing of 3.5 Å [6], [7] . These edge sites are highly reactive and allow strong adsorption tendency and chemical modifications. The enhanced electron-transfer kinetics observed at the EGGP are attributed to the presence of the edge sites.

These results in general show that the electrochemical oxidation of TBP involves a one electron per proton transfer, leading to the formation of 2,4,6-tri-tert-butylphenoxy radical. Additionally, EPPG electrode appears as the more suitable material for our analysis because of its high sensitivity, excellent electronic conductivity and good detection limit. However, there is a problem with adsorption due the presence of the edge sites in its microstructure as mentioned in section 3.3.1. Although EPPG is used in further studies the effect of adsorption must be considered during analysis.

3.3.2 Cyclic Voltammetry of Phenol

Figure 3.5 shows the electrochemical response of 0.5 mM phenol in 50:50(v:v) 0.1 M potassium phosphate buffer (pH11) and ethanol at a scan rate of 0.2 Vs^{-1} at the EPPG electrode. It is observed that phenol starts to undergo irreversible oxidation at 0.45 V, rising to two distinct peaks centred at 0.57 V (peak I) and 0.67 V (peak II) on the first scan. A reduction peak at about 0.14 V (peak IV) is also observed on the reverse scan and on the second scan a corresponding oxidation peak is seen at 0.22 V (peak III). The peak separation of this couple $|E_{p(III)} - E_{p(IV)}|$ is 80 mV and this shows a reversible redox reaction occurring. The second oxidation peak (II) observed at 0.67 V may suggest that, some of the products formed at peak (I) rapidly undergo further oxidation. A significant decrease in the oxidation peak current associated with peaks (I) and (II) is observed on the second and subsequent cycles. This might be due to the blocking of the electrode surface by the oxidation products formed through polymerization. These polymeric products tend to stick at the surface of the electrode as a film, therefore preventing the diffusion of further phenoxide ions to the electrode surface for oxidation, thereby

resulting in significant decrease in the oxidation peak current during the 2nd and subsequent cycles [1]. This is discussed further in section 3.3.2.3.

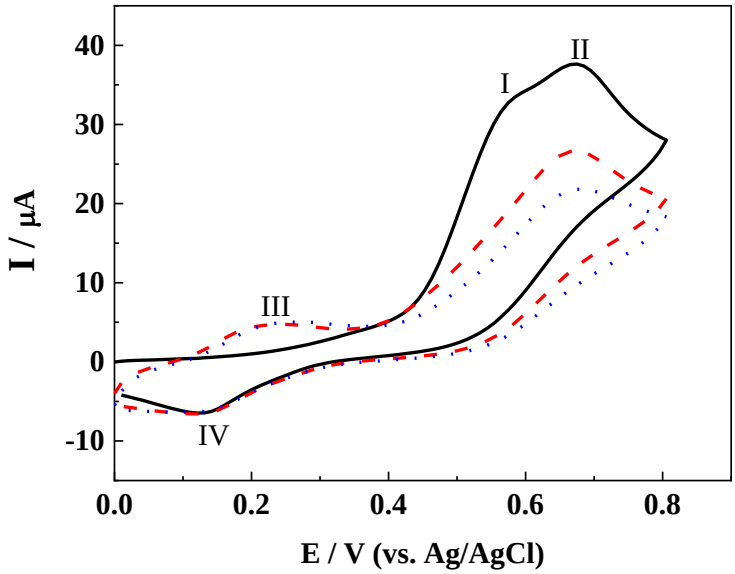

Figure 3.5: Cyclic voltammogram for the electro-oxidation of 0.5 mM phenol in 50:50 (v:v) 0.1 M potassium phosphate buffer of pH11 and Ethanol at EPPG electrode at a scan rate of 0.2 Vs^{-1}: (black) 1st scan, (red) 2nd scan and (blue) 3nd scan.

Under the reaction conditions used here, the reactant is phenoxide species as the pH of the solution is above the pKa value of phenol (pKa = 10). This can be verified by applying the Henderson – Hasselbach equation:

$$pH = pK_a + log\ \frac{[A^-]}{[HA]} \tag{3.3}$$

where [HA] and $[A^-]$ are the concentrations of the undissociated acid and the acid's base conjugate respectively. Using this equation, a value of 10 was obtained for ($[A^-]$ / [HA]) and this mean than the concentration of the deprotonated phenol is 10 times bigger than the initial phenol at pH = 11.

To further analyse the results obtained, the charge associated with the area under the reduction peak (IV) (Q_{red}) on the first reduction scan was calculated and divided by the charge associated with the area under the oxidation peaks (I) and (II) (Q_{ox}), and the result obtained was then multiplied by 100 to give the percentage of phenol converted into the

species that undergoes reversible reduction at (IV). After calculation, a value of ca.10% was obtained and this means that only a tenth of the phenol is converted into these species. The rate of formation of the species that undergo reversible reduction at (IV) depends on the experimental conditions, as will be explored below (concentration, the nature of the electrode, the pH, solvent, electrode potential and current density).

3.3.2.1 Influence of pH on the Cyclic Voltammetry Response of Phenol

The CV response of 0.5 mM phenol in 50:50 (v:v) PBS:Ethanol in different pH solutions varying from 6 to 11 at EPPG electrode is presented in Figure 3.6. These results show a shift in the oxidation peak potential from 0.77 V to 0.58 V as the pH increases from 6 to 11. A decrease of the peak current from pH6 (20.77 µA) to pH9 (13.17 µA) is observed, but this peak current increases up to 33.55 µA at pH11.

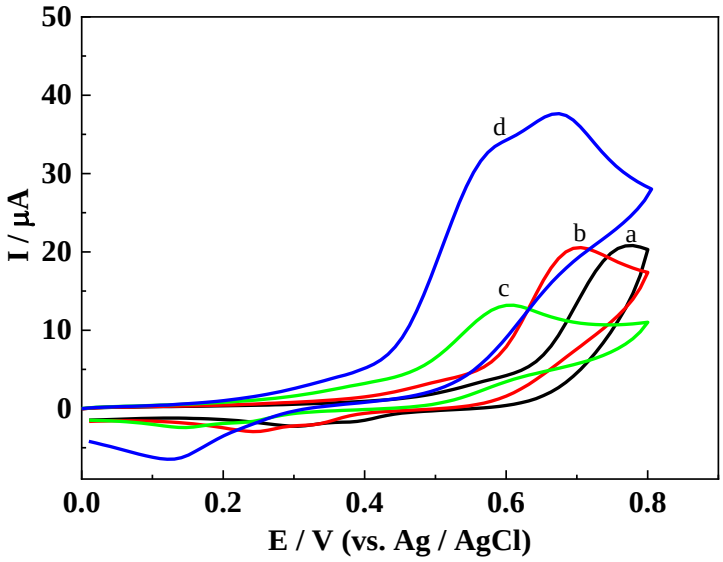

Figure 3.6: Cyclic Voltammogram of 0.5 mM phenol in 50:50(v:v) EtOH:0.1M PBS solution with varying pHs: (a) pH6; (b) pH7; (c) pH9 and (d) pH11 at EPPG electrode and scan rates of 0.2 Vs^{-1}.

A plot of the oxidation peaks potential against pH (Fig 3.7) reveals a linear response in the pH 6.0 – 9.0 range (pH dependence) with a slope of 56 ± 4 mV per pH unit which is close to the theoretically predicted and calculated value of 59 mV for a one electron transferred per proton transferred process. Above pH9 the oxidation peak potential is observed to be independent of the pH. As the pKa of phenol is approximatively equal to 10, it is likely to be present in majority as the phenolate anion in the pH range above pH9

and the oxidation process is likely to be associated with the loss of electron from the phenolate anion to produce the phenoxy radical as shown in equation (3.4):

$$Ph{-}O^{-} \rightarrow Ph{-}O^{\bullet} + e^{-} \qquad (3.4)$$

The initial oxidation of the unsubstituted phenol at pH below 9 is pH dependent and it is associated with a loss of proton from the initial phenol, while at pH above 9 the initial oxidation involves the loss a proton from the phenolate anion to produce the radical. This is in contrast with what was observed with the TBP at pH9 where the initial oxidation is associated with a reversible loss of electron from its protonated molecule to produce the phenoxy radical, as the pKa of TBP is 12 which is higher than the pH values used in the study.

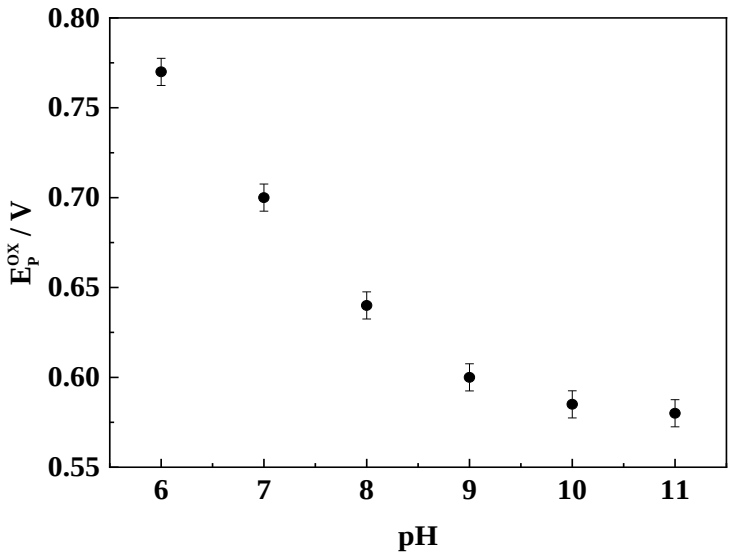

Figure 3.7: Plot of the oxidation peak potential at pH values varying from 6 to 11.

The ratio of the charge associated with the area under the reduction peak (IV) (Q_{red}) and the charge associated with the area under the oxidation peaks (I) and (II) (Q_{ox}) was evaluated and plotted against pH (Figure 3.8). It can be observed that the percentage of phenol which is converted into species associated with the reversible reduction process at peak (IV) increases from ca.13 % to ca.15 % between pH6 and pH7 before decreasing as the pH increases to reach a value of ca.10 % at pH11.This suggest that different oxidation mechanisms proceed at different pH.

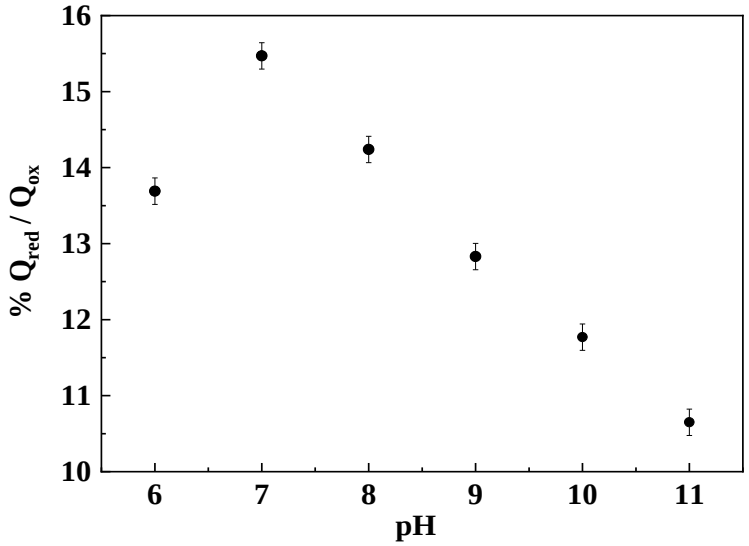

Figure 3.8: Plot of the ratio of the charge associated with the area under the reduction peak (IV) (Q_{red}) and the charge associated with the area under the oxidation peaks (Q_{ox}) of 0.5 mM phenol at different pHs and at scan rate of 0.2 Vs^{-1}.

3.3.2.2 Effect of Scan Rates

The scan rate dependence of phenol oxidative and reductive peaks current at the EPPG electrode was investigated and the results obtained are shown in Figure 3.9. It can be seen that both the oxidative and reductive peaks current against the square root of the scan rate shows a linear dependence. This linear relationship is indicative of a diffusion controlled redox process. This is different to what was observed with the TBP where a non-linear response was obtained and this difference might be due to the adsorption effect which is less for the unsubstituted phenol compared to TBP due the absence of the tert-butyl groups. This makes the interpretation of the phenol results easier as the adsorption effect does not need to be taken into account.

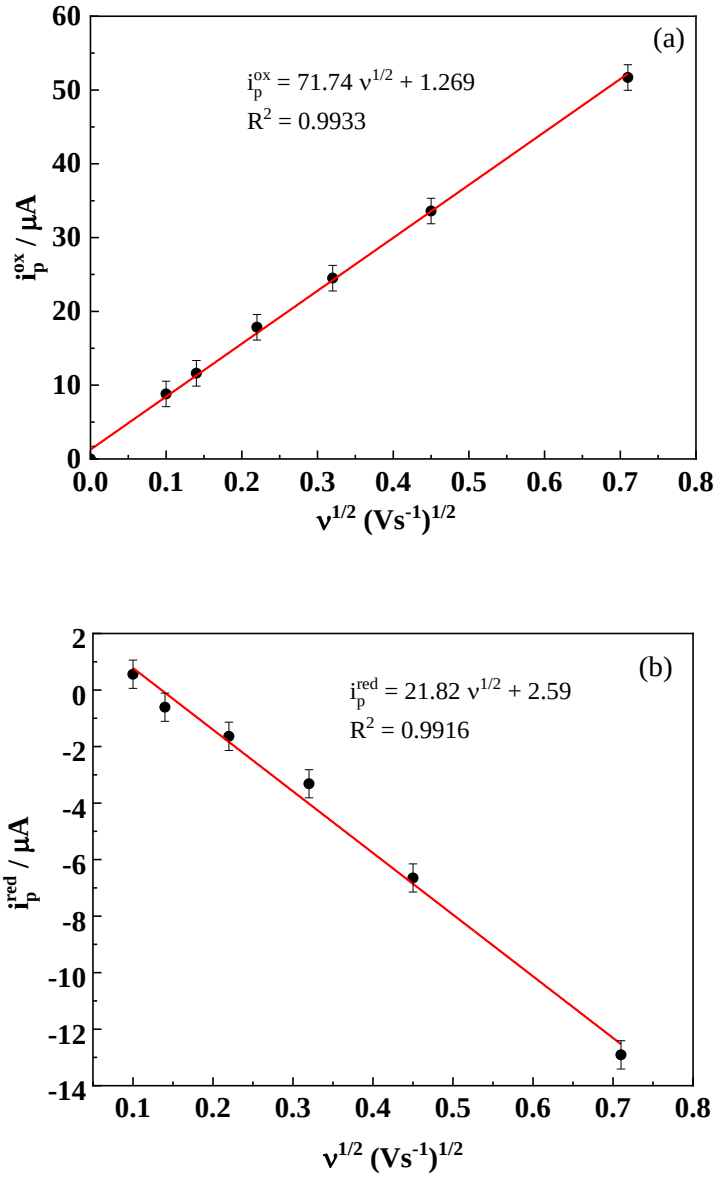

Figure 3.9: Linear dependence of: (a) oxidative and (b) reductive peak current with square root of scan rates for 0.5 mM phenol in 50:50(v:v) 0.1 M potassium phosphate buffer at pH11 and ethanol at EPPG electrode.

3.3.2.3 Effect of Concentration

The influence of phenol concentration on the CV response at pH11 was also examined and the results obtained are presented in Figure 3.10 below. These results show that the peak current increases with the increase in phenol concentration, but this relationship is hindered in the concentration ranging from 0.5 to 1 mM where a decreasing current is observed. This result is unexpected but reproducible and this will be discussed further.

A very little increase of the current is observed as the concentration is increased above 5 mM. This little increase of the current at higher concentration may be related to a decrease in the activity of the electrode probably due to the formation of larger amount of phenoxy radicals produced during oxidation. These radicals are known to be involved in electro-polymerization processes, resulting in the blockage of the electrode active surface at higher concentration.

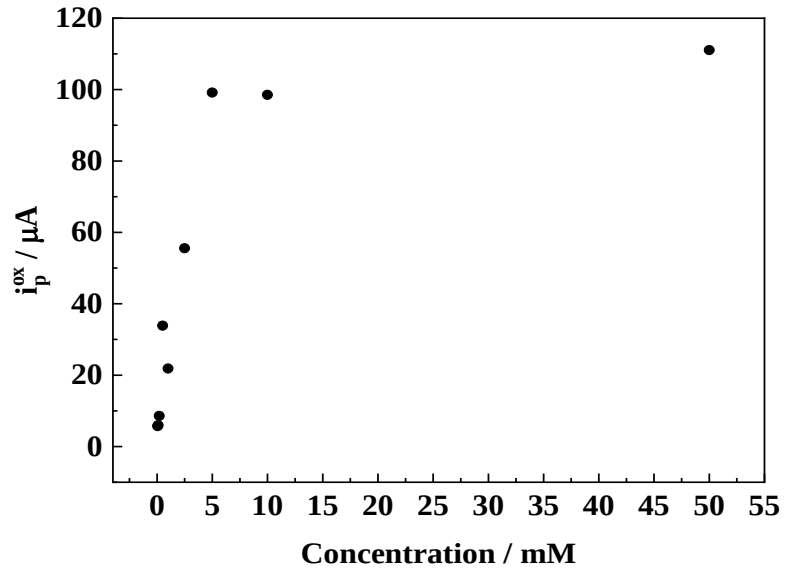

Figure 3.10: Plot showing concentration dependence of phenol in 50:50(v:v) EtOH:PBS (pH11) at EPPG electrode.

The ratio % Q_{red} / Q_{ox} at different phenol concentration is plotted and the results are shown in Figure 3.11. It can be observed that the ratio decreases initially from ca.4.6 % to ca.3.7 % between 0.05 mM to 0.2 mM. A big increase is then seen at 0.5 mM (ca.10.6 %), before decreasing with the increasing concentration to reach a value of ca. 6.5 %. An unexpected result is observed in the concentration ranging from 1 to 2.5 mM where a little increase of the ratio is observed. This will be discussed further later.

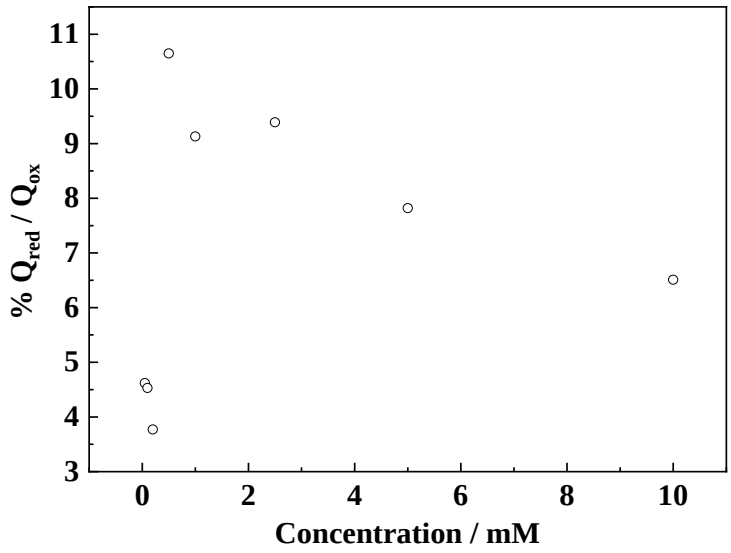

Figure 3.11: Plot of ratio % (Q_{red} / Q_{ox}) of phenol at different concentration at pH11 and scan rate of 0.2 Vs^{-1}.

3.3.2.4 Proposed Electrochemical Oxidation Mechanism of Phenol at EPPG Electrode

In order to propose a reaction mechanism for phenol, an attempt was made to evaluate the number of electrons which might be involved in the oxidation process. This was performed by comparing the oxidation current of phenol with the oxidation current of TBP and by using the Randles Sevick equation as shown in section 3.3.1.2 which describes the relationship between peak current and the number of electrons transferred (i is proportional to $n^{3/2}$). After calculation, the peak current of phenol was found to be 4.38 times larger than the peak current of TBP and by assuming that the diffusion coefficient calculated above for TBP is also the same for phenol, a 2 or 3-electrons oxidation should give a current 2.8 or 5.2 times larger respectively. This suggests that the number of electrons transferred for phenol oxidation can be estimated to be between 2 and 3 electrons per phenol molecule.

As discussed above, at pH11 the dominant solution species is the phenolate. First, a one electron transfer occurs between the phenolate and the electrode to produce phenoxy radical (I) alongside radicals (II), (III) and (IV) due to the delocalisation of the electron in the ring (scheme 3.2). This reaction might be assigned to the first oxidation peak (I)

observed in the CV response (Figure 3.5). Further oxidation of the phenoxy radical (I) to give phenoxy cations (V) and (IV) can occur under very acid condition (pH < 4). As discussed in the introduction in acidic conditions a coupled H^+ and e^- transfer means $2e^-$ route to phenoxy cations is energetically viable [8]. However, this is assumed not to happen under the experimental conditions used in this study (pH > 4) as equation (3) requires much higher potentials than applied in this study.

$$PhO^{\bullet} \rightarrow PhO^{+} + e^{-} \qquad (3.5)$$

The next step involves the coupling of the different radicals (I to IV) formed to produce firstly dimers (1) through O−O coupling which terminates the reaction. In addition, dimers (2) and (3) can be formed and can undergo further two electrons transfer to yield the dipheno-quinone molecules (XI) and (XII) respectively. This is due to the fact that dimers (3) and (4) can be easily oxidised at same potential as the original phenolate. The pathways (C_1 and D_1) lead to the formation of the mono and dipheno-quinones molecules (XI and XII) and hence the reduction peak (IV) (Fig 3.5) is assigned to the reduction of the quinoid molecules on the reverse scan. An alternative pathway is the coupling reaction of two molecules of the phenoxy radical (I) through ether C−O−C linkage via the phenoxy group to form the compound (VII). This is followed by a further one electron transfer oxidation process at the same potential leading to formation of molecule (VIII) and then the polymerised product (IX) as shown in pathway (A_1). Such products are responsible for the fouling of the electrode surface through passivation [9]. This passivation is responsible for the decreasing current on the second and subsequent scan on the CV response.

Taking the reactions altogether it is clear to see how the number of electrons transferred per phenol molecule during oxidation is > 1. The exact number of electrons will depend on the relative rates of reactions A_1, B_1, C_1 and D_1.

The rate of formation of the quinoid compounds calculated from the Q_{red} / Q_{ox} ratio under different pH and concentrations above shows that more quinone species are formed under lower pH, lower concentrations, while lower rate of formation is observed under higher pHs and higher concentration. These suggest that under condition where more quinone is obtained, the oxidation reaction tends to follow more pathways C_1 and D_1 that lead to the quinoid compounds formation than the pathways which result in the oxidation

products IX and dimer 1. Inversely the oxidation reaction follows more pathways A_1 and B_1, which give the polymeric product (IX) and dimer 1 respectively under condition where lower rate is observed (at higher pHs and higher concentration). A further explanation is that the oxidation reaction is more likely to go via 2e- / $2H^+$ route that leads to the formation of cation (V) and (VI) at pH values below 9 and via routes C_1 and D_1 (quinoid formation) but with stronger competition of polymerisation (route A_1) at pH values above 9. Furthermore, less dimerization or polymerisation is observed near the electrode by any route (A_1, B_1, C_1 and D_1) at lower concentration, and this is because less phenoxy radicals are produced or they diffused away from the electrode before reacting. At intermediate concentration (~1mM) little polymerisation is obtained as the concentration is still quite low for dimerization to take place. This might explain the unexpected results observed in the 1− 2.5 mM concentration range in Figure 3.11. At high concentration, the polymer formation blocks the response from the quinones on the reverse scan.

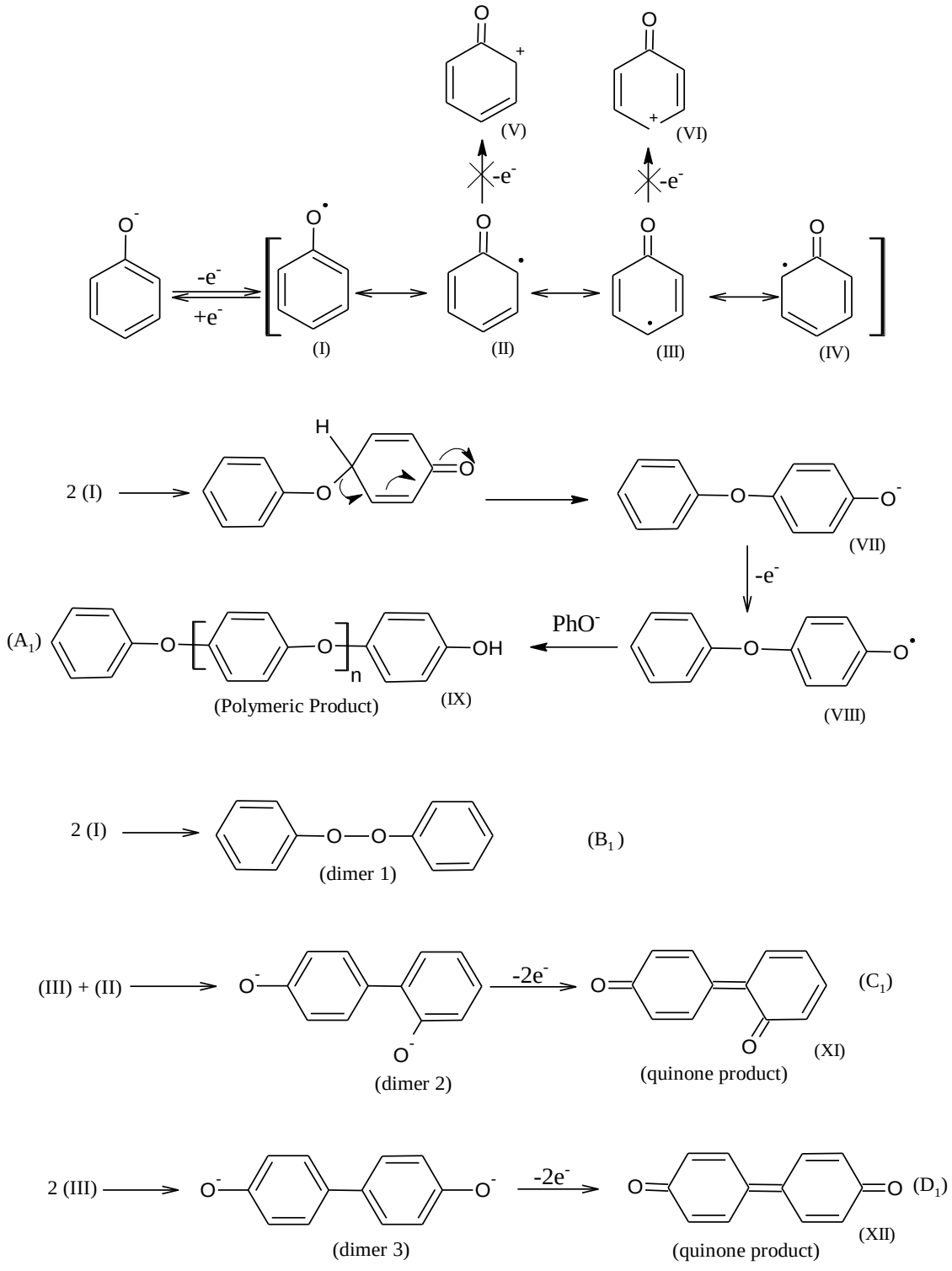

Scheme 3.2 Proposed phenol electrochemical oxidation mechanism at EPPG electrode.

3.3.3 Comparative Study between Phenols, o, m, p-Cresols and TBP

Figure 3.12 shows the electrochemical response of o-cresol, m-cresol and p-cresols obtained under the same conditions (pH11) as the unsubstituted phenol and TBP.

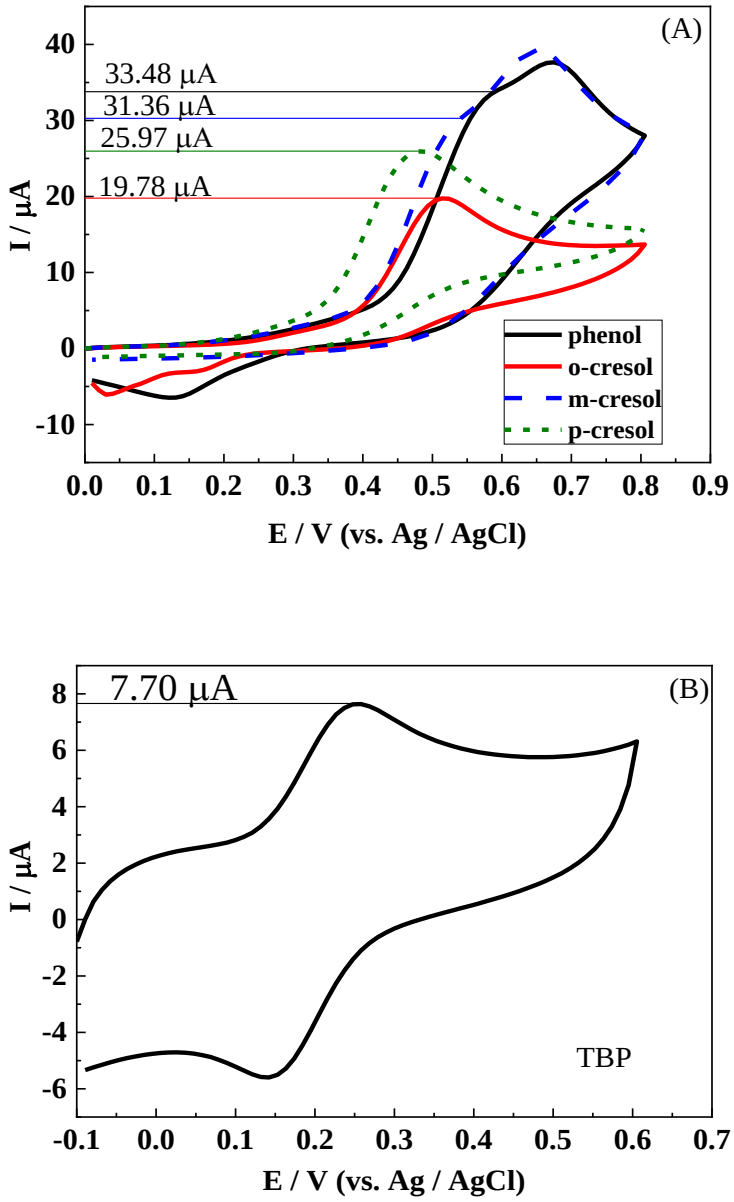

Figure 3.12: Electrochemical response of 0.5 mM: (A) (black) phenol, (red) o-cresol, (blue) m-cresol and (olive) p-cresol. (B) TBP in 50:50(v:v) EtOH:PBS(pH11) at EPPG electrode and at a scan rate of 0.2 Vs^{-1}.

Two oxidation peaks are observed in the forward scan for meta-cresol similarly to the unsubstituted phenol at ca. 0.54 V and ca.0.65 V, but no reverse peak is observed on the backward scan. Para-cresol shows an oxidation response at ca.0.55 V but no reduction

peak is observed on the backward scan. Ortho-cresol displays an oxidation peak at ca.0.52 V and two reduction peaks at ca.0.16 V and ca.0.035 V. Furthermore, a higher peak current is observed for the oxidation of the unsubstituted phenol and meta-cresol compared to para-cresol and o-cresol respectively.

Similarly, as described in section 3.3.2.4 the number of electrons which might be involved in the oxidation reaction of ortho, meta and para-cresols was evaluated in order to propose a reaction mechanism. After evaluation, the peak current of o-cresol, m-cresol and p-cresols were found to be 2.56, 4.07 and 3.37 times larger than the peak current of TBP respectively, therefore, the number of electrons transferred during oxidation is estimated between 1 and 2 electrons for ortho-cresol and between 2 and 3 electrons for meta- and para-cresols. This suggest that different reaction mechanisms take place depending on the substitution position of the methyl group on the phenyl ring.

Proposed Reaction for Substituted Phenols

Similarly to the unsubstituted phenol, meta-cresol undergoes a one electron transfer to produce the phenoxy radical (2) (scheme 3.3). This radical may be delocalised around the aromatic ring leading to the formation of radical in ortho (3) and para-position (4). It is assumed that a second electron transfer leading to the formation of the phenoxy cation does not take place due to the reasons mentioned in section 3.3.2.4. The reaction leading to the formation of the phenoxy radical (2) can be assigned to the oxidation peak observed at ca.0.54 V on the CV response (cf blue CV) in Fig 3.13. The generated phenoxy radical (2) then reacts with other radicals or other molecules of the initial para-cresol (1) to form a polymeric product (pathway A_2). Such reactions are responsible for the fouling of the electrode through passivation. An alternative reaction pathway is the coupling reaction of the intermediate radicals (2), (3) and (4) to give dimer (5) through O–O coupling which terminates the reaction. There is also possibility of formation of dimers (5) and (6) based on radical coupling reaction, however, these two dimers even if they are formed, are likely to be present at low concentration due to the fact that the molecules will be too sterically crowded because of the position of the methyl group, hence unlike the unsubstituted phenol no quinoid species are formed during oxidation of m-cresol. This explains for m-cresol the absence of the reduction peak (IV) previously assigned to quinone reduction on the reverse scan for phenol. The radical coupling reaction which

leads to the formation of dimers (5) and (6) is therefore likely to be slower than the polymerization reaction and the reactions leading to the formation of dimer (4).

The fact that the peak current for m-cresol is comparable to that for unsubstituted phenol, suggests that for both species oxidation primarily proceeds via process A, the formation of the polymer.

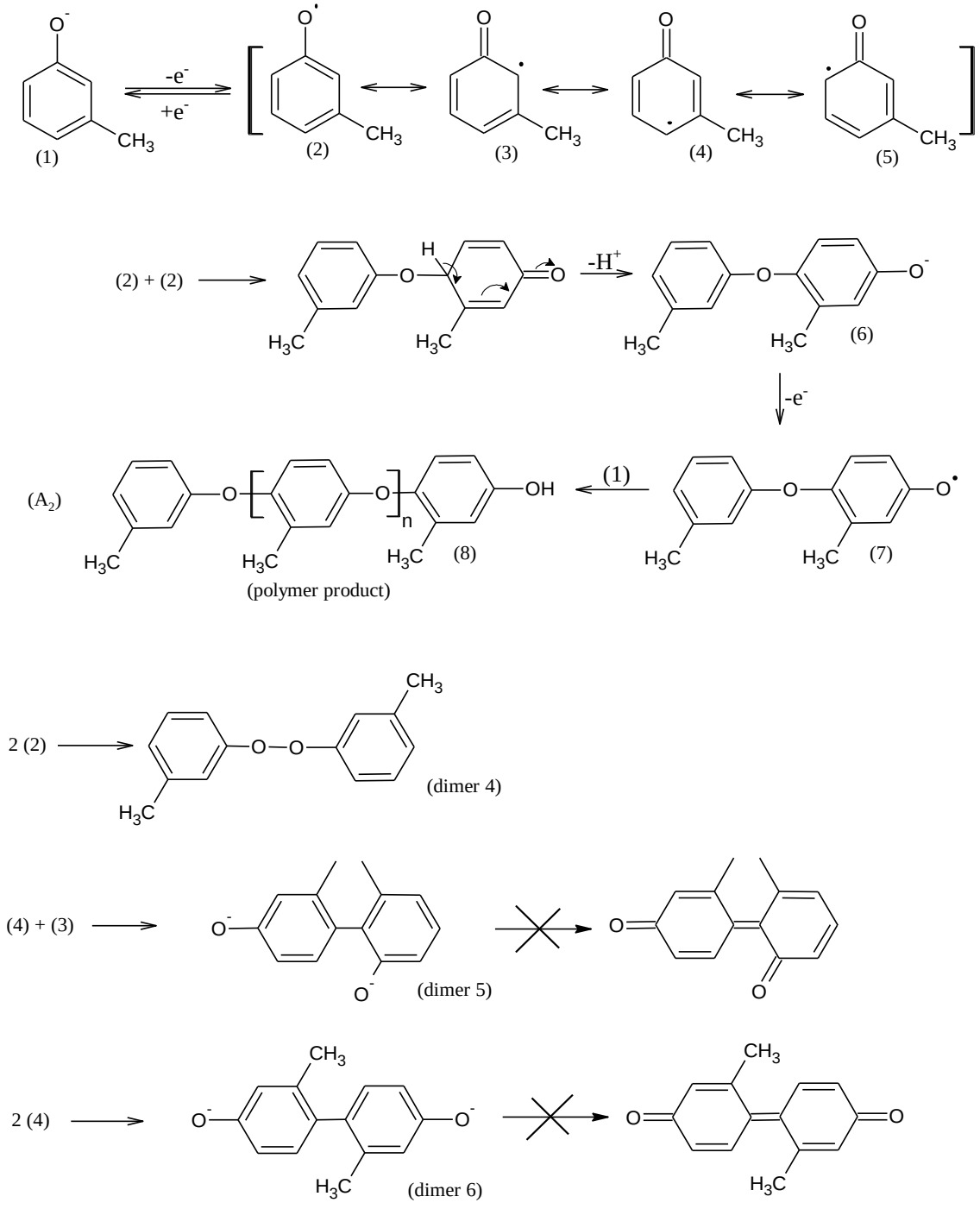

Scheme 3.3 Proposed oxidation mechanism for meta-cresol at EPPG electrode.

In scheme 3.4 is shown the proposed electrochemical oxidation mechanism of o-cresol at EPPE electrode. The oxidation results in either the formation of polymeric compound through C−O−C coupling of radicals (ii) following pathways (A_3) or dimer (7) through O−O linkage, which terminates the reaction. There is also the possibility of formation of dimers (8) and (9) which lead to the formation of the quinone products (ix) and (x) respectively as shown in pathways (C_3) and (D_3). As mentioned in the oxidation mechanism of phenol, the formation of these quinone compounds is due to the fact that the corresponding dimers (dimers (8) and (9)) are easily oxidized at the same potential as the initial phenolate (1).The first oxidation peak observed at ca.0.52 V on the CV data can be assigned to the oxidation of the phenolate molecule which leads to the formation of radical (ii) as well as contributions from further oxidation of dimer 8 and 9. In addition the generation of the polymer product via route A_3 will also contribute to the oxidation charge passed. The much smaller oxidation current for o-cresol compared to unsubstituted phenol and m-cresol suggests less charge is passed in the A_3 pathways, which is consistent with steric crowding resulting in slower polymer growth. The reduction peaks obtained on the reverse scan at ca.0.16 V and ca.0.035 V can be assigned to the reduction of compounds (ix) and (x).

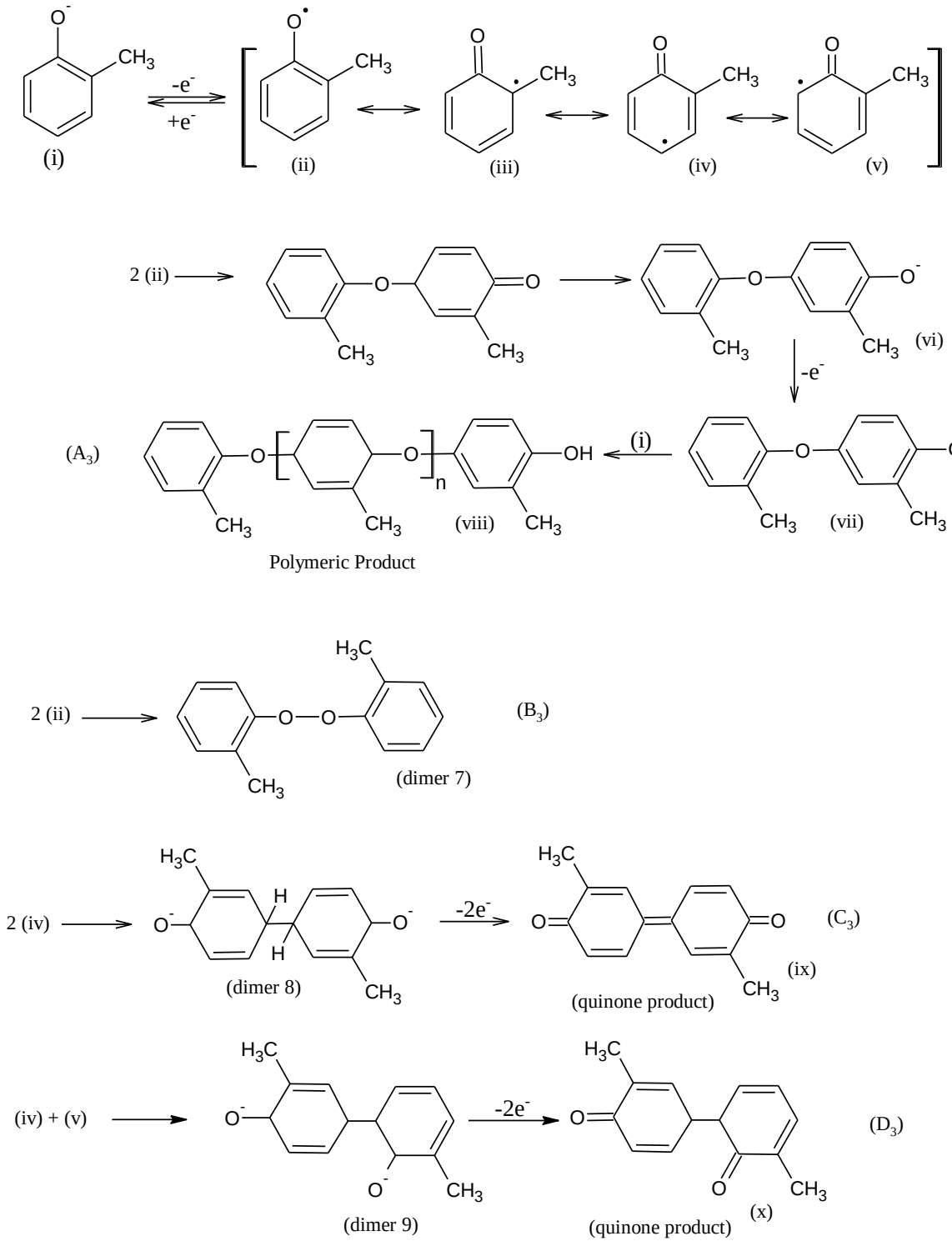

Scheme 3.4 Proposed oxidation mechanism for m-cresol at EPPG electrode

Finally, for p-cresol shown in scheme 3.5, the formation of the polymeric product through C−O−C coupling of radicals (b) is not likely due to the presence of the methyl group in the para-position. However, as seen in the previous mechanism there is possibility of O−O coupling of two radicals (b) to produce dimer (10) which terminates the reaction.

The formation of dimers (11) and (12) and their subsequent oxidation to quinoids is also less probable due to the molecule being too sterically crowded or they might be formed at low concentration and kept way from the electrode surface by dimer (10). This explains the absence of quinoid reduction peak on the reverse scan. The first oxidation peak observed at ca.0.55 V can be assigned to the oxidation of the p-cresol to produce radical (b).

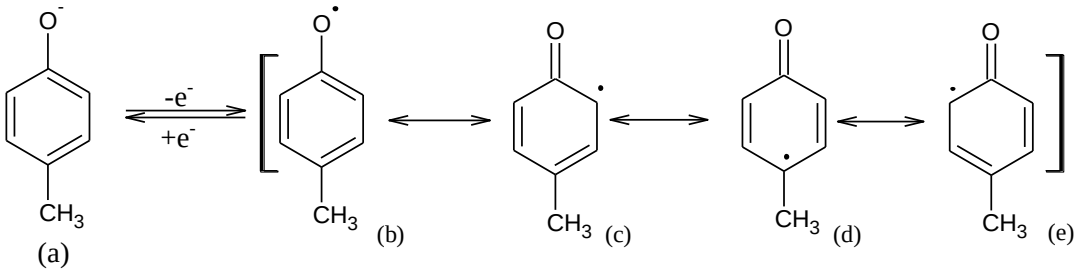

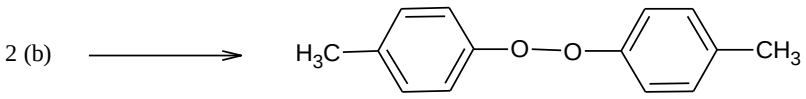

(dimer 10)

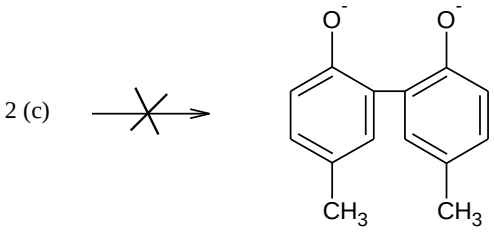

(dimer 11)

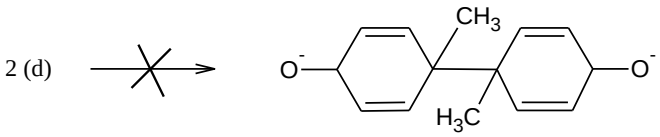

(dimer 12)

Scheme 3.5 Proposed oxidation mechanism for p-cresol at EPPG electrode

3.4 Summary and Conclusion

In this study, the electrochemical oxidation of TBP, phenol and o,m,p-cresols were monitored using cyclic voltammetry techniques. In the earlier experiments, the electrochemical oxidation of TBP at various carbon materials electrode such as GC, EPPG and BDD was studied in order to choose the suitable substrate for our investigations. The results obtained show a reversible or quasi-reversible process at the EPPG electrode and a quasi-process at the GC electrode. The electrochemical response at the BBD electrode was not taken into account as the response observed was weak and sluggish. The effect of pH and scan rate on the electrochemical response of TBP at the EPPG and GC electrodes were also investigated. This revealed that TBP undergoes a reversible one electron transferred oxidation process at both electrodes as shown in section 3.3.1.1 and that the process is diffusion controlled at the GC electrode and at the EPPG electrode a mixture of diffusion and adsorption processes is observed. These results in general show that TBP undergoes a one electron per proton transfer oxidation, leading to the formation of 2,4,6-tri-tert-butylphenoxy radical. Additionally, EPPG electrode was used for our analysis because of its high sensitivity, excellent electronic conductivity and good detection limit. However, there was a problem with adsorption due the presence of the edge sites in its microstructure as mentioned in section 3.3.1 and this was considered during analysis. Thus then an oxidation mechanism was proposed for the TBP where 2,4,6-tri-tert-butylphenoxyl was obtained as oxidation product (cf scheme 3.1).

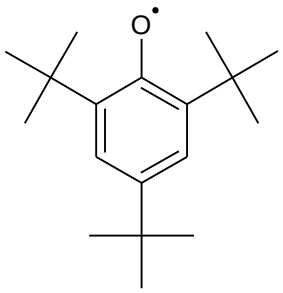

2,4,6-tri-tert-butylphenoxyl

Similarly to the TBP, the electrochemical oxidation of phenol was also investigated in order to get more insight into the oxidation mechanism (section 3.3.2) and the results obtained revealed a reversible reaction occurring in the oxidation process. The oxidation current was observed to be significantly decreasing on the second and subsequent scan and this was attributed to the fouling of the electrode due to the deposition of the

polymeric oxidation product at the surface of the electrode therefore preventing the diffusion of further phenoxy radical for oxidation. In order to find out the amount of phenol converted into species that undergoes reversible reduction at (IV), the charge associated with the area under the reduction peak (IV) (Q_{red}) on the first reduction scan was calculated and divided by the charge associated with the area under the oxidation peaks (I) and (II) (Q_{ox}). The result obtained was then multiplied by 100 to give the percentage of phenol converted into species that undergoes reversible reduction at (IV). A value of approximately 10% was obtained and this suggests that that only the tenth of the initial phenol is converted onto quinones species. The effect of pH and scan rate was also investigated in order to detect approximately the number of electron and protons that could possibly be transferred during oxidation of the unsubstituted phenol. These results show that the initial oxidation of the unsubstituted phenol at pH below 9 is pH dependent and it is associated with a loss of proton from the initial phenol, while at pH above 9 the initial oxidation involve the loss of electron from the phenolate anion to produce the radical. The study of the effect of the scan rate on the CV response shows a linear relationship between the oxidation current and the square root of the scan rate and this is indicative of a diffusion controlled redox process. This is different to what was observed with the TBP where a non-linear response was obtained and this difference might be due to the adsorption effect which is less for the unsubstituted phenol compared to TBP due the absence of the tert-butyl groups.

Based on these findings, an attempt was made to evaluate the number of electrons which might be involved in the oxidation process. This was performed by comparing the oxidation current of phenol with the oxidation current of TBP and by using the Randles Sevick equation as shown in section 3.3.1.2 which describes the relationship between peak current and the number of electrons transferred (i is proportional to $n^{3/2}$). After calculation, the peak current of phenol was found to be 4.38 times larger than the peak current of TBP and by assuming that the diffusion coefficient calculated above for TBP is also the same for phenol, a 2 or 3-electron oxidation should give a current 2.8 or 5.2 times larger respectively. This suggests that the number of electrons transferred for phenol oxidation can be estimated to be between 2 and 3 electrons per phenol molecule. Thus, then an oxidation mechanism was proposed for the unsubstituted phenol at pH11 (cf scheme 3.2) where the oxidation products were found to be:

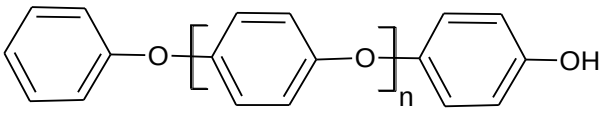

(Polymeric Product) (IX)

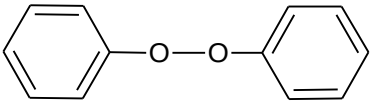

(d i m e r 1)

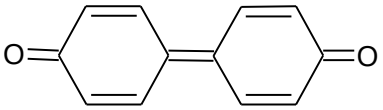

dipheno-quinone (XII)

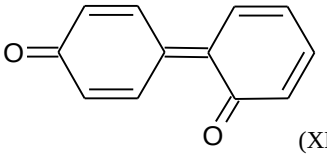

(XI)

(quinone product)

Finally, the electrochemical oxidation of substituted phenols such as ortho-, meta- and para-cresols were studied under the same experimental conditions as the unsubstituted phenol and TBP using cyclic voltammetry technique in order to propose an oxidation mechanism for each of them. While the CV response obtained for o-cresol shows a peak assigned to quinoid species reduction on the reverse scan, no such peak was observed for meta- and para-cresols. Similarly as described in section 3.3.2.4 the number of electrons, which might be involved in the oxidation reaction of ortho, meta and para-cresol, was evaluated to be approximately between 1 and 2 electrons for ortho-cresol and between 2 and 3 electrons for meta- and para-cresols. These suggest that different reaction mechanisms take place depending on the substitution position of the methyl group on the phenyl ring. A reaction mechanism was then proposed for each cresol compound where the oxidation products were found to be:

- For o-cresol:

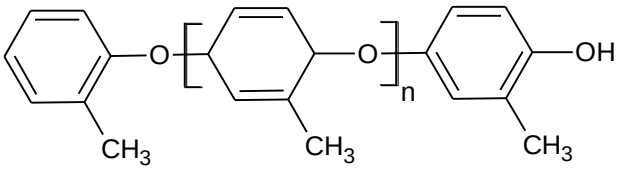

Polymeric product (viii)

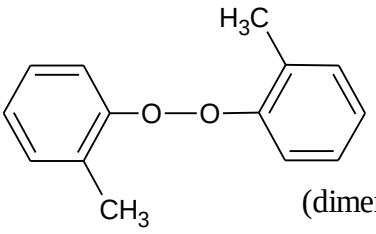

(dimer 7)

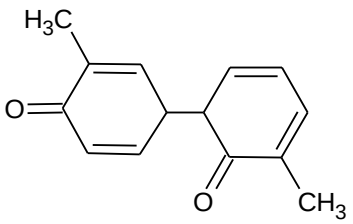

quinone (x)

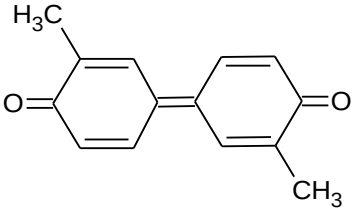

dipheno-quinone (ix)

- For m-cresol:

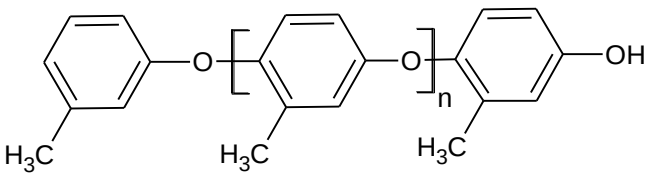

Polymeric product (8)

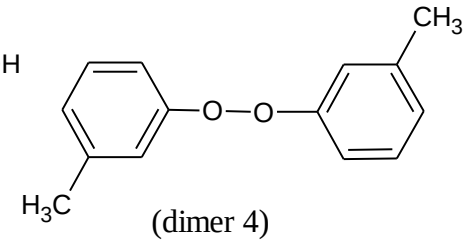

(dimer 4)

- For p-cresol:

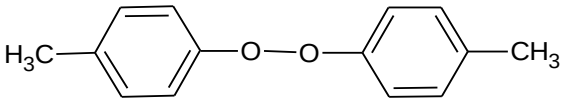

dimer 10

These oxidation mechanisms described above for all these phenolic compounds were proposed after interpretation of the results obtained. The oxidation mechanism proposed for TBP agreed well with the mechanism proposed in the literature. However, the mechanism proposed for the unsubstituted phenol shows some differences in the oxidation products with the mechanism proposed by other authors. In most published works on phenol oxidation, a four electron and protons transferred mechanism leading to monomeric quinone and polymeric product formation were reported and this was due to the experimental conditions used. In this work, pH11 was used and therefore the second route leading to the formation of phenoxy cation is not considered in here and this can explain the difference in oxidation products obtained. It is also important to note that other possible mechanism pathways that proceeds by formation of intermediate hydroperoxy compounds are also not considered here. These pathways would result from reaction with oxygen which has not been considered above. These possible mechanisms are investigated in chapter 5.

Although the oxidation mechanism proposed for each compound in this work is consistent with the results obtained under the experimental condition used here (at concentration of 0.5 mM and at pH11), further experiments needed to be carried out in order to confirm these proposed mechanisms. Therefore, a combined technique of chronoamperometry and in situ ATR-FTIR spectroscopy was design in order to confirm these oxidation mechanisms and this work is presented in the next chapter (Chapter 4).

References for Chapter 3

[1] J. Mathiyarasu, J. Joseph, K. L. N. Phani, and V. Yegnaraman, "Electrochemical Detection of Phenol in Aqueous Solutions," *Indian J. Chem. Technol.*, vol. 11, no. 6, pp. 797–803, 2004.

[2] H. Nady, M. M. El-rabiei, and G. M. A. El-hafez, "Electrochemical Oxidation Behavior of Some Hazardous Phenolic Compounds in Acidic Solution," *Egypt. J. Pet.*, vol. 10, no. 9, pp. 1–10, 2016.

[3] J. A. Richards, P. E. Whitson, and D. H. Evans, "Electrochemical oxidation of 2,4,6-tri-tert-butylphenol," *J. Electroanal. Chem.*, vol. 63, no. 3, pp. 311–327, 1975.

[4] J. A. Richards and D. H. Evans, "Electrochemical Oxidation of 2,6-di-Tert-Butyl-4-Isopropylphenol," *J. Electroanal. Chem. Interfacial Electrochem.*, vol. 81, no. 1, pp. 171–187, Aug. 1977.

[5] N. S. Neghmouche and T. Lanez, "Calculation of Diffusion Coefficients and Layer Thickness for Oxidation the Ferrocene using Voltammetry Technique," *Int. J. Chem. Stud.*, vol. 1, no. 1, pp. 28–32, 2013.

[6] O. Fazlolahzadeh, A. Rouhollahi, and M. Hadi, "Electroanalytical Determination of Atorvastatin in Pharmaceutical Formulations based on Edge-Plane Pyrolytic Graphite Electrode," *Anal. Bioanal. Electrochem.*, vol. 8, no. 5, pp. 566–577, 2016.

[7] W. Yuan *et al.*, "The Edge- and Basal-Plane-Specific Electrochemistry of a Single-Layer Graphene Sheet," *Sci. Rep.*, vol. 3, pp. 1–7, 2013.

[8] W. A. Waters, "Comments on the Mechanism of One-Electron Oxidation of Phenol: A Fresh Interpretation of Oxidative Coupling Reactions of Plant Phenols," *J. Chem. Soc. B Phys. Org.*, pp. 2026–2029, 1971.

[9] T. A. Enache and A. M. Oliveira-Brett, "Phenol and para-substituted phenols Electrochemical Oxidation pathways," *J. Electroanal. Chem.*, vol. 655, no. 1, pp. 9–16, May 2011.

[10] J. L. N. Xavier, E. Ortega, J. Z. Ferreira, A. M. Bernardes, and V. Pérez-Herranz, "An Electrochemical Study of Phenol Oxidation in Acidic Medium," *Int. J. Electrochem. Sci.*, vol. 6, no. 3, pp. 622–636, 2011.

[11] K. Omura, "Electron Transfer Between Protonated and Unprotonated Phenoxyl Radicals," *J. Org. Chem.*, vol. 73, no. 3, pp. 858–867, 2008.

[12] M. Ferreira, H. Varela, R. M. Torresi, and G. Tremiliosi-Filho, "Electrode Passivation Caused by Polymerization of Different Phenolic Compounds," *Electrochim. Acta*, vol. 52, no. 2, pp. 434–442, Oct. 2006.

[13] M. E. Tessensohn, H. Hirao, and R. D. Webster, "Electrochemical Properties of Phenols and Quinones in Organic Solvents are Strongly Influenced by Hydrogen-Bonding with Water," *J. Phys. Chem. C*, vol. 117, no. 2, pp. 1081–1090, 2013.

[14] A. M. Zaky and B. P. Chaplin, "Mechanism of p-substituted Phenol Oxidation at a Ti4O7 Reactive Electrochemical Membrane," *Environ. Sci. Technol.*, vol. 48, no. 10, pp. 5857–5867, 2014.

[15] G. Grampp, S. Landgraf, and C. Mureşanu, "Redox Properties and Bond Dissociations Energies of Phenoxyl Radicals," *Electrochim. Acta*, vol. 49, no. 4, pp. 537–544, 2004.

[16] M. Lu and R. G. Compton, "Voltammetric pH Sensor Based on an Edge Plane Pyrolytic Graphite Electrode.," *R. Soc. Chem.*, vol. 139, no. 10, pp. 2397–2403, 2014.

[17] D. H. Evans, P. J. Jimenez, and M. J. Kelly, "Reversible Dimerization of Phenoxyl Radicals Formed by Anodic Oxidation of Phenolates. A Quantitative Study by Cyclic Voltammetry," *J. Electroanal. Chem.*, vol. 163, pp. 145–157, 1984.

[18] P. Hapiot and J. Pinson, "Multiple Reaction Pathways for the Oxidation of 2,6-Diphenylphenolates," *J. Electroanal. Chem.*, vol. 362, pp. 257–265, 1993.

[19] S. Patai, *The Chemistry of Phenols*, 1st ed. Chichester: John Wiley & sons, Ltd, 2003.

[20] F. Wantz, C. E. Banks, and R. G. Compton, "Edge Plane Pyrolytic Graphite Electrodes for Stripping Voltammetry: A Comparison with Other Carbon Based Electrodes," *Electroanalysis*, vol. 17, no. 8, pp. 655–661, 2005.

[21] Z. Taleb, F. Montilla, C. Quijada, E. Morallon, and S. Taleb, "Electrochemical and In Situ FTIR Study of O-Cresol on Platinum Electrode in Acid Medium," *Electrocatalysis*, vol. 5, no. 2, pp. 186–192, 2014.

[22] H. Eickhoff, G. Jung, and A. Rieker, "Oxidative phenol coupling - Tyrosine dimers and libraries containing tyrosyl peptide dimers," *Tetrahedron*, vol. 57, no. 2, pp. 353–364, 2001.

[23] H. J. Salavagione, J. Arias-Pardilla, J. L. Vázquez, M. C. Miras, E. Morallón, and C. Barbero, "Spectroelectrochemical Study of the Oxidation of Diaminophenols on Platinum Electrodes in Acidic Medium," *Electrochim. Acta*, vol. 50, no. 27, pp. 5414–5422, 2005.

[24] N. T. Belhadj and A. Savall, "Electropolymerization of Phenol on a Vitreous Carbon Electrode in Acidic Aqueous Solution at Different Temperatures," *J. Appl. Electrochem.*, vol. 41, no. 8, pp. 983–989, 2011.

[25] S. M. Sayyah, F. Mohamed, and M. Shaban, "Electropolymerization of (ortho cresol-co-pyrrole) and Characterization of the Obtained Film," *IOSR J. Appl. Chem.*, vol. 7, no. 9, pp. 09–21, 2014.

[26] D. S. Shishmarev, N. V. Rees, and R. G. Compton, "Enhanced Performance of Edge-Plane Pyrolytic Graphite (EPPG) Electrodes Over Glassy Carbon (GC) Electrodes in the Presence of Surfactants: Application to the Stripping Voltammetry of Copper," *Electroanalysis*, vol. 22, no. 1, pp. 31–34, 2010.

[27] M. Khafaji, S. Shahrokhian, and M. Ghalkhani, "Electrochemistry of Levo-Thyroxin on Edge-Plane Pyrolytic Graphite Electrode: Application to Sensitive Analytical Determinations," *Electroanalysis*, vol. 23, no. 8, pp. 1875–1880, 2011.

[28] N. Song and D. M. Stanbury, "Overoxidation of Phenol by Hexachloroiridate(IV)," *Inorg. Chem.*, vol. 50, no. 24, pp. 12762–12773, 2011.

[29] G. V Kornienko, N. V Chaenko, N. G. Maksimov, V. L. Kornienko, and V. P. Varnin, "Electrochemical Oxidation of Phenol on Boron – Doped Diamond Electrode," *Short Commun.*, vol. 47, no. 2, pp. 225–229, 2011.

[30] N. Oyama, T. Ohsaka, Y. Ohnuki, and T. Suzuki, "Anodic Oxidation of 2,6-Dimethylphenol in Various Electrolytic Solutions," *J. Electrochem. Soc.*, vol. 134, no. 12, pp. 3068–3073, 1987.

[31] A. M. Polcaro, S. Palmas, F. Renoldi, and M. Mascia, "On the Performance of Ti/SnO2 and Ti/PbO2 Anodesin Electrochemical Degradation of 2-Chlorophenol for Wastewater Treatment," *J. Appl. Electrochem.*, vol. 29, no. 2, pp. 147–151, 1999.

[32] S. Stucki, R. Kötz, B. Carcer, and W. Suter, "Electrochemical Wastewater Treatment using High Overvoltage Anodes Part II: Anode Performance and Applications," *J. Appl. Electrochem.*, vol. 21, no. 2, pp. 99–104, 1991.

[33] C. A. Martínez-Huitle and S. Ferro, "Electrochemical Oxidation of Organic Pollutants for the Wastewater Treatment: Direct and Indirect Processes," *Chem. Soc. Rev.*, vol. 35, no. 12, pp. 1324–1340, 2006.

[34] M. Sathish and R. P. Viswanath, "Electrochemical Degradation of Aqueous Phenols using Graphite Electrode in a Divided Electrolytic Cell," *Korean J. Chem. Eng.*, vol. 22, no. 3, pp. 358–363, 2005.

[35] M. E. Tessensohn, H. Hirao, and R. D. Webster, "Electrochemical Properties of Phenols and Quinones in Organic Solvents are Strongly Influenced by Hydrogen-Bonding with Water," *J. Phys. Chem.*, vol. 117, no. 2, pp. 1081–1090, 2013.

[36] N. B. Tahar, R. Abdelhédi, and A. Savall, "Electrochemical Polymerisation of Phenol in Aqueous Solution on a Ta/PbO2 Anode," *J. Appl. Electrochem.*, vol. 39, no. 5, pp. 663–669, 2009.

[37] C. Comninellis and A. Nerini, "Anodic Oxidation of Phenol in the Presence of NaCl for Wastewater Treatment," *J. Appl. Electrochem.*, vol. 25, no. 1, pp. 23–28, 1995.

[38] F. Trabelsi *et al.*, "Oxidation of Phenol in Wastewater by Sonoelectrochemistry," *Chem. Eng. Sci.*, vol. 51, no. 10, pp. 1857–1865, May 1996.

[39] J. L. Boudenne, O. Cerclier, J. Galéa, and E. Van Der Vlist, "Electrochemical Oxidation of Aqueous Phenol at a Carbon Black Slurry Electrode," *Appl. Catal. A Gen.*, vol. 143, no. 2, pp. 185–202, 1996.

[40] M. M. Musiani, F. Furlanetto, P. Guerriero, and J. Heitbaum, "Phenol Electropolymerization on Phosphated Mild Steel via Zinc Electrodeposition," *J. Appl. Electrochem.*, vol. 23, no. 10, pp. 1069–1075, Oct. 1993.

[41] N. Belhadj Tahar and A. Savall, "Electrochemical Removal of Phenol in Alkaline Solution. Contribution of the Anodic Polymerization on Different Electrode Materials," *Electrochim. Acta*, vol. 54, no. 21, pp. 4809–4816, 2009.

[42] A. Safavi, N. Maleki, and F. Tajabadi, "Highly Stable Electrochemical Oxidation of Phenolic Compounds at Carbon Ionic Liquid Electrode," *Analyst*, vol. 132, pp. 54–58, 2007.

[43] C. Comninellis and C. Pulgarin, "Electrochemical Oxidation of Phenol for Wastewater Treatment Using SnO2, Anodes," *J. Appl. Electrochem.*, vol. 23, no. 2, pp. 108–112, 1993.

[44] X. Li, J. Cui, Z. Gu, Y. Xie, and Y. Feng, "Reaction Pathways and Mechanisms of the Electrochemical Degradation of Phenol on Different Electrodes," *Water Res.*, vol. 39, no. 10, pp. 1972–1981, 2005.

[45] L. Gui, H. Jin, Y. Zheng, R. Peng, Y. Luo, and P. Yu, "Electrochemical Degradation of Bisphenol A Using Different Modified Anodes Based on Titanium in Aqueous Solution," *Int. J. Electrochem. Sci.*, vol. 13, no. 7, pp. 7141–7156, 2018.

[46] M. A. Ajeel, M. K. Aroua, and W. M. A. W. Daud, "Anodic Degradation of 2-Chlorophenol by Carbon Black Diamond and Activated Carbon Composite Electrodes," *Electrochim. Acta*, vol. 180, pp. 22–28, 2015.

[47] Y. J. Feng and X. Y. Li, "Electro-Catalytic Oxidation of Phenol on Several Metal-Oxide Electrodes in Aqueous Solution," *Water Res.*, vol. 37, no. 10, pp. 2399–2407, 2003.

[48] A. A. Al-Zahrani, A. H. El-Shazly, M. A. Daous, and S. S. Al-Shahrani, "Enhancement of Electrochemical Oxidation of Phenol in Aqueous Solutions Using Polyaniline Coated Graphite Electrode," *Int. J. Electrochem. Sci.*, vol. 12, no. 8, pp. 7048–7063, 2017.

[49] J. Iniesta, P. A. Michaud, M. Panizza, G. Cerisola, A. Aldaz, and C. Comninellis, "Electrochemical Oxidation of Phenol at Boron-Doped Diamond Electrode," *Electrochim. Acta*, vol. 46, pp. 3573–3578, 2001.

Chapter 4

In Situ Spectroelectrochemical Study of Phenol and Substituted Phenols

4.1 Introduction

In this work, the electro-oxidation of phenol, TBP and cresols were studied in situ using ATR-FTIR spectroscopy technique in order to gain more insight into the oxidation processes and support the oxidation mechanisms proposed for these phenolic compounds in the last chapter. The analysis of the absorption spectra obtained will allow the identification of several IR absorption bands that could be assigned to the oxidation products. Infrared ATR-FTIR spectroscopy has been shown to be a useful technique for monitoring phenols oxidation in situ. Webster and co-workers have used this technique to monitor the one electron oxidation of 2,4,6-tri-tert-butylphenolate in CH_3CN. From their results, the authors identified several IR absorption bands notably in the 1592 −1573 cm^{-1} and 1509 −1505 cm^{-1} ranges which were assigned to C_oC_m (carbon in the ortho-and meta-position) ring and $C- O^{\bullet}$ stretching vibration of 2,4,6-tri-tert-butylphenoxyl respectively [1]. Other authors such as Haracio and co-workers have also reported the use of this technique to detect the oxidation products for para, meta, and ortho-aminophenols while studying the electrochemical oxidation of aminophenols on platinum electrode in acid medium. In their study, the authors observed that the three isomers of aminophenols showed different behaviour with the platinum electrode, leading to different oxidation products. While meta- and para-aminophenol give polymeric compounds, quinone and CO_2 as oxidation products, electroactive dimers were observed as the oxidation product for ortho-aminophenols and these active dimers can polymerize to form an electroactive layer on the electrode surface [2]. Others authors have also used the same technique to successfully monitor the oxidation process of phenolic compounds such as o-cresols [3] on platinum electrode in acid medium.

In most of these published works, platinum electrode was used in acid medium and the limitations of the technique was not mentioned.

4.2 Experimental

The TBP, Phenol and cresols were used as received and the electrolyte solutions were 50:50(v:v) 0.05 M $Na_2SO_4.10H_2O$ / EtOH. All in situ FTIR experiments were performed using a combined technique of chronoamperometry and in situ ATR-FTIR spectroscopy. In this technique, a three electrode electrochemical cell was used which consists of a working electrode (EPPG coated with singlet walled carbon nanotubes (SWCNT)), a reference electrode (Ag / AgCl) and a counter electrode (platinum wire) dipped in the electrolyte. The working electrode was prepared by drop-coating 3µL of SWCNT suspension (1.5 mg / mL) onto the electrode surface and leaving it to dry at room temperature for 30 mins before use. Oxidation potentials ranging from 0.2 to 0.95 V were applied to the working electrode and the difference spectra collected over time between $4000 - 600$ cm^{-1} with a resolution of 4 cm^{-1} in absorbance mode using a Bruker Tensor 27 Fourier-transform spectrometer equipped with a diamond crystal prism and having an Opus data collection program. All background spectra were collected with the electrode in solution with no potential applied. The absorption band between 2500 cm^{-1} and 1800 cm^{-1} related to absorption by the diamond prism was cut out from the spectra for more accurate data analysis. The SWCNT layer was added onto the electrode surface in order to increase the surface area and hence improve the signal to noise ratio resolution of the IR spectral features (see section 4.2.2).

4.2.1 In Situ FTIR Experimental Set - up

A schematic diagram of a typical experimental set-up is presented in Figure 4.1. In this set up, the working electrode (EPPG coated with SWCNT) was immersed in the electrolyte as close to the ATR prism as possible. The distance limit between the unmodified electrode and the prism was determined to be around ca.17 µm by other colleagues in our research group while investigating the acid deprotonation and protonation state at the interface of a BBD electrode modified with graphene nanoflakes (GNF). The GNF-Ca layer was found to swell when immersed in solution and fills the gap between the electrode and the prism, thus as the penetration depth of the IR

evanescence is < 2 µm only the region of the GNF layer furthest from the modified BBD electrode surface is probed [4].

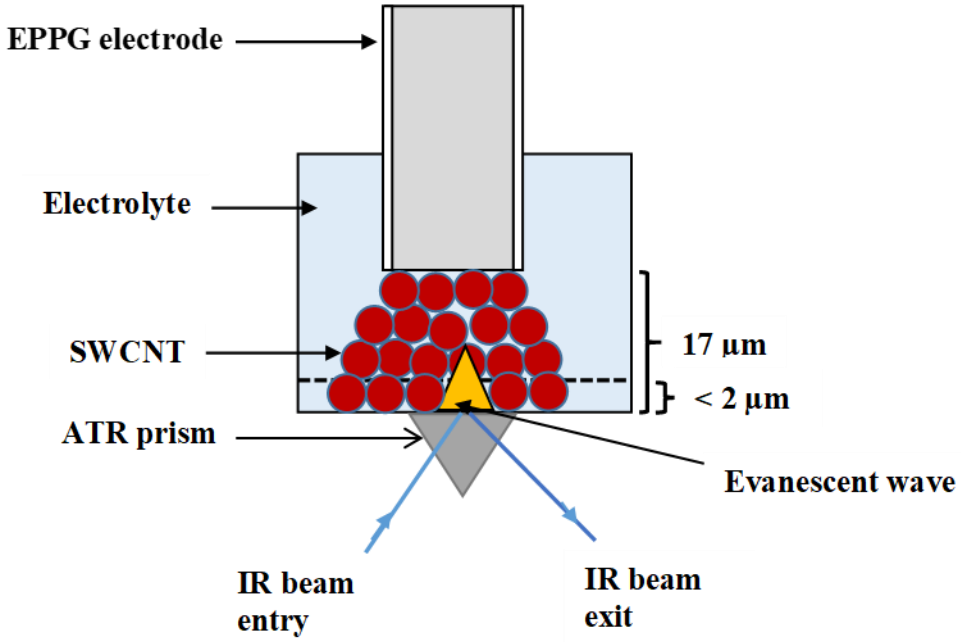

Figure 4.1: Schematic representation of the interface region of the in situ ATR-FTIR experimental set up.

This effect is illustrated in Figure 4.2 below. This graph shows that the spectral intensity of the GNF-Ca increases considerably after 5mins of immersion of the electrode in the electrolyte solution and this was reported to be the consequence of the swelling of the GNF-Ca layer upon interaction with water and hence filling the gap between the BDD electrode surface and the ATR. This led to more of the layer been probed by the evanescent IR radiation and an increase in spectral intensity is observed.

In our work EPPG electrode coating with single walled carbon nanotube (SWCNT) was used as the working electrode. These SWCNT have an average diameter of 1.4 nm ± 0.1nm and their solubility in water is 5mg / mL. Early experiments in our work have shown that the SWCNT increase the surface area and increase the noise ratio resolution of the IR spectral features (see section 4.2.2). This might be explained by the fact that the SWCNT behave in the same way as the GNF-Ca layer when immersed in solution as described above. i.e. the SWCNT provides a high surface area electroactive layer close to the prism and therefore within probing depth of the IR evanescent wave.

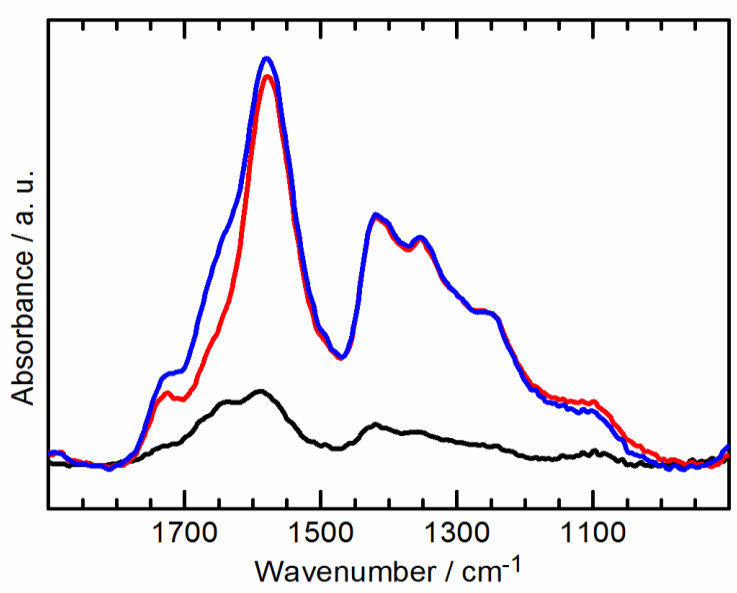

Figure 4.2: IR absorbance difference spectra of GNF-Ca modified electrode after immersion into 0.1 M K_2SO_4 electrolyte at pH 6.8. (black) immediately after immersion, (red) 5mins after immersion, (blue) 35 mins after immersion. This Graph is taken from [4].

4.2.2 Effect of SWCNT on the Spectral Response of $Na_2SO_4.10H_2O$ Solution at the EPPG Electrode Interface.

Figure 4.3 shows the FTIR difference spectra of 0.1 M $Na_2SO_4.10H_2O$ solution at both the EPPG and SWCNT modified EPPG electrodes interface when 0.5 V was applied. In these experiments, the modified EPPG electrode was prepared by drop-coating 3µL of SWCNT solution onto the electrode surface and leaving it to dry at room temperature for 15 mins before use. The background spectra were collected with the electrodes immersed in the solution along with the counter and reference electrode with no potential applied. Difference spectra for both electrodes were then collected overtime relative to the background for 30 mins with a delay time of 5 mins between measurements after applying a potential of 0.5 V. Two broad and intense positive bands are observed in the 1800 − 1550 cm^{-1} and 1150 − 1000 cm^{-1} ranges on the spectrum of EPPG coated with SWCNT. These bands are attributed to the bending mode of water and asymmetric SO_4^{2-} stretch respectively. The intensity of the later band indicates that application of the potential results in increase in this band in the IR sampling region. In contrast only weak features are seen on the spectrum of EPPG only in the same range.

This implies that the SWCNT increase the spectral intensity and this is explained by the increased electrode surface area within the IR probing region described in section 4.2.1. Hence this increase in spectral intensity was our aim so this is why we continue with SWCNT modified electrodes throughout this study.

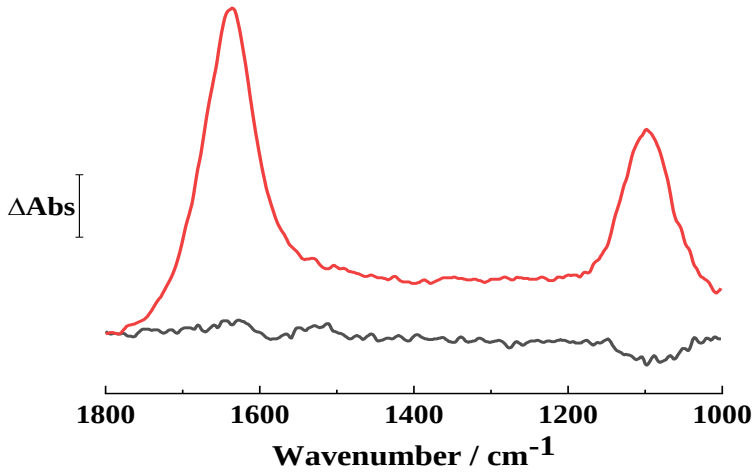

Figure 4.3: FTIR difference spectra of: EPPG (Black) and EPPG coated with 3µL SWCNT (Red) in 0.1 M $Na_2SO_4.10H_2O$. 0.5 V was applied and the difference spectra were recorded for 30 mins with a delay time of 5 mins between measurements. The background spectra were recorded with the electrodes immersed in the supporting electrolyte with no potential applied.

4.2.3 FTIR Spectra of PBS and Sodium Sulfate Hydrate

Figure 4.4 shows the FTIR difference spectra of EPPG electrode coated with SWCNT in 0.1M PBS (pH9) and in 0.1M $Na_2SO_4.10H_2O$. These experiments were performed in order to choose the most appropriate electrolyte for more accurate data analysis. In the early stage of our in situ FTIR spectroscopy experiments, PBS was used as the supporting electrolyte solution because the main objective of this chapter was to support the electro-oxidation mechanism of the phenolic compounds investigated in Chapter 3 where 50:50 (v:v) PBS (pH11) / EtOH was used as the supporting electrolyte. However, the spectra obtained were difficult to analyse as certain bands of the PBS buffer interferes with the bands expected for the oxidation products of these phenolic compounds. In the spectrum of PBS several bands are observed in the 1800 – 1600 cm^{-1} range where the C=O vibration stretch is expected with the more distinct band seen in the 1700 – 1600 cm^{-1} region.

Bands similar to C=C and C−O stretches are also seen in the 1600 − 1400 cm^{-1} and 1300 − 1000 cm^{-1} regions. The presence of all these bands in the spectrum of the PBS will make the interpretation of our in situ results difficult. Therefore $Na_2SO_4.10H_2O$ solution was used instead of the PBS as its spectrum shows only two distinct bands; one in the 1800 − 1600 cm^{-1} range which have a characteristic of O–H bending mode of water present in the solution and the second band in the 1200 – 1000 cm^{-1} range which is attributed to the asymmetric stretch of SO_4.This latter band may also interfere with the C− O and C− O− C vibration stretch bands expected for certain oxidation products. However, the interpretation of our in situ spectra will be less problematic in this solvent. However, it is important to note the pH in the sulfate solution is ~ 6.8 which is different to the pH of the PBS solution used in the electrochemical chapter. This implies that the oxidation mechanism will be expected to be different to the one in the previous chapter where pH11 was used, therefore the second electron transfer route leading to the formation of the phenoxy cations should also be considered while using the sulfate as electrolyte.

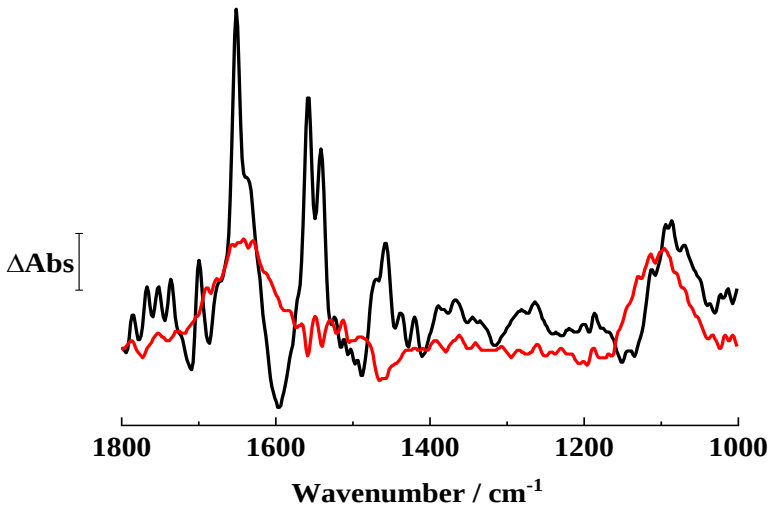

Figure 4.4: FTIR difference spectra of EPPG coated with SWCNT in: (black) 0.1 M PBS (pH9) and (Red) 0.1M $Na_2SO_4.10H_2O$. The sample scan was used as background. Difference spectra were collected for 30 mins between 4000 – 500 cm^{-1} with a resolution of 4 cm^{-1} with no potential applied.

4.3 Results and Discussions

In Figure 4.5 is shown the CV of 0.5 mM TBP in 50:50(v:v) 0.05M $Na_2SO_4.10H_2$ /EtOH at the SWCNT modified EPPG electrode. This experiment was performed in order to determine in which potential the TBP undergoes oxidation in this electrolyte as the potentials will be different to those determined in pH11. This allowed us to apply the correct potentials in our in situ experiment. Arrow (1) represents the potential before oxidation (+ 0.2 V), arrow (2) the potential in which the TBP begins to undergo oxidation (+ 0.4 V) and (3) the peak oxidation potential of TBP (+ 0.6 V). In this CV the oxidation potential for the TBP is 0.35 V higher than the oxidation potential observed in the CV of TBP in PBS (pH11) presented in the electrochemistry chapter and in addition to that less distinct oxidation and reduction peaks are also seen in this case. These differences can be explained mainly by the difference in pH observed between the sulfate solution (pH 6.8) and the PBS (pH11) and also the SWCNT modification, where electron transfer (ET) kinetics may be slower and the porous nature of the electrode leads to less distinct diffusion- controlled peaks.

Similar CV experiments under the same experimental condition as the TBP, were carried out for the phenol and cresols and their oxidation potentials were found to be 0.85 V. A summary of the oxidation potentials applied in the in situ spectroelectro-chemistry for the different compounds is presented in table 4.1 below:

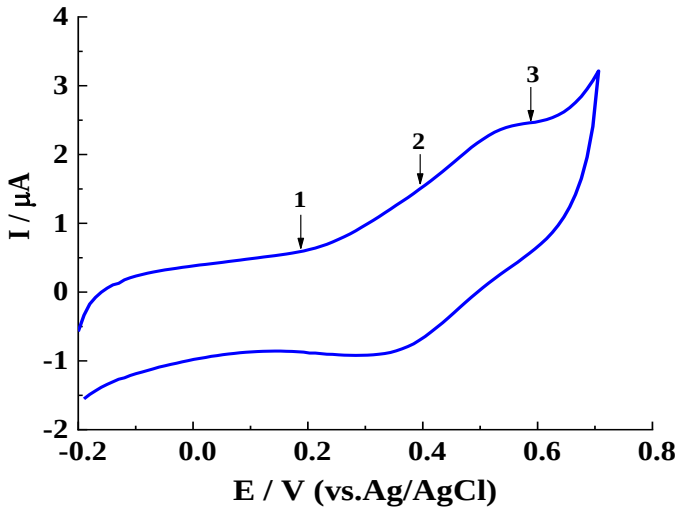

Figure 4.5: CV of 2.5 mM TBP in 50:50(v:v) 0.05 M $Na_2SO_4.10H_2O$ / EtOH using EPPG electrode coated with SWCNT at a scan rate of 0.1 mVs^{-1}: (1) + 0.2V, (2) + 0.4 V and (3) + 0.6 V.

Table 4.1:Oxidation potentials applied in the in situ spectroelectrochemistry experiments for the different compounds.

Phenolic compounds	Oxidation peaks potential (V) vs Ag / AgCl
TBP	+ 0.6
Phenol	+ 0.85
o-cresol	+ 0.85
m-cresol	+ 0.85
p-cresol	+ 0.85

4.3.1 Infrared Characterization of TBP, Phenol and o,m,p-cresols

In the earlier stage of this work, the solvated TBP, phenol and cresols were characterized using ATR-FTIR spectroscopy and the resulting spectra obtained are presented below. In these experiments the different solution samples were drop-coated onto the ATR prism and the spectra collected for 30 mins between 4000 − 600 cm^{-1} with a resolution of 4 cm^{-1} with a delay time of 5 mins between measurements where first a spectrum of the blank ATR prism was collected and used as the background for all subsequent spectra. The resulting spectra obtained are background subtracted. In Figure 4.6(a) is presented the FTIR absorbance spectrum of 2.5 mM of TBP between 1800 and 600 cm^{-1}. The bands observed at 1476 and 1436 cm^{-1} are associated with the CC ring vibration stretches, the band seen at 1361 cm^{-1} is assigned to the OH bending mode, the band at 1234 cm^{-1} is due to C−O vibration stretch and the band at 994 cm^{-1} is assigned to the out of plane C−H stretches in the tert-butyl groups.[1] The additional intense bands observed in the 1200 − 1000 cm^{-1} and 650 – 620 cm^{-1} range are associated with the vibration stretches modes of the solvent (0.1 M $Na_2SO_4.10H_2O$ / EtOH) used to dissolved the TBP and these vibration modes will be discussed later**.** Figure 4.6 (b) shows the FTIR spectrum of phenol, the intense peak at 1596 cm^{-1} is associated with the aromatic C=C stretch, the intense peaks observed at 1500 and 1474 cm^{-1} are assigned to the CC stretches and the broad bands at 1367 cm^{-1} and 1230 cm^{-1} are attributed to the OH bending and the C−O stretching vibration respectively.

The in plane C−H stretch is observed at 1072 cm^{-1} and the out of plane C−H at 811, 752 and 690 cm^{-1}. In Figure 4.6(c) is presented the FTIR absorbance spectra of o,m,p-cresols. The band observed at 1593 cm^{-1} in the spectrum of o-cresol is assigned to the aromatic C=C vibration stretch. This band appears at 1590 cm^{-1} and 1607 cm^{-1} in the spectra of meta and para-cresol respectively. The bands seen at 1466 cm^{-1} in the spectra of ortho and meta-cresol, and at 1512 cm^{-1} and 1450 cm^{-1} in the spectrum of para-cresol are associated with the CC vibration stretches. The OH bending vibration is observed at 1351 cm^{-1} in the spectrum of o-cresol and at 1342 cm^{-1} and 1361 cm^{-1} in meta and para-cresol respectively. The band around 1200 cm^{-1} seen in the spectra of o-cresol and little bit shifted toward higher wavenumber in the spectrum of meta (1243 cm^{-1}) and para-cresol (1224 cm^{-1}) is associated with the C−O vibration stretches. The additional bands observed in the 1200 – 1000 cm^{-1} and 900 – 650 cm^{-1} range are due to the in plane and out of plane C−H stretches in ring and in the methyl group attached to the ring. These bands define the substitution pattern in the ring.

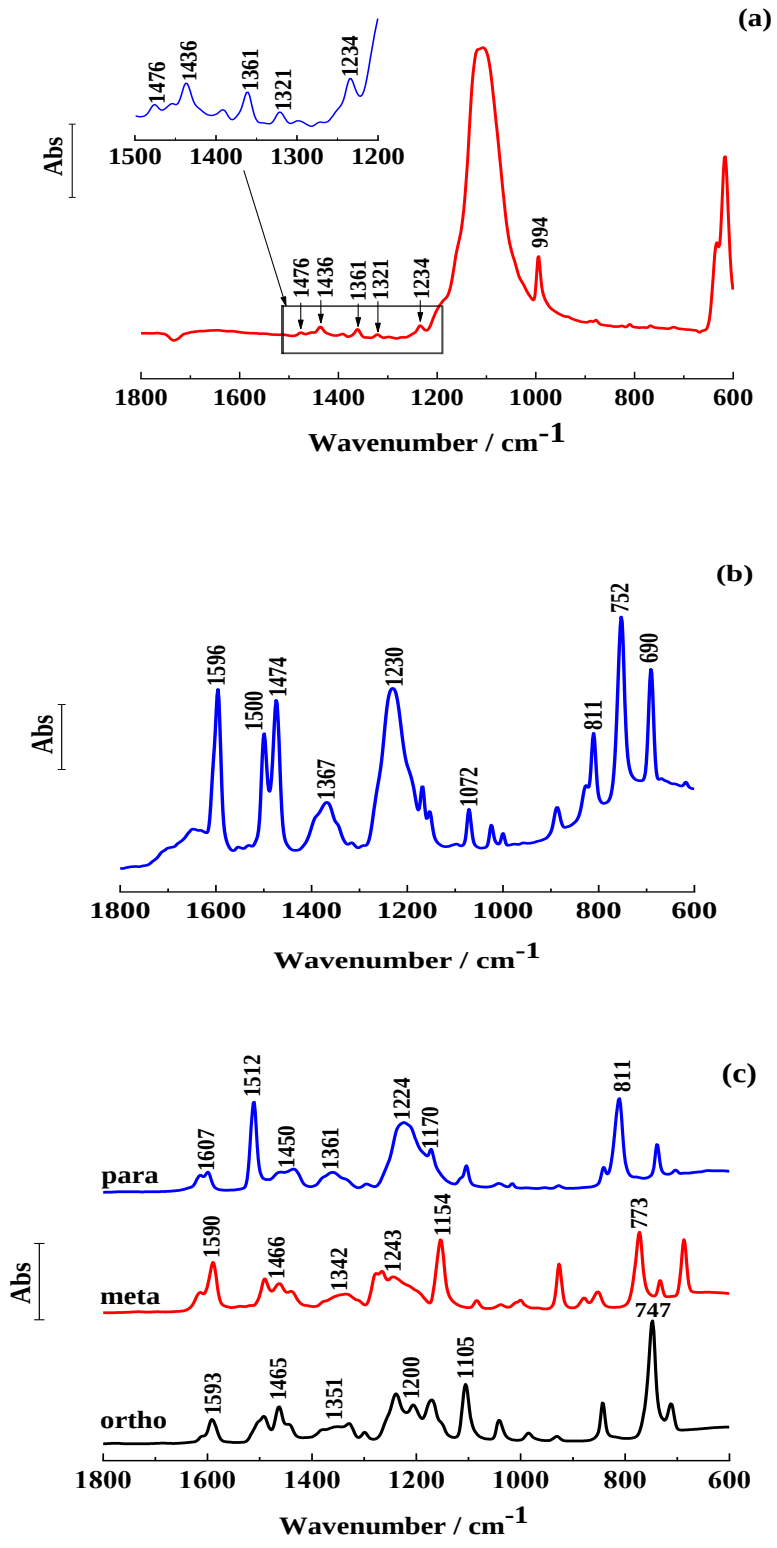

Figure 4.6: (a) Background subtracted FTIR absorbance spectra of: (a) TBP; (b) phenol and (c) cresols: (Black) o-cresol; (Red) m-cresol and (Blue) p-cresol. The spectra were recorded between 4000 – 500 cm^{-1} with a resolution of 4 cm^{-1} and averaged over 100 scans.

4.3.2 In Situ ATR-FTIR Study of the Electrolyte

Figure 4.7 shows the in situ FTIR absorbance spectra obtained for the EPPG electrode coated with SWCNT in 0.1 M $Na_2SO_4.10H_2O$ solution (electrolyte) without any phenol species present. The working electrode was immersed in the spectroelectrochemical cell along with the reference and counter electrode and left to settle for 5 mins before collecting the background spectrum. A potential of 0.6 V was then applied and difference spectra collected overtime relative to the background for 30 mins with a delay time of 5mins between measurements. The strong positive bands observed at 1090 cm^{-1} and 1047 cm^{-1} are attributed to the C−O vibration stretch of ethanol. The bands at 1196 cm^{-1} and 879 cm^{-1} are assigned to the OH bending and out of plane C−H stretch of ethanol respectively. The negative band observed at 1120 cm^{-1} is assigned to the asymmetric SO_4^{2-} stretch of the sulfate and the broad band at 1653 cm^{-1} to the OH bending mode of water present in the solvent. In summary, it can be observed that the difference spectra of the electrolyte at + 0.6 V which consist of 50:50(v:v) $Na_2SO_4.10H_2O$/EtOH is dominated by the positive absorption bands of ethanol and the only band observed for the $Na_2SO_4.10H_2O$ is the negative band assigned to the asymmetric SO_4^{2-} stretch. This is in contrast with what was observed above when the same experiment was done in 0.1 M $Na_2SO_4.10H_2O$ with no ethanol present where the sulfate band increases when a positive potential was applied as expected. Here it is the opposite which is unexpected but the only thing that has changed is the ethanol and we are assuming that the SWCNT might not swell as much when the ethanol is present. Hence rather than probing within the porous electrode as shown in Figure 4.1 we may be probing the outside interface of the SWCNT layer with the electrolyte as shown in
Figure 4.8.

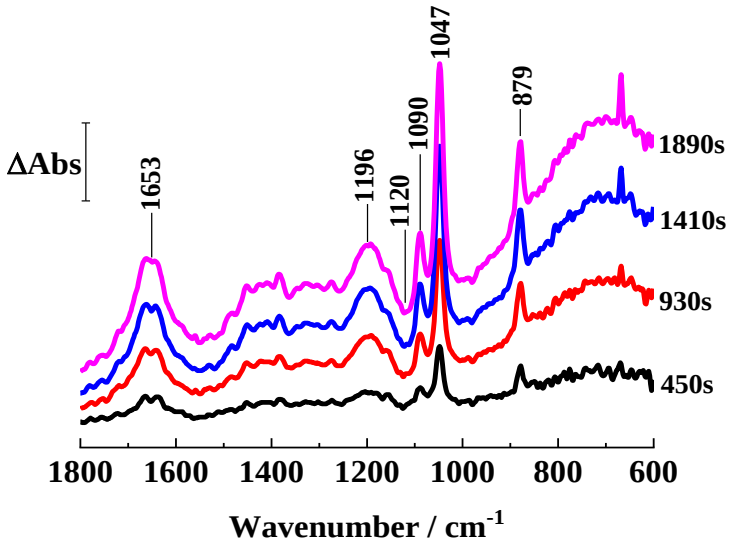

Figure 4.7: FTIR spectra collected for EPPG electrode coated with SWCNT in 0.05 M $Na_2SO_4.10H_2O$ / EtOH solution at + 0.6 V. The background was taken 5 mins after sample deposition and the spectra were collected between 4000 – 500 cm^{-1} with a resolution of 4 cm^{-1} and averaged over 500 scans.

A tentative explanation of the electrolyte interaction with the electrode surface is presented in Figure 4.8. In this representation both the sodium and sulfate ions are solvated by water and ethanol molecules such that the δ- oxygen will interact with the positively charged sodium (Na^+) ion, and the δ+ hydrogen will interact with the negatively charged sulfate (SO_4^{2-}). Thus then when a positive potential is applied to the electrode, the positively charged solvated sodium is repelled from the electrode surface and moves towards the IR probing area, while the negatively charged solvated sulfate moves in the opposite direction as it is attracted to the positive electrode. Hence in the difference spectrum for the electrolyte the sulfate band is negative as there is a smaller concentration in the probing region. Na^+ does not possess IR bands but if ethanol is more strongly associated with Na^+ than SO_4^{2-}, an increase in Na^+ in the probing region would explain the increase in the ethanol bands when the potential is applied.

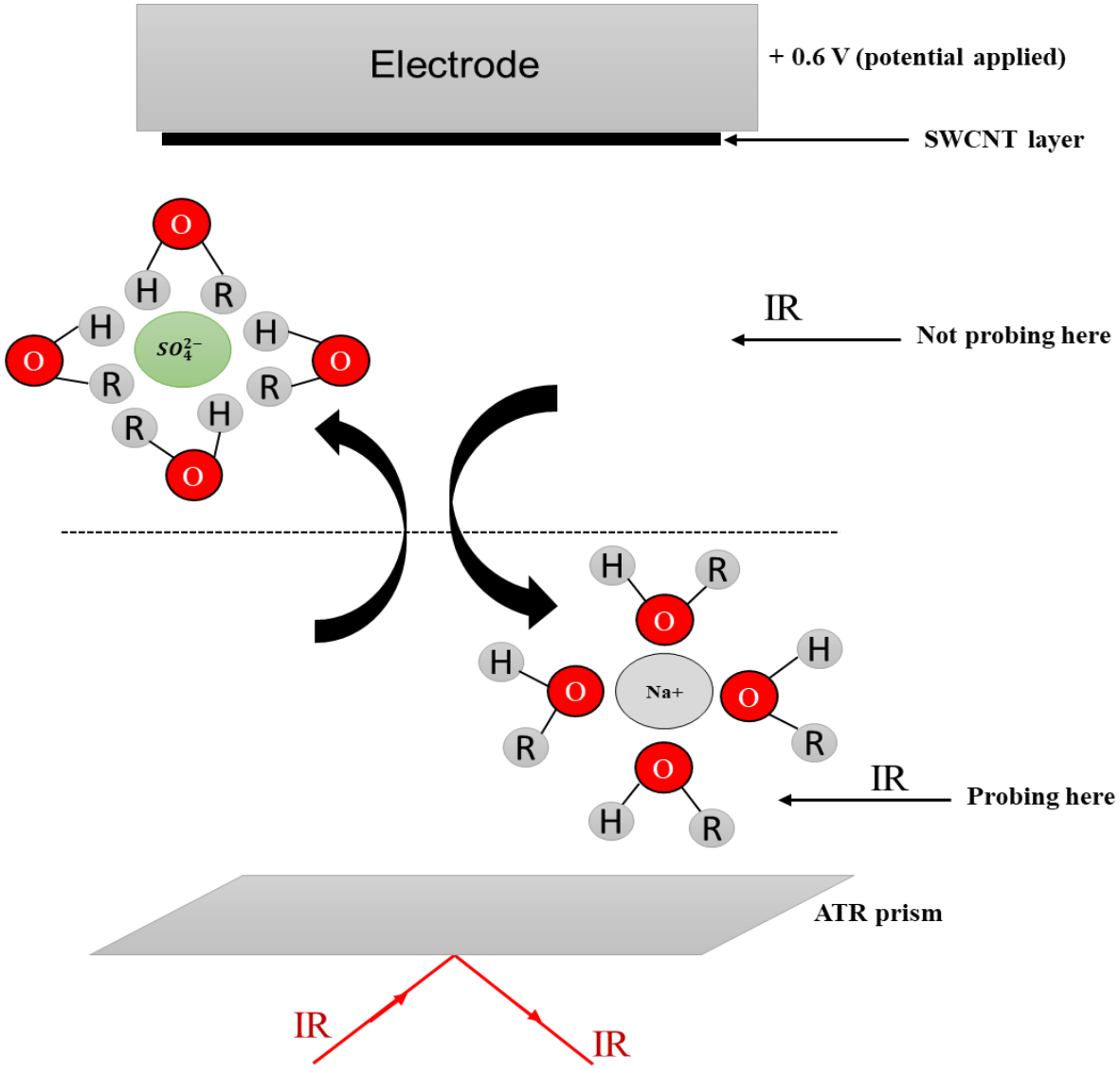

Figure 4.8: Schematic representation of the electrolyte interaction with the EPPG electrode.

4.3.3 In situ FTIR Spectra of TBP

The oxidation reaction of TBP was monitored using in situ FTIR spectroscopy in order to confirm the oxidation mechanism proposed in chapter 3 in which the oxidation product was proposed to be 2,4,6-tri-tert-butylphenoxyl.

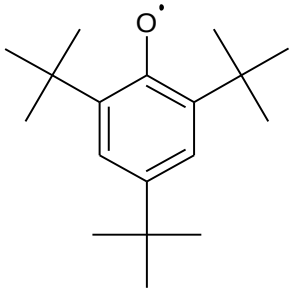

Five important bands were observed in the spectra of the solvated TBP when + 0.6 V (oxidation potential) was applied to the working electrode immersed in the solution (Figure 4.9); at 1650, 1558, 1548, 1513 and 940 cm^{-1}. The negative band at 1558 cm^{-1} and the positive band at 1548 cm^{-1} can be both assigned to the CC ring stretch and indicate a change in electron density in the ring (cf scheme 4.1). These two bands indicates the loss of one type of CC ring stretch (negative band) and the gain of another (positive band) and this might be due to the delocalisation of the electron in the phenoxyl ring after oxidation. The band at 1513 cm^{-1} is associated with the C−O• stretch in the phenoxy radical. The positive band observed at 940 cm^{-1} is attributed to the out of plane C−H in the tert-butyl groups. The intense band centred at 1650 cm^{-1} is broader and sharper in comparison to the band seen in the spectra of the electrolyte. This band may incorporate both the OH bending vibration mode of water and a C=O band; the presence of this latter group indicates the formation of a quinone type structure of the radical as shown in scheme 4.1 below.

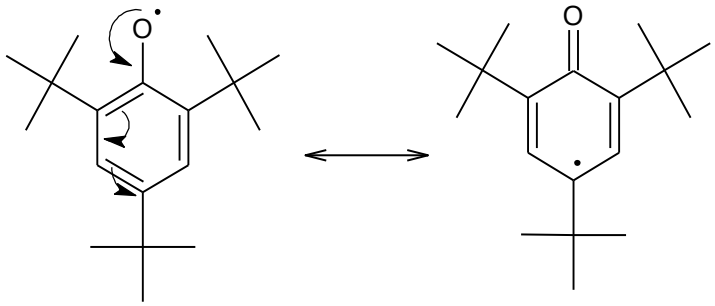

Scheme 4.1 Electrons delocalisation in the 2,4,6-tri-tert-butylphenoxyl leading to quinone type structure of the radical.

These assignments are consistent with those reported by Webster and co-workers while monitoring the oxidation reaction of 2,4,6-tri-tert-butylphenolate and 2.6-di-tert-butyl-4-methoxyphenolate in acetonitrile (CH_3CN) solution at room temperature using in situ FTIR spectroscopy. Several IR absorption bands were identified and assigned to the vibration stretches in the 2,4,6-substituted phenoxyl radicals notably the CC ring and C−O• stretches observed in the 1592 − 1573 cm^{-1} and 1509 − 1505 cm^{-1} ranges. These bands show many similarities with the bands reported in our study, the position of the C−O• in our work is shifted upward to 1513 cm^{-1} and agrees within 3 − 4 cm^{-1} with the same band reported by Webster and the position of this band (C−O•) has also been reported to vary between 1518 cm^{-1} and 1505 cm^{-1} in the resonance spectra of other

substituted phenoxyls. This shift in the position of the band in our study may be explained by the difference in the experimental conditions used. Webster et al have produced the radical by oxidizing the phenolate anion in acetonitrile in a controlled potential electrolysis cell at negative potentials varying from − 0.68 V to − 0.84 V while in our work the TBP oxidation was monitored in situ in 0.05 M $Na_2SO_4.10H_2O$ / EtOH solution at an applied potential of + 0.6 V. It is also important to mention that our different solvent will lead to local changes in the bonding environment which could shift the spectra.

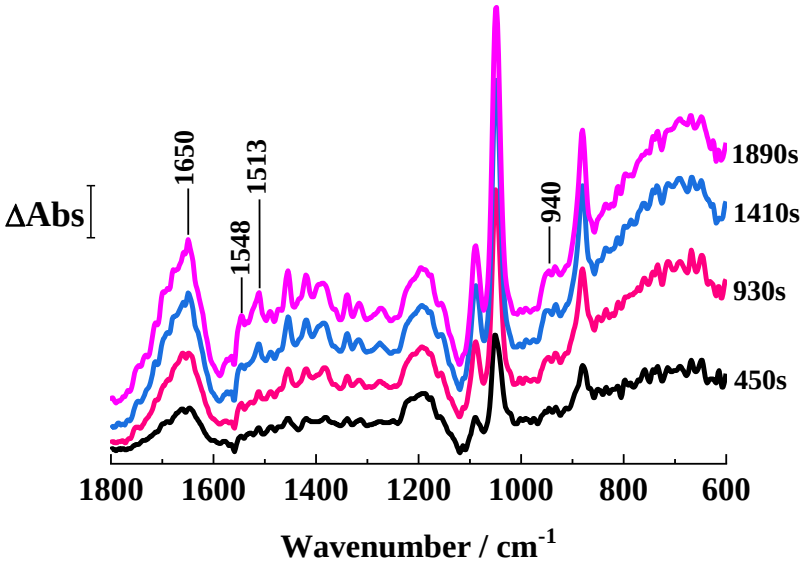

Figure 4.9: FTIR spectra collected for EPPG electrode coated with SWCNT in 0.05 M $Na_2SO_4.10H_2O$ / EtOH solution containing 2.5 mM TBP. The potential applied was + 0.6 V and the spectra were averaged over 500 scans.

4.3.4 In situ FTIR Spectra of Phenol

The oxidation of 10 mM of phenol in the electrolyte solution was investigated in the same electrolyte as the TBP at an applied potential of + 0.85 V and the resulting spectra obtained are presented in Figure 4.10. These spectra should give valuable information confirming the oxidation mechanism proposed in the previous chapter in which the oxidation products obtained were proposed to be:

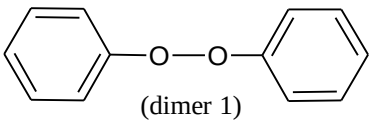

(dimer 1)

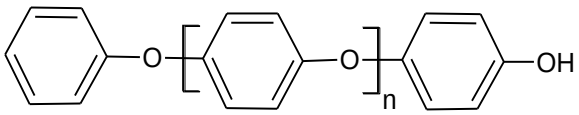

(Polymeric Product) (IX)

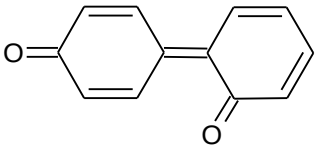

quinone

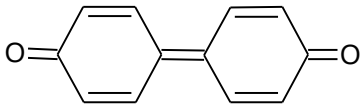

dipheno-quinone

The difference spectra at + 0.85 V show evidence for aliphatic C=O as well as OH bend of water in the positive band centred at 1636 cm^{-1} indicating some quinone type products formation (quinone and dipheno-quinone). The negative band at 1597 cm^{-1} is attributed to the changes in C=C stretch in the phenol ring. The bands centred at 1196 cm^{-1} and 1054 cm^{-1} are associated with the C−O−C vibration stretch. These latter two positive bands are concurrent with the negative band centred at 1096 cm^{-1} which is attributed to C−OH vibration stretch. These features indicate the loss of C−OH and formation of oxidation product through ether C−O−C linkage (polymeric product). The band observed at 868 cm^{-1} has a characteristic of the vibrational stretch of aromatic C−O−O−C and this might be due to the formation of dimer 1.

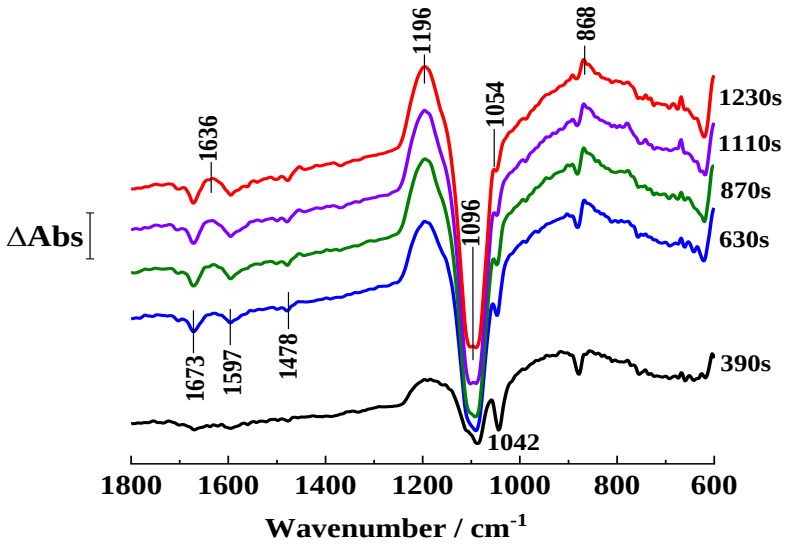

Figure 4.10: In situ FTIR spectra collected for an EPPG electrode coated with a SWCNT in 10 mM phenol dissolved in 0.05 M $Na_2SO_4.10H_2O$ / EtOH solution during oxidation up to + 0.85 V. The spectra were averaged over 100 scans.

4.3.5 In situ FTIR Spectra of o-cresol

Similarly to the phenol and TBP, the oxidation of orthocresol was monitored using the same experimental conditions in order to monitor the main products of oxidation proposed in chapter 3:

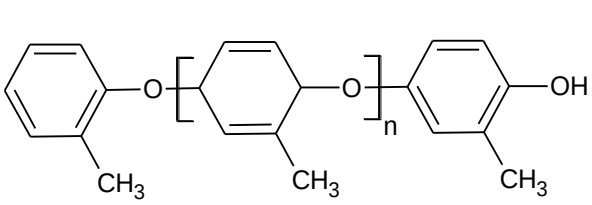

polymeric product

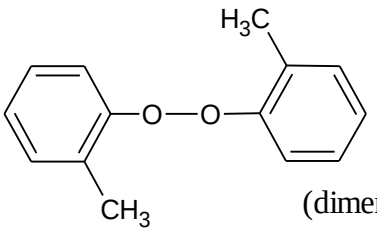

(dimer 7)

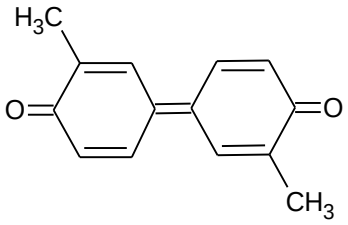

dipheno-quinone

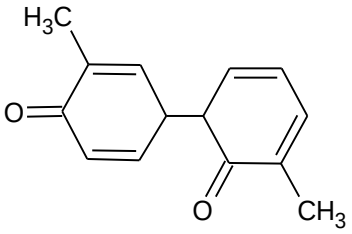

quinone

In Figure 4.11 a positive band centred at 1660 cm^{-1} can be observed and this band can be assigned to the aromatic C=O stretches in the quinone and dipheno-quinone products formed. The broad positive band seen at 1196 cm^{-1} which increases in intensity overtime can be assigned to C−O−C vibration stretch in the oxidation product and this latter band is linked with the negative band observed at 1110 cm^{-1} associated with C−OH vibration stretch in the o-cresol. This indicates the formation of oxidation product link through C−O−C coupling and this suggests the formation of the polymeric product. The band at 877 cm^{-1} is associated with the C−O−O−C vibration in product 7. Bands at 1089 cm^{-1} and 1048 cm^{-1} are associated with the characteristic C−O stretches in ethanol as described in section 4.3.1. Similar bands assigned have been reported by Taleb and co-workers in their study of electrochemical and in situ FTIR study of o-cresol on platinum electrode in 0.5 M H_2SO_4. Oxidation potentials ranging from 0.5 V to 1.2 V were applied to the platinum electrode immersed in solution containing 1mM o-cresol and 0.5 M H_2SO_4 and the oxidation of the o-cresol monitored using in situ FTIR spectroscopy technique. The

bands seen at 1600, 1457 and around 1150 cm^{-1} were assigned to the aromatic C=C, C−C and C−O−C vibration stretches mode respectively. These assignments agree to a large extent with the assigned reported above for the o-cresol. The small shift in position of these bands observed in our spectra may be due again to the difference in our experimental conditions.

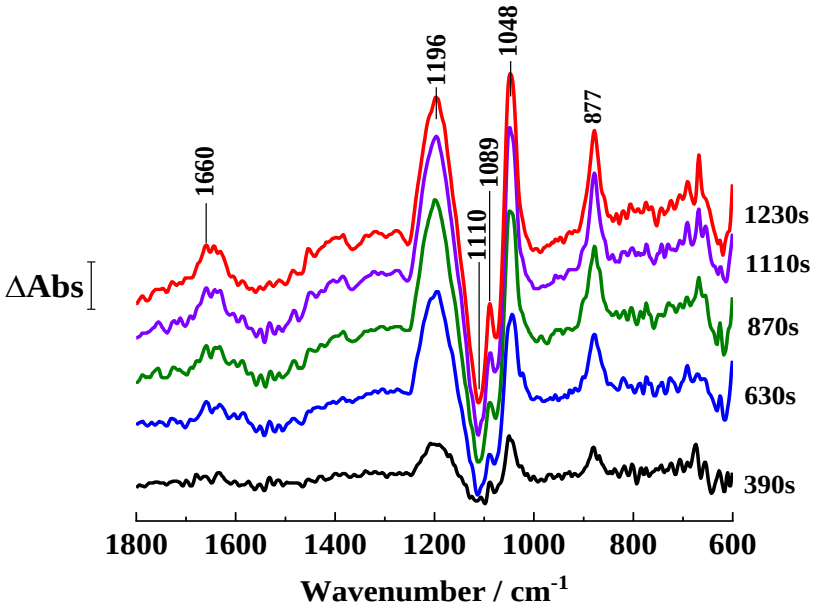

Figure 4.11: In situ FTIR spectra collected for an EPPG electrode coated with a SWCNT in 10 mM o-cresol dissolved in 0.05 M $Na_2SO_4.10H_2O$ / EtOH solution during oxidation up to 0.85 V. The spectra were averaged over 100 scans.

4.3.6 In Situ FTIR Study of m-cresol

This experiment was carried out with the goal of supporting the oxidation mechanism proposed in the last chapter with the oxidation product proposed as:

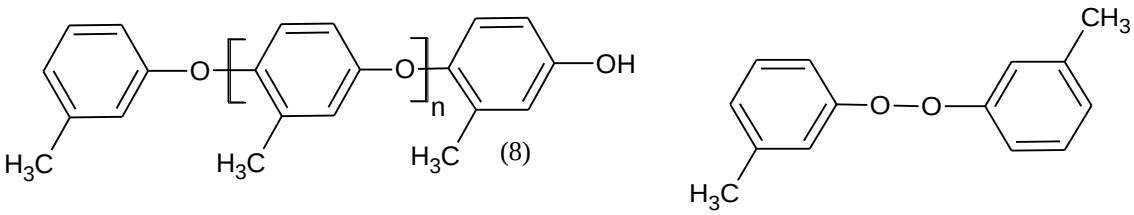

Figure 4.12 shows the in situ FTIR spectra obtained for 10mM m-cresol under the same experimental conditions as the phenol, TBP and o-cresol. The broad positive band observed between 1254 cm^{-1} and 1139 cm^{-1} is assigned to the C−O−C vibration stretch

in the polymer product formed (product 8). The increase in intensity of this band over time is associated with the decrease in intensity of the broad negative band centred at 1096 cm^{-1} which is attributed to the C−O vibration stretch in the m-cresol leading to the formation of the polymer. The band observed at 878 cm^{-1} is associated with the C−O−O−C vibration stretch in product 2. The broad band at 1642 cm^{-1} has a characteristic of O−H bending of water in the solution.

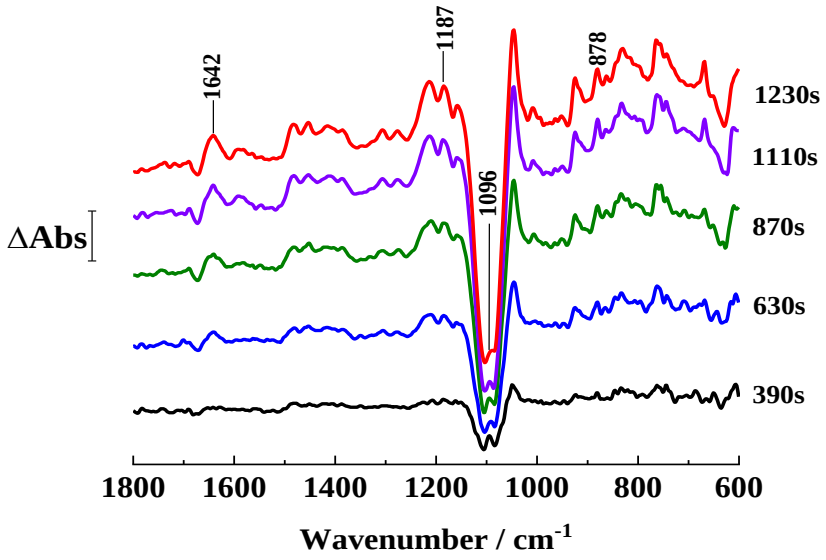

Figure 4.12: In situ FTIR spectra collected for an EPPG electrode coated with a SWCNT in 10 mM m-cresol dissolved in 0.05 M $Na_2SO_4.10H_2O$ / EtOH solution during oxidation up to 0.85 V. The spectra were averaged over 100 scans.

4.3.7 In Situ FTIR Spectra of p-cresol

The in situ FTIR difference spectra of 10 mM p-cresol in 0.1 M $Na_2SO_4.10H_2O$ / EtOH solution obtained during oxidation up to + 0.85 V under the same experimental conditions as the phenol is presented in Figure 4.13 below. This experiment was performed in order to confirm the oxidation product proposed for p-cresol in the electrochemistry chapter which was proposed to be:

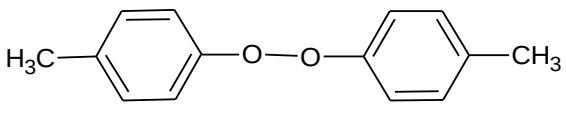

dimer 10

In the electrochemistry of p-cresol proposed in the last chapter, only dimer 10 is proposed to be formed for this compound, the polymer and quinone products are not formed. In these spectra an intense positive band having the characteristic of C−O−O−C vibration stretch is observed at 878 cm^{-1}. This band increases in intensity over time and this suggests the formation of dimer 10. Little evidence of polymer formation is seen in these spectra. The positive and negative bands seen at 1198 cm^{-1} and 1118 cm^{-1} respectively situated in the region assigned to C−O−C of the polymer product and C−O vibrations stretches in the spectra of phenol and the o-cresols are less intense in this case, therefore suggesting a little or no polymer products formation. The broad positive band observed at 1653 cm^{-1} is assigned to the OH bending of water.

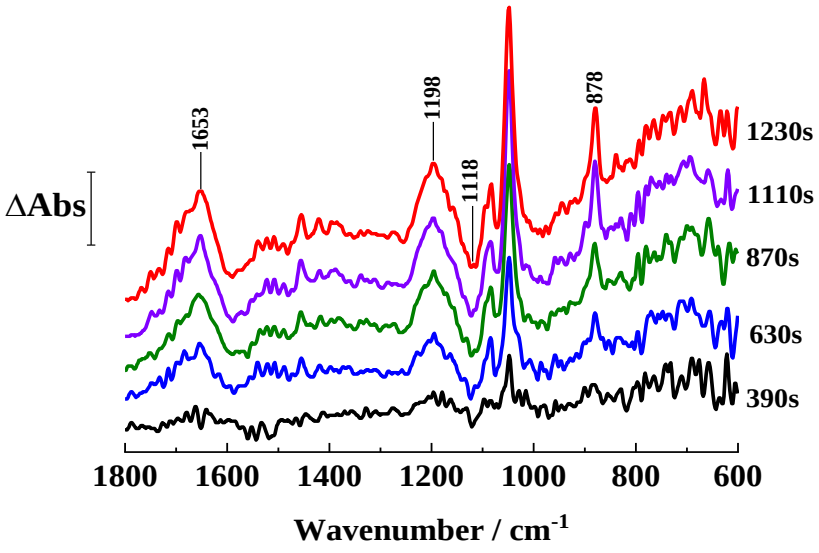

Figure 4.13: In situ FTIR spectra collected for an EPPG electrode coated with a SWCNT in 10 mM p-cresol dissolved in 0.05 M $Na_2SO_4.10H_2O$ / EtOH solution during oxidation up to + 0.85 V. The spectra were averaged over 100 scans.

4.4 Summary of Results

In the early experiments, the different phenolic compounds were characterized using ex situ FTIR spectroscopy. The samples solutions were dropped coated onto the ATR prism and overtime spectra collected for each compound for 30 mins between 4000 cm^{-1} and 500 cm^{-1} with a spectral resolution of 4 cm^{-1}. The blank ATR disc scan was taken as background and the spectra were averaged over 100 scans.

The spectral assignments for the different products between 1800 – 600 cm^{-1} is presented in Table 4.2 below. These assignments agreed well with the assignments in the literature [1],[2],[3].

Table 4.2: Summary of the assignment of the different absorption bands obtained for the different phenolic compounds after ex situ FTIR characterization.

	Vibration stretches (cm^{-1})					
	C−O	C−C	C=C	C−H oop	C−H in plane	OH bending
Phenol	1230	1500 & 1474	1596	811 & 752 & 690	1072	1367
o-cresol	1200	1466	1593	-	-	1351
m-cresol	1243	1466	1590			1342
p-cresol	1124	1512 & 1450	1307	-		1361
TBP	1234	1476 & 1436	-	-		1361

The effect of SWCNT material on the EPPG electrode surface was also investigated. This was performed by comparing the resulting spectra of 0.1 M $Na_2SO_4.10H_2O$ solutions at the EPPG with and without SWCNT electrodes interface with 0.5 V applied. This revealed that the SWCNT increases the spectral intensity of the sulfate and water bands and this was suggested to be due to the swelling of the SWCNT material and filled the existing gap between the surface of the EPPG electrode and the ATR prism upon immersion in the electrolyte. Thus then the surface area and the noise ratio resolution of the IR spectral features are increased.

Furthermore, in situ spectroscopy experiments were also carried out in PBS and $Na_2SO_4.10H_2O$ solutions in order to choose the most appropriate electrolyte for more accurate data analysis. The analysis of the resulting spectral data obtained from these experiments shows that PBS present bands which will interfere with the bands expected for the oxidation product of the different phenolic compounds notably in the region

between 1800 −1600 cm^{-1} where the C=O bands of quinone are expected. This will therefore make the analysis of the data obtained for the different phenolic compounds difficult to analyse in this solvent. In contrast, the spectra obtained for $Na_2SO_4.10H_2O$ show only two broad bands. One band in the 1800 − 1600 cm^{-1} assigned to OH bending vibration of water present in the solution and another band in the 1200 – 1000 cm^{-1} range attributed to the asymmetric stretch of SO_4^{2-}.This latter band may also interfere with the C−O and C−O−C vibration stretches bands expected for certain oxidation products. However, the interpretation of our in situ spectral data will be less problematic in this solvent. Therefore, $Na_2SO_4.10H_2O$ solution was used as electrolyte for the in situ FTIR spectroscopy experiments for the different phenolic compounds.

After the above investigations, the electrochemical oxidation of TBP, phenol and cresols on EPPG electrode coated with SWCNT were monitored in situ using ATR-FTIR spectroscopy technique. These works were carried out in order to confirm the electrochemistry mechanisms proposed for the different phenolic compounds in the electrochemistry chapter. The resulting spectra obtained at + 0.6 V for TBP show evidence of 2,4,6-tri-tert-butylphenoxyl and this radical was shown in the previous chapter to be the main oxidation product of TBP. The spectra of phenol show evidence of polymeric compound (product IX) with the bands at 1196 cm^{-1} assigned to the C−O−C vibration stretch in the polymeric products. Dimer 1 and quinone species were also confirmed as oxidation products for phenol with the bands seen at 877 cm^{-1} and at 1636 cm^{-1} assigned respectively to the C−O−O−C and C=O vibration stretches in dimer1 and the quinone compounds (quinone and dipheno-quinone) formed. The resulting spectra obtained for ortho-, meta- and paracresol show that these three isomers produced different oxidation products. While the difference spectra obtained for orthocresol show evidence of polymeric product (band at 1196 cm^{-1}assigned to the C−O−C vibration stretch), quinone species (band at 1660 cm^{-1} attributed to the C=O vibration mode) and dimer 7 type compounds (band at 877 cm^{-1} assigned to the C−O−O−C groups), polymeric and product 2 type compounds are observed in the spectra of meta-cresol with bands associated with C−O−C vibration mode in the polymer (1255 −1139 cm^{-1} range) and C−O−O−C in product 2 (at 878 cm^{-1}). In contrast to the ortho- and meta-cresol, para-cresol produces only dimer 10 as oxidation product and this is product is related to the band observed at 878 cm^{-1}.

4.5 Discussion

The suggested spectral assignments described above agreed with the electrochemistry conclusions to a large extent, however, differences have been observed particularly in the spectra of p-cresol in the 1800 – 1600 cm^{-1} range. The broad and sharp band attributed to OH bending mode of water also has a characteristic of C=O vibration stretch and this implies that quinone compound might also be formed in this case in contrast to what was observed in the electrochemistry. This can be explained by the difference in the experimental conditions (pH, concentration, change of solvent). In the electrochemistry chapter, PBS at pH11 was used as the electrolyte while $Na_2SO_4.H_2O$ / EtOH at pH ~ 7 was used as electrolyte instead in here. In this later electrolyte at the lower pH the second electron transfer route leading to the production of the phenoxium cation in the electrochemistry chapter should be taken into account as shown in scheme 3.2 in section 3.3.2.4 (chapter 3). These cations can undergo hydrolysis to produce monomeric quinone compounds. Thus then additional bands that can be relate to the C=O vibration of these monomeric quinone species can also be observed in the spectra of phenol and the cresols.

In the electrochemistry chapter, it was shown that only 10% of these phenolic compounds are converted into quinone species and the rest is converted into polymeric products. Therefore, there is a higher percentage of these polymeric products in the probing area. This might explain the increasing spectral intensity of the band attributed to the C−O−C vibration mode of the polymeric compounds and the greater sensitivity of these measurements to the polymer compared to dissolved quinones.

In comparison to previous studies on in situ spectroelectrochemical study of phenolic compounds using FTIR spectroscopy technique where the electrochemical cell used limits the spectroscopy technique to the detection of species of concentration approximately greater than 20 mM, the cell used in here allow species with concentration below 20 mM to be detected. For example, 2.5 mM of TBP and 10 mM of phenols and cresols were needed to obtain high resolution spectra of these compounds in this work. In addition, the experimental set-up in this work is easy to understand and only required small samples preparation. However, some limitations of the technique have been observed. The first problem encountered was the presence of ethanol in our system. Ethanol was used to help dissolved the TBP, so to maintain the same experimental conditions for all the phenolic compounds, ethanol was used in all in situ FTIR

spectroscopy experiments, but the presence of the ethanol has make our system very complex. The second limitation is that the existing gap between the EPPG electrode surface and the ATR prism. Even if we assumed that, this gap was filled due to SWCNT modification, we are not sure about the exact electrode-prism separation and where we are actually probing and this needs to be investigated further in future works.

4.6 Conclusion

Extending on the work presented in chapter 3, the spectroelectrochemical oxidation of TBP, phenol and cresols were investigated in situ using FTIR spectroscopy in order to confirm the oxidation mechanism of these phenolic compounds proposed. Firstly, this work has shown that the use of SWCNT on the EPPG electrode surface increase the surface area and hence improve the signal to noise ratio resolution of the IR spectral features. This was shown by the increase in intensity of the sulfate band when a positive potential was applied to the SWCNT modified EPPG electrode immersed in 0.05 M $Na_2SO_4.H_2O$ / EtOH in comparison to the sulfate band observed under the same experimental conditions but with the non- modified EPPG electrode.

Secondly, the changes in the solution electrolyte species at the electrode interface when a positive potential was applied was also observed.

Thirdly and more importantly, the analysis of the spectral data obtained has revealed that this technique can be successfully used to detect the product of the phenolic compounds oxidation. The different peaks obtained for the different compound suggest that different oxidation mechanism is observed with different phenolic compounds. The analysis of the spectral data obtained has allowed us to identify several peaks that were related to the oxidation products of the different phenolic compound proposed in the last chapter.

References for Chapter 4

[1] R. D. Webster, "In Situ Electrochemical-ATR-FTIR Spectroscopic Studies on Solution Phase 2 , 4 , 6-tri-substituted Phenoxyl Radicals," *Electrochem. commun.*, vol. 5, pp. 6–11, 2003.

[2] H. J. Salavagione, J. Arias, P. Garcés, E. Morallón, C. Barbero, and J. L. Vázquez, "Spectroelectrochemical Study of the Oxidation of Aminophenols on Platinum Electrode in Acid Medium," *J. Electroanal. Chem.*, vol. 565, no. 2, pp. 375–383, 2004.

[3] Z. Taleb, F. Montilla, C. Quijada, E. Morallon, and S. Taleb, "Electrochemical and In Situ FTIR Study of O-Cresol on Platinum Electrode in Acid Medium," *Electrocatalysis*, vol. 5, no. 2, pp. 186–192, 2014.

[4] M. Lounasvuori, "Electrochemical and Spectroscopic Studies of Graphene Nanoflakes with Functionalised Edges," University College London, 2017.

[5] M. C. Pham, F. Adami, and P. C. Lacaze, "In Situ Study by Multiple Internal Reflection Fourier Transform Infrared Spectroscopy (MIRFTIRS) of the Phenoxy Radical during Anodic Oxidation of Phenol Derivatives on Iron," *J. Electrochem. Soc.*, vol. 136, no. 3, pp. 677–679, 1989.

[6] M. Lounasvuori and K. B. Holt, "Acid Deprotonation Driven by Cation Migration at Biased Graphene Nanoflake Electrodes," *Chem. Commun.*, vol. 53, no. 15, pp. 2351–2354, 2017.

[7] G. J. Wilson, C. Y. Lin, and R. D. Webster, "Significant Differences in the Electrochemical Behavior of the α-, β-, γ-, and δ-Tocopherols (Vitamin E)," *J. Phys. Chem*, vol. 110, no. 23, pp. 11540–11548, 2006.

[8] J. G. Radziszewski, "Electronic States of the Phenoxyl Radical," *J. Chem. Physic*, vol. 115, no. 21, pp. 9733–9740, 2001.

[9] T. M. Craw and C. M. Depew, "Contributions of Electron Spin Resonance Spectroscopy to the Study of Vitamins C, E and K," *Rev. Chem. Intermed.*, vol. 6, no. 1, pp. 1–31, 1985.

[10] L. Valgimigli, T. J. Banks, U. K. Ingold, and J. Lusztyk, "Kinetic Solvent Effects on Hydroxylic Hydrogen Atom Abstractions Are Independent of the Nature of the Abstracting Radical. Two Extreme Tests Using Vitamin E and Phenol," *J. Am. Chem. Soc.*, vol. 117, no. 40, pp. 9966–9971, 1995.

[11] M. Matsuo and S. Matsumoto, "Electron Spin Resonance Spectra of the Chromanoxyl Radicals Derived from Tocopherols (vitamin E) and their Related Compounds," *J. Am. Oil Chem. Soc.*, vol. 18, no. 1, pp. 81–86, 1983.

[12] R. D. Webster, "In situ electrochemical-ATR-FTIR spectroscopic studies on solution phase carboxylate radical anions," *J. Chem. Soc. , Perkin Trans. 2*, no. 11, pp. 1882–1888, 2002.

[13] R. M. Silverstein, F. X. Webster, and D. J. Kiemle, *Spectrometric Identification of Organic Compounds*, 7th ed. New York: John Wiley & sons, inc, 2005.

[14] H. J. Salavagione, J. Arias-Pardilla, J. L. Vázquez, M. C. Miras, E. Morallón, and C. Barbero, "Spectroelectrochemical Study of the Oxidation of Diaminophenols on Platinum Electrodes in Acidic Medium," *Electrochim. Acta*, vol. 50, no. 27, pp. 5414–5422, 2005.

[15] Y. Song, "Theoretical studies on electrochemistry of p-aminophenol," *Spectrochim. Acta - Part A Mol. Biomol. Spectrosc.*, vol. 67, no. 3–4, pp. 611–618, 2007.

[16] C. Barbero, J. J. Silber, and L. Sereno, "Formation of a Novel Electroactive Film by Electropolymerization of Ortho-Aminophenol. Study of its Chemical Structure and Formation Mechanism. Electropolymerization of Analogous Compounds," *J. Electroanal. Chem.*, vol. 263, pp. 333–352, 1989.

[17] A. Chtaini, S. Zaroual, A. Bellouchou, M. Boulghallat, A. Gamouh, and R. Najih, "Electrochemical Study of the Capacity of Moringa Oleifera to Chelate p-Aminophenol," *Glob. J. Med. Res. B Pharma, Drug Discov. Toxicol. Med.*, vol. 15, no. 5, pp. 9–18, 2015.

[18] T. Ohsaka, S. Kunimuna, and N. Oyama, "Electrode Kinetics of Poly (o-aminophenol) Film Prepared by Electro-Oxidative Polymerization of O-Aminophenol and its Electrochromic Properties," *Electrochem. Acta*, vol. 33, no. 5, pp. 639–645, 1988.

[19] Y. Yang and Z. Lin, "Effects of Surface Oxide Species on the Electropolymerization of O-Aminophenol on Pretreated Glassy Carbon Electrodes," *Synth. Met.*, vol. 78, no. 2, pp. 111–115, 1996.

[20] R. Tucceri, P. Arnal, and A. Scian, "Electrosynthesis and Spectroscopic Characterization of Poly(o-Aminophenol) Film Electrodes," *Polym. Sci.*, vol. 12, pp. 1–26, 2012.

[21] R. Tucceri, P. Arnal, and A. Scian, "Spectroscopic Characterization of Poly(ortho - aminophenol) Film Electrodes," *J. Spectrosc.*, vol. 1, no. 1, 2013.

[22] S. K. Devi, J. Malviya, L. K. Sharma, and R. K. P. Singh, "Electro Organic Synthesis and Characterization of Phenol–Aniline Based Copolymers," *Polym. Sci. Ser. B*, vol. 59, no. 3, pp. 300–307, 2017.

[23] K. M. Richard and A. A. Gewirth, "In Situ STM and IR Studies of Phenoxide Electrooxidation on Au(111) Electrode Surfaces," *J. Phys. Chem*, vol. 99, pp. 12288–12293, 1995.

[24] A. D. Long, *Infrared and Raman Characteristic Group Frequencies Tables and Charts*, 3nd ed. Chichester: John Wiley and Sons, Ltd, 2001.

[25] I. J. D. Ebenezar, S. Ramalingam, C. R. Raja, and P. C. Jobe, "Vibrational Spectroscopic [IR and Raman] Analysis and Computational Investigation [NMR , UV-Visible , MEP and Kubo gap] on L-Valinium Picrate," *J. Nanotechnol. Adv. Mater.*, vol. 2, no. 1, pp. 11–25, 2014.

[26] F. Hernandez and H. Baltruschat, "Electrochemical Characterization of Gold Stepped Surfaces Modified With Pd," *Langmuir*, vol. 18, no. 12, pp. 4659–4666, 2002.

[27] C. Morin, D. Simon, and P. Sautet, "Density-Functional Study of the Adsorption and Vibration Spectra of Benzene Molecules on Pt(111)," *J. Phys. Chem. B*, vol. 107, no. 2995–3002, 2003.

[28] F. N. Ajjan, M. J. Jafari, T. Rębiś, T. Ederth, and O. Inganäs, "Spectroelectrochemical Investigation of Redox States in a Polypyrrole/Lignin Composite Electrode Material," *J.*

Mater. Chem. A, vol. 3, no. 24, pp. 12927–12937, 2015.

[29] F. Matemadombo, M. D. Maree, K. I. Ozoemena, P. Westbroek, and T. Nyokong, "Synthesis, Electrochemical and Spectroelectrochemical Studies of Octaphenylthio-Substituted Phthalocyanines," *J. Porphyr. Phthalocyanines*, vol. 09, no. 07, pp. 484–490, 2005.

[30] M. Gattrell and D. W. Kirk, "A Fourier Transform Infrared Spectroscopy Study of the Passive Film Produced During Aqueous Acidic Phenol Electro-Oxidation," *J. Electrochem. Soc.*, vol. 139, no. 10, pp. 2736–2744, 1992.

[31] A. Almeida, J. A. Moulijn, and M. Guido, "In Situ ATR-FTIR Study on the Selective Photo-Oxidation of Cyclohexane over Anatase TiO2," *J. Phys. Chem.*, vol. 112, no. 5, pp. 1552–1561, 2008.

[32] N. B. Colthup, L. H. Daly, and S. E. Wiberley, *Introduction to Infrared and Raman Spectroscopy*, 3rd ed. New York: Academic Press, 1990.

[33] R. A. Nyquist, *Interpreting Infrared, Raman, and Nuclear Magnetic Resonance Spectra*, 3rd ed. New York: Academic Press, 2001.

[34] A. Q. Zhanga, Q. C. Cuia, Z. Y. Chen, and Y. J. Lee, "Synthesis and Electrochromic Properties of Poly-O-Aminophenol," *J. Electroanal. Chem.*, vol. 373, no. 1–2, pp. 115–121, 1994.

[35] L. H. Mascaro, A. N. Berton, and L. Micaroni, "Electrochemical Synthesis of Polyaniline / Poly-O -Aminophenol Copolymers in Chloride Medium," *Int. J. Electrochem.*, vol. 2011, pp. 1–8, 2011.

[36] C. Barbero, J. J. Silber, and L. Sereno, "Electrochemical Properties of Poly-Ortho-Aminophenol Electrodes in Aqueous Acid Solutions," *J. Electroanal. Chem.*, vol. 291, pp. 81–101, 1990.

[37] A. Guenbour, A. Ben Bachir, L. Aries, and A. Kacemi, "Electropolymerization of 2-Aminophenol: Electrochemical and Spectroscopic Studies," *Prog. Org. Coatings*, vol. 38, pp. 121–126, 2000.

[38] R. D. Little and K. D. Moeller, "Organic Electrochemistry as a Tool for Synthesis," *Electrochem. Soc. Interface*, pp. 36–42, 2002.

[39] R. M. Silverstein, G. C. Bassler, and T. C. Morrill, "Spectrometric Identification of Organic Compounds," 1981.

[40] J. Shwarz, H. Kaden, F. Schumer, and W. Oelbner, "Voltammetric and Spectroelectrochemical Studies on 4-aminophenol at Gold Electrodes in Aqueous and Organic Media," *Electrochem. Acta*, vol. 48, no. 17, pp. 2479–2486, 2003.

[41] I. Brand, J. J. Debinska, L. Wickramasinghe, and C. N. Verani, "An in Situ Spectroelectrochemical Study on the Orientation Changes of an [FeIIILN2O3] Metallosurfactant Deposited as LB Films on Gold Electrode Surfaces," *Dalt. Trans.*, vol. 47, no. 40, pp. 14218–14226, 2018.

[42] Š. Komorsky-Lovrić, V. Mirčeski, C. Kabbe, and F. Scholz, "An in Situ Microscopic Spectroelectrochemical Study of a Three-Phase Electrode Where an Ion Transfer at the Water|Nitrobenzene Interface is Coupled to an Electron Transfer at the Interface ITO|Nitrobenzene," *J. Electroanal. Chem.*, vol. 566, pp. 371–377, 200

Chapter 5

Chemical Oxidation of Polystyrene Studied with In Situ Infrared Spectroscopy

5.1 Introduction

Polystyrene (PS) is a synthetic polymer made from vinyl polymerization of the monomer styrene, and structurally it is composed of a long hydrocarbon chain with a phenyl group attached to every other carbon atom. Polystyrene due to its exclusive properties (durability, appearance, low cost, etc.) is one of the most used polymers in the manufacturing industry [1]. However, the accumulation of the polystyrene waste in the environment has become a great source of concern leading to pollution problems. Therefore, it is important to study polystyrene degradation in order to understand the degradation mechanisms to help in preventing or reducing environmental pollution [2].

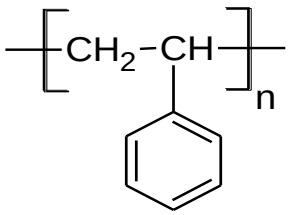

Structure of Polystyrene

Although degradation of polystyrene has been the subject of extensive studies, the degradation mechanisms are still not well understood especially in chemical oxidation. Therefore, this work will focus on monitoring the changes in chemical structure to polystyrene upon treatment with oxidising agents in order to understand the oxidation mechanisms. Polystyrene can undergo chemical oxidation under the effect of oxidising agents such as $IrCl_6^{2-}$ which has a reduction potential of 0.75 V (vs Ag / AgCl) [3]. This is hard to rationalise considering the structure of polystyrene, as the saturated hydrocarbon backbone and phenyl ring should not be easily oxidised at this potential

(benzene and toluene are known to undergo oxidation at a potential above 2 V (vs. Ag / AgCl)) [3]. But polystyrene has defect sites present in its structure such as substituted phenols that can be oxidised at 0.70 V (vs. Ag / AgCl) and it may be these that undergo oxidation under the action of relatively mild oxidising agent.

The aim of this work is to acquire further insight into the oxidation mechanisms of polystyrene. For this purpose, in situ infrared experiments have been designed to detect changes to the polystyrene structure in the presence in solution of oxidizing agents such as iridium (IV) tetrachloride, iridium (IV) hexachloride, hydrogen peroxide and potassium ferricyanide. Before these experiments, ex situ infrared spectra were obtained and assigned for the unoxidised and oxidised polystyrene (see section 5.3.1.1 and 5.3.1.2), the effect of adsorbed water on the spectra of the non-oxidised and oxidised PS was also investigated.

5.2 Experimental Methods

In this study, a cleaned suspension of monodisperse 800 nm diameter polystyrene beads was used. This was obtained from sulfate-terminated PS beads purchased from Sigma-Aldrich (LB7, 10% solids in aqueous suspension) that were cleaned by membrane dialysis against water to remove the extraneous agents (sodium dodecyl sulfate surfactant, potassium sulfate and sodium bicarbonate). The TEM image and chemical structure of this PS beads are presented in Fig.5.1.

The oxidising agents (iridium (IV) tetrachloride, iridium (IV) hexachloride, potassium ferricyanide and hydrogen peroxide) were purchased from Sigma-Aldrich.

The oxidised polystyrene bead samples were obtained by chemically treating the non-oxidised polystyrene bead suspension with 5 mM solution of the oxidising agent under study.These PS samples were separated from the oxidizing reagent solution by centrifugation using an Eppendorf centrifuge 5415D instrument (with four cleaning and rinsing steps) followed by re-suspension in de-ionized water and stored in polypropylene centrifuge tubes for later use.

For all ATR-FTIR analysis a Bruker Tensor 27 Fourier-transform spectrometer equipped with a diamond crystal prism and an Opus data collection program in absorbance mode was used. The spectra were recorded from 4000 cm^{-1} to 400 cm^{-1} with a resolution of

4 cm^{-1}. The absorption band between 2500 cm^{-1} and 1800 cm^{-1} related to absorption by the diamond prism was cut out from the spectra for more accurate data analysis.

For some experiments, polystyrene pre-treated with Ir (IV) tetrachloride chloride solution were analysed under dry air, water vapour and Argon. The oxidised sample was drop-coated onto the ATR prism and allowed to dry at room temperature for 2 hours. Either dry air, Ar and H_2O saturated air was then passed over the sample.

In order to investigate the effect of water on non-oxidised and oxidised PS, 5µL of the non-oxidised and oxidised PS suspension were separately drop-coated onto the ATR prism and allowed to dry at room temperature for 1 hour and exposed to vacuum for 15 mins to remove any excess of water. 1mL of de-ionised water was then added to the sample compartment and the solvated films allowed to equilibrate for 5 min before collecting the background spectrum. Difference spectra were then collected relative to this background every 5 min for 2 hours (see Fig 5.2). For all the in situ oxidation experiments, 5 µL of non-oxidised PS suspension was drop-coated onto the ATR prism and left to dry for 1 hour to form an adherent film.1 mL of water was then added to the sample compartment and the solvated PS film allowed to equilibrate for 5 min before collecting the background spectrum. 100 µL of the corresponding oxidising agent solution was added to the sample compartment and left to settle for 10 min. Difference spectra were then collected relative to this background, every 5 min for 3 hours between $4000 - 400$ cm^{-1} with a spectral resolution of 4 cm^{-1}.

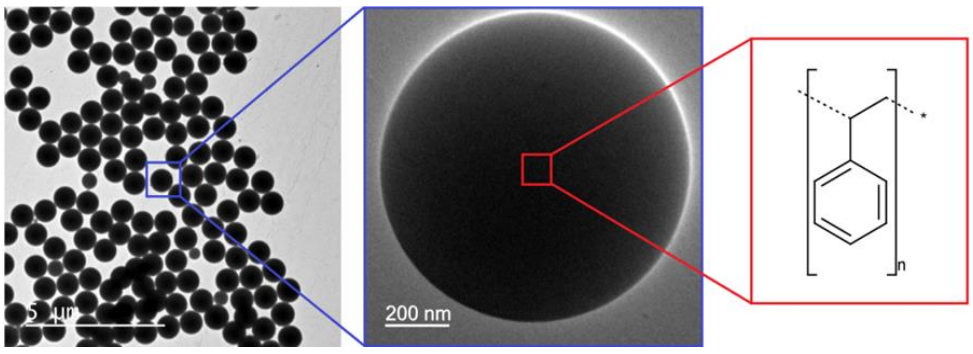

Figure 5.1: TEM image and chemical structure of polystyrene under study [3].

5.3 Results and Discussions

5.3.1 FTIR Analysis of the Polystyrene under Study

5.3.1.1 Analysis of the non-oxidised Polystyrene

In early stages of our study, the as-received polystyrene was characterised using FTIR spectroscopy and the resulting spectrum is presented in Figure 5.2. The absorption bands at 3059 cm^{-1} and 3026 cm^{-1} are assigned to the aromatic C−H stretching vibrations. The peaks at 2925 cm^{-1} and 2848 cm^{-1} are attributed to the asymmetric and symmetric stretching vibrations of the methylene groups (CH_2) respectively. The absorption band at 1600 cm^{-1} is assigned to the C=C stretching vibration in the ring [4], [5]. The peaks at 1494 cm^{-1} and 1453 cm^{-1} correspond to the C−C stretching vibrations in the aromatic ring. However, the band at 1453 cm^{-1} maybe also assigned to the methylene $–CH_2$ deformation vibration [6]. The in-plane C−H bending (also called rocking where the structural unit swings back and forth in the plane of the molecule) of the aromatic ring are observed in the 1200 − 1000 cm^{-1} range. The absorption bands ranging from 906 − 690 cm^{-1} correspond to the out of plane (oop) C−H bending (also called twisting; this is where the structural unit rotates about the bond which joins it to the rest of the molecule) of the phenyl ring, with the most intense peaks at 699 cm^{-1} and 754 cm^{-1}. These bands are characteristic of the substitution pattern in the ring. A summary of the band assignments is given in Table 5.1.

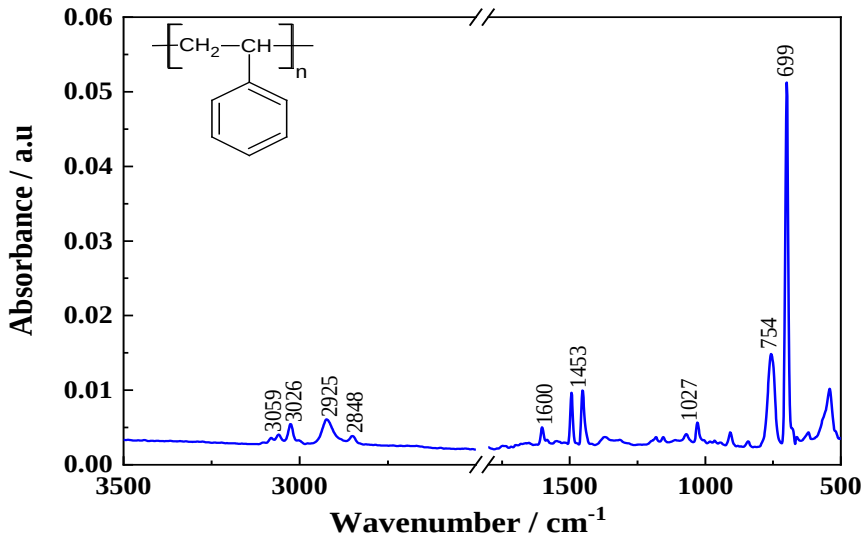

Figure 5.2: FTIR spectrum of non - oxidised polystyrene film under study. The background was taken prior to sample deposition. The spectrum was averaged over 100 scans.

Table 5.1: Summary of characteristic infrared absorption bands of the non-oxidised polystyrene under study [4], [5], [6].

Wavenumber (cm^{-1})	Bands Assignment
3100 − 3000	C−H aromatic stretching
2925	-CH_2 asymmetric stretching
2848	-CH_2 symmetric stretching
1600	C=C Aromatic stretching
1500 − 1300	C−C Aromatic stretching
1200 − 1000	C−H in plane bending stretching in the ring
950 − 690	C−H out of plane bending stretching in the ring

The individual band assignments of the polystyrene under study are in accordance with the published data. The diamond cut-out band between 2500 and 1800 cm^{-1} is known to contain anomalous absorption bands and has been excluded from the graphs for more accurate data analysis.

5.3.1.2 Analysis of Polystyrene treated with different Oxidising Agents

5.3.1.2.1 FTIR Characterization of PS treated with Iridium (IV) Tetrachloride and Hydrogen Peroxide.

The effect of strong oxidising agents such as iridium (IV) tetrachloride and hydrogen peroxide (H_2O_2) on the PS surface was investigated by pre-treating the PS with the relevant oxidising agent and the resulting FTIR spectra obtained are presented in Figure 5.3. A very broad signal with maxima at 3399 cm^{-1} and 3367 cm^{-1} typical of OH stretches appears in the 3600 − 2500 cm^{-1} region for the PS treated with iridium (IV) tetrachloride and H_2O_2 solutions respectively. Within this band, the sharp aromatic and aliphatic C−H stretches in the polystyrene are seen in the 3100 − 3000 cm^{-1} and 3000 − 2800 cm^{-1} regions respectively. The intense signal seen in the range 1800 − 1600 cm^{-1} is assigned to C=O groups. The broadness of this band suggests the formation of various carbonyl compounds such as carboxylic acids, ketones and aldehydes. The peaks observed in the 1600 − 1400 cm^{-1} region are attributed to C=C in the phenyl ring. The in plane and out

of plane C−H stretches are observed in the 1300 −1000 cm^{-1} and 900 − 690 cm^{-1} ranges respectively for the PS treated with iridium tetrachloride. In the spectrum of PS treated with H_2O_2 the in-plane C− H bands are replaced by a broad band between 1200 − 1000 cm^{-1} characteristic of C− O stretch of carboxylic acids and alcohol. The out of plane C−H bands range extending around 900 cm^{-1} also suggests a di-substitution (1,3-disubstitution) in the phenyl ring [7] . In the band attributed to OH stretches (3600 − 2500 cm^{-1}), it was not possible to distinguish between the OH stretches resulting from the oxidation of the polymer (i.e. alcohol, carboxylic acid or phenol functionalities on the PS surface) and physisorbed water, and therefore this was investigated further (see section 5.3.1.2.2). Comparing the two spectra in Fig.5.3a and Fig.5.3b, they look similar to some extent, however, some differences can be observed in the C=O, C−C, in plane and out of plane C−H bending region. The peak attributed to C−O stretch seen in spectra (b) is not observed in spectra (a). The C−C band in the 1500 − 1400 cm^{-1} region which is broad for PS treated with H_2O_2 (Fig. 5.3b), splits into two distinct peaks for the PS treated with Ir (IV) tetrachloride (Fig.5.3a). Additionally, the band associated with in plane C− H bending vibration in the 1300 −1000 cm^{-1} region are not seen for the PS treated with hydrogen peroxide but a broad band characteristic of C− O vibration stretch is observed instead. Two additional peaks in the 1000 − 850 cm^{-1} range associated with the out of plane C−H stretch is also observed in the spectrum of PS treated with H_2O_2. The changes to the spectra in these regions may be attributed to different substitution patterns in the phenyl ring upon oxidation.

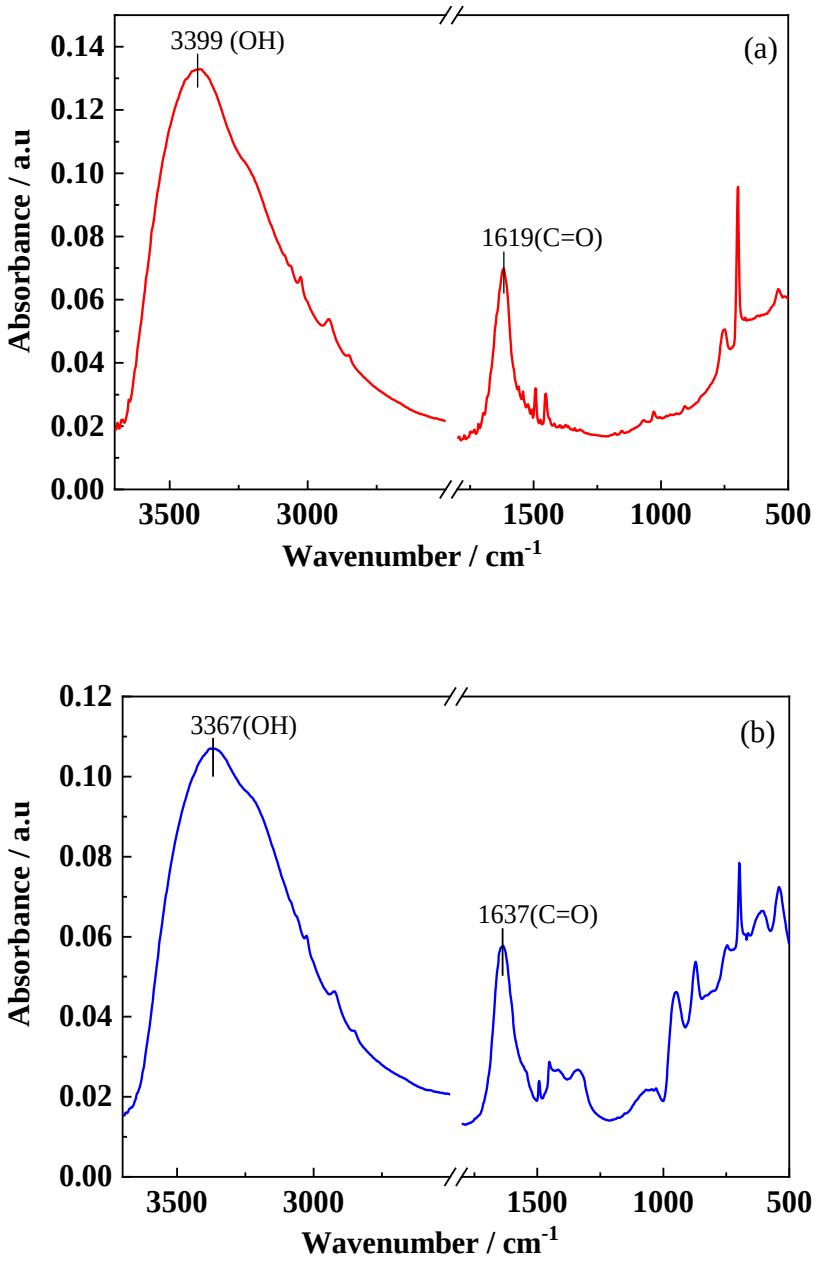

Figure 5.3: FTIR spectra of polystyrene: (a) treated with iridium (IV) tetrachloride and (b) treated with hydrogen peroxide. The background was taken prior to sample deposition. The spectra were collected between 4000 − 400 cm^{-1} with spectral resolution of 4 cm^{-1} and each spectrum averaged over 100 scans.

In order to investigate if substituted phenols are also formed during oxidation as reported in other studies [8], [9], substituted phenols such as ortho-, meta- and paracresols were characterized under the same experimental condition as the PS treated with iridium (IV) tetrachloride and hydrogen peroxide. The spectra obtained (Fig.5.4) were then compared to the spectra in Fig.5.3.

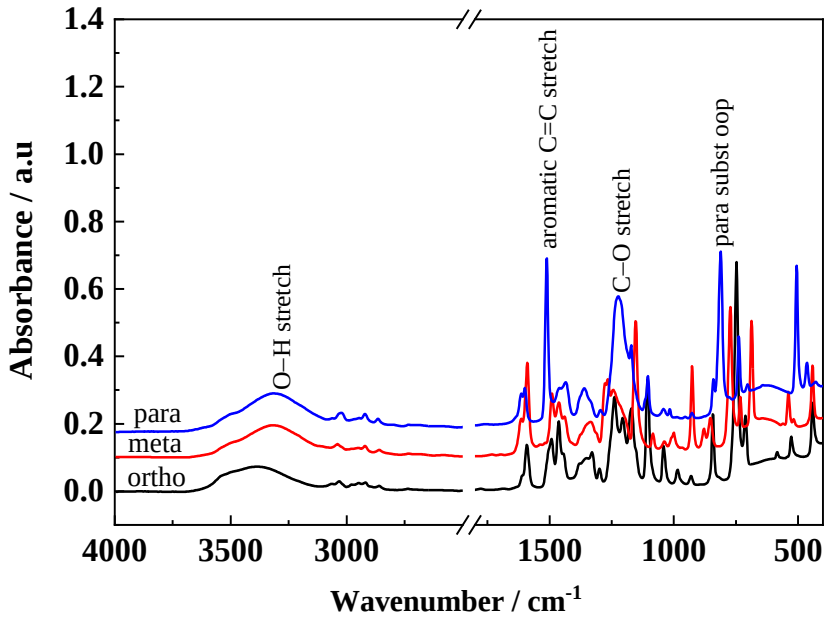

Figure 5.4: FTIR spectra of methylphenols: (black) o-cresol; (red) m-cresol; (blue) p-cresol. The background was taken with no sample deposition. The spectra were collected between 4000 − 400 cm^{-1} with spectral resolution of 4 cm^{-1} and averaged over 100 scans.

The IR spectra of methylphenols are well known in the literature and the broad absorption band located at 3600 −3100 cm^{-1} is attributed to OH stretch. These compounds also show C−O band in the 1260 − 1000 cm^{-1} region. The band observed in the 1540 − 1420 cm^{-1} region is attributed to C=C stretch in the ring. The in plane C− H bending vibration bands are seen in the 1123 − 1000 cm^{-1} region for o-cresol, this bands are 52 cm^{-1} and 7 cm^{-1} shifted towards higher wavenumber in the spectra of m-cresol and para-cresol respectively. The bands observed in the 1000 − 600 cm^{-1} range are assigned to the out of plane C−H bending vibration. This band differentiates the isomers (ortho, meta, and para). Within this bands associated with the oop C−H bending, additional intense peaks are observed in the 950 − 850 cm^{-1} region in the spectrum of m-cresol only and these peaks are also observed in the spectrum of PS treated with H_2O_2, suggesting formation of a meta substituted product.

The difference in spectra observed for the oxidised polystyrene suggests incorporation of oxygen at different sites in the phenyl ring depending on which oxidising agents is used.

By analogy to past findings and the interpretation of the IR spectra obtained for the two PS samples a reaction mechanism can be proposed. For the PS treated with H_2O_2, the reaction is more likely to be initiated by the hydroxyl radical resulting from the decomposition of H_2O_2 (cf scheme 5.1). This radical can then abstract hydrogen either from the tertiary carbon attached to the ring or the ring (in meta position) to produce a polystyryl radical and water (see scheme 5.1).

Initiation

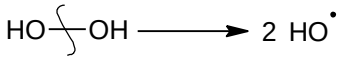

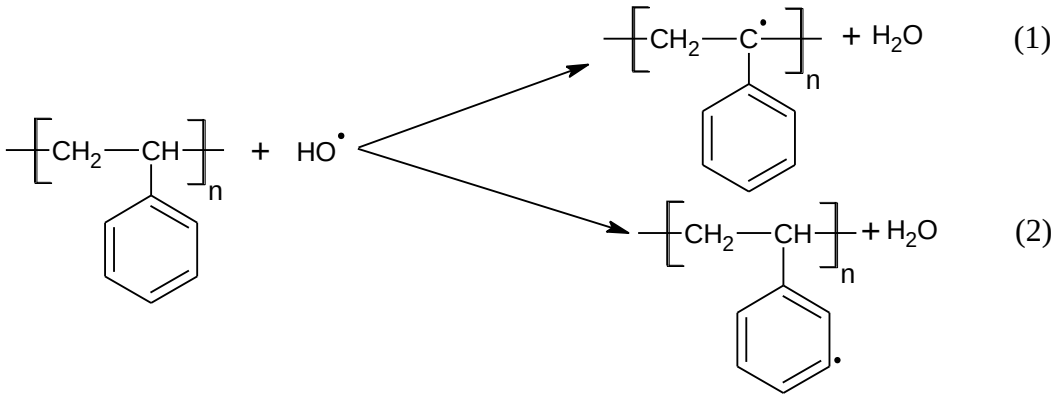

Scheme 5.1

Further reaction of the radical with dissolved oxygen can result in a hydroxyl group being incorporated either along the main chains or in the meta position in the ring (this is confirmed by the C−H out of plane bands observed between 1000 − 690 cm^{-1} in the IR spectrum, attributed to 1,3 disubstitution in the ring) [9] resulting in the formation of different alcohols, ketones and carboxylic acid type compounds (see scheme 5.2). In this scheme, the polystyryl radical generated through route (1) reacts with oxygen (O_2) to give peroxy radical with the OO group linked to the carbon attached to the phenyl ring. This peroxy radical can abstract hydrogen from another polystyrene molecule to form compound 1. This compound is known to be unstable and can decompose to give a polystyryl carbonyl that can abstract hydrogen from another polystyrene molecule to form an alcohol (compound 2) or can undergo β chain scission of the C− Ph bond leading to compound 5 or scission of the C−CH_2 bond which can result in the formation of

compounds 3 and 4. The polystyryl radical produced through route (2) also results in a peroxy radical after reacting with oxygen but the peroxide group is formed in the meta position on the phenyl ring in this case. The reaction then follows similar pathways as in route (1), leading to the formation of phenol (compound 6) only. There is also possibility of formation of carbonyl type compound with formation of hydroxyl group in meta positon in the phenyl ring following similar pathway as in Scheme 3.5 [10],[11]. The bands observed in the $1800 - 1600\ cm^{-1}$ region can then be related to compound 3, 4 and 5; and the broad band in the $3600 - 2500\ cm^{-1}$ range to compounds 4 and 6. Although, route (1) is possible, the interpretation and comparison of the IR spectrum with the spectra of methylphenols, suggests a meta-substituted phenol oxidation product formation which is consistent with route (2) and leading to compound 6.

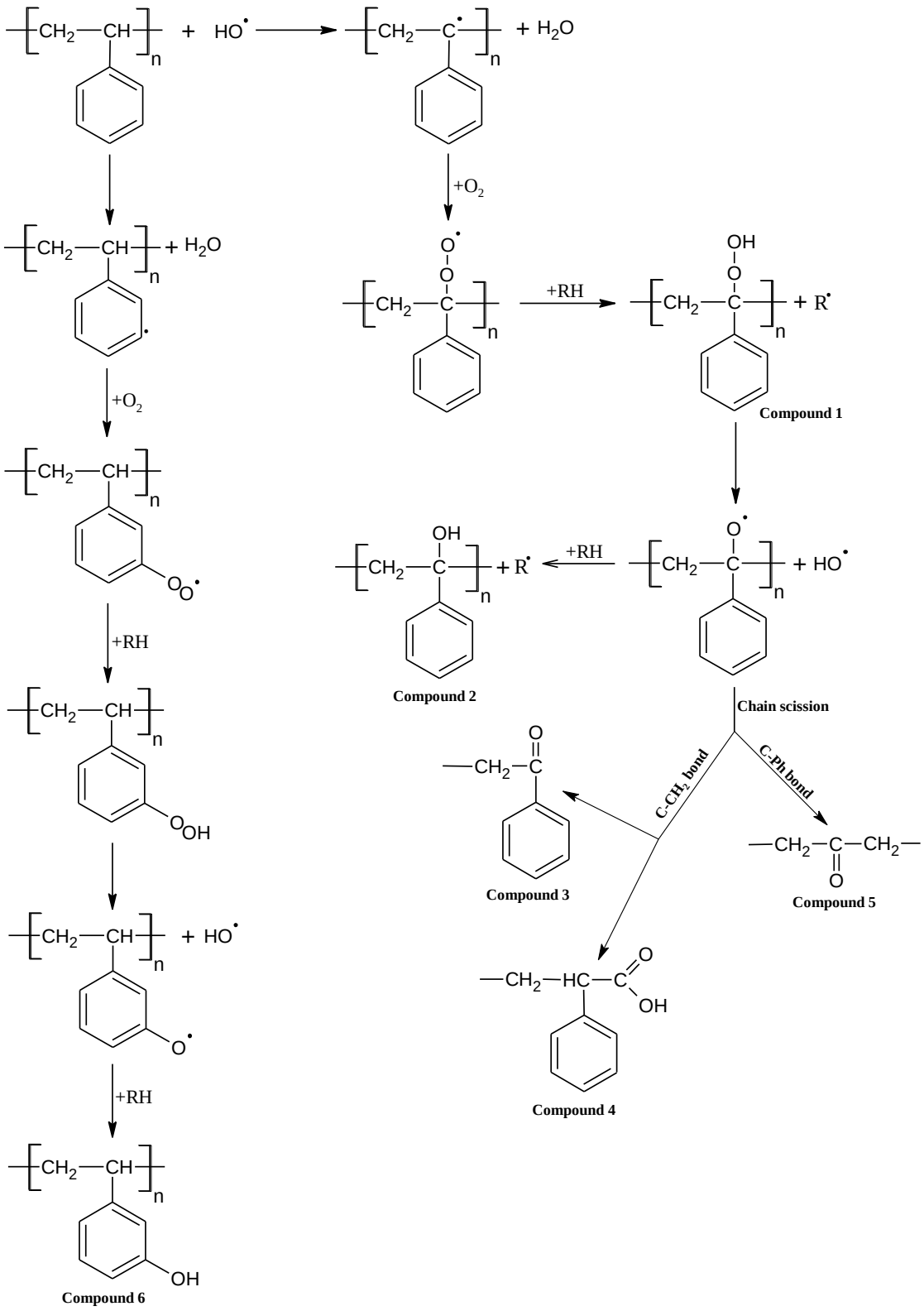

Scheme 5.2 Proposed Oxidation Mechanism for PS treated with H_2O_2 and iridium (IV) tetrachloride.

Two reaction mechanisms can possibly be suggested for PS treated with iridium (IV) tetrachloride. The first mechanism is initiated by the hydroxyl radical generated from the reaction of iridium (IV) with water (cf scheme 5.3). The reaction then follows similar pathways as in scheme 5.2.

$$Ir^{4+} + H_2O \rightarrow {}^{\bullet}OH + H^{+} + Ir^{3+}$$

Scheme 5.3

Alternatively, direct oxidation of polystyrene by the iridium (IV) can take place (see scheme 5.4), leading to the formation of the polystyryl radical as in route (1) (scheme 5.1). The reaction then follows similar pathways, resulting in the formation of alcohol (compound 2), ketones (compound 3 and 5) and carboxylic acid (compound 4). In this case, the interpretation and comparison of the IR spectrum in Fig.5.3a with the spectra of substituted phenols (in Fig.5.4), suggests little evidence of substituted phenols being formed, therefore the oxidation reaction leading to route (1) is predominant.

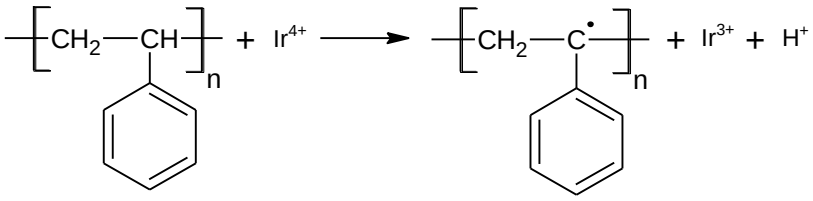

Scheme 5.4

5.3.1.2.2 Investigation of the broad OH stretches band seen in the 3600 - 2600cm^{-1} region in section 5.3.1.2.1

In order to distinguish between the OH stretching vibration at 3600 − 2600 cm^{-1} from physisorbed water and surface bound hydroxyl group resulting from the oxidation of the polystyrene (Fig.5.3), experiments were carried out where polystyrene previously treated with Ir (IV) tetrachloride chloride was analysed under dry air, water vapour and argon. In each experiment, the treated PS sample was drop-coated onto the ATR prism and allowed to dry at room temperature for 2 hours. The spectrum of the dry film was collected as the background spectrum. Either dry air, Ar or H_2O saturated air was then passed over the sample. The spectra were then collected every 5 min for 2 hours between 4000 − 400 cm^{-1} with a spectral resolution of 4 cm^{-1}.

The resulting difference spectra are shown in Figure 5.5. In these difference spectra the variation of the absorbance intensity of the OH stretching vibration band in the 3600 − 2600 cm^{-1} region will be examined. The treated PS sample purged with argon (in Figure 5.5a) shows three dependent bands located between 3650 − 3320 cm^{-1}, 3320 − 2900 cm^{-1} and 2900 − 2600 cm^{-1} in the OH region. While the absorbance intensity of the bands in the 3650 − 3320 cm^{-1} and 2900 − 2500 cm^{-1} range increase with time, the intensity of the band located between 3320 cm^{-1} and 2900 cm^{-1} decreases. In the spectra of oxidised PS purged with dry air (Fig.5.5b) the OH band is split into two broad bands located in the 3680 − 3200 cm^{-1} and 3200 −2500 cm^{-1} regions, with absorbance intensity increasing with time. These bands were expected to decrease with time if the bands were due to physisorbed water as the argon or dry air was supposed to dry the film further and therefore remove all the excess of water overtime. When the sample was exposed to water vapour (Fig.5.5c) a single OH band was observed in the 3650 − 3000 cm^{-1} region. The absorbance intensity of this band decreases slightly with time while it was expected to increase as more H_2O groups are adsorbed onto the surface of the polymer.

The pattern of the difference infrared spectra obtained for all these experiments suggest that this broad OH band is not only due to water vibration stretching as if it was the case this band would be expected to decrease with time as the water is removed through treatment with dry air or argon. This might be explained by the fact that initially before the argon and dry air were introduced, the broad OH band had contributions from OH of carboxylic acid, alcohol, hydroperoxy and water groups. So when the argon was passed over the surface of the PS sample, water was lost, resulting in less hydrogen bonding to surface alcohol, acid and hydroperoxy groups. This might explain the loss of intensity of the band in the 3320 − 2900 cm^{-1} range corresponding to H-bonded OH. Concomitantly an increase in the intensity of the band in the 3650 − 3320 cm^{-1} and 2900 − 2500 cm^{-1} ranges associated with the vibration stretches of free OH of alcohols (compound 2), carboxylic acid (compound 4) or hydroperoxy (compound 1) respectively is observed (Fig.5.5a). Similar patterns in changes to the OH band is also observed when the PS oxidised sample was purged with dry air (Fig.5.5b), the only difference is that the big loss of the band in the 3320 − 2900 cm^{-1} range associated with the loss of water and hydrogen bonded OH of alcohol and carboxylic acids is not seen here (in Fig 5.5b). The intensity of the band in the 3200 − 2500 cm^{-1} range associated with free OH of carboxylic acid and hydroperoxy is bigger in this case, and this might be due to more carboxylic

acid and hydroperoxy formation when the dry air was introduced due to the presence of oxygen, hence leading to the increase in intensity of this band. The broadness of the OH band observed in Fig.5.5c shows the typical contribution to the OH band expected from water. This broad band can then be associated to inter- and extra-molecular bonded OH groups from water, alcohol and carboxylic acids.

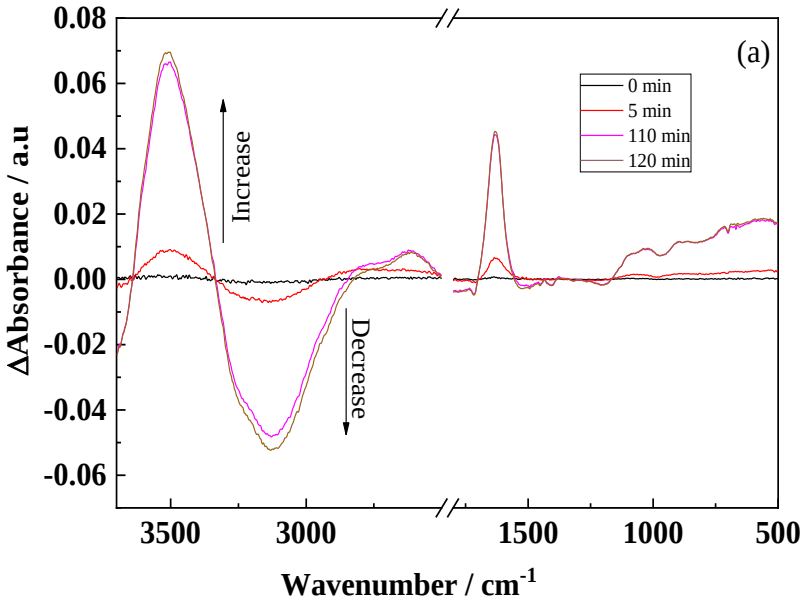

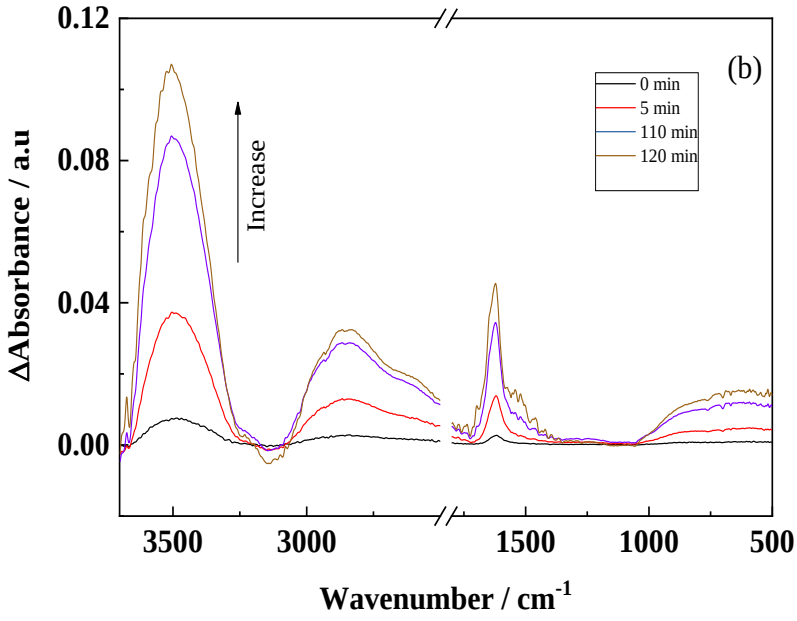

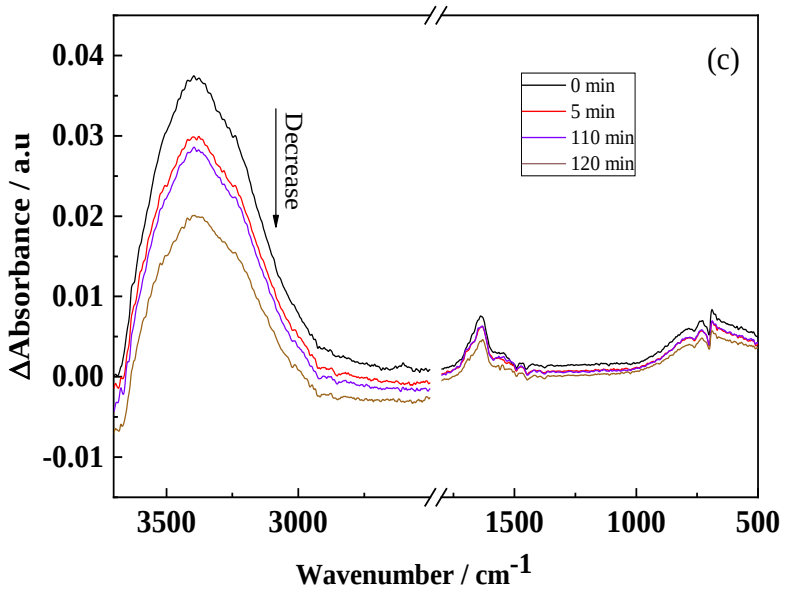

Figure 5.5: Evolution of the FTIR difference spectra of Polystyrene treated with Iridium (IV) tetrachloride solution: (a) purged with Argon, (b) purged with dry air and (c) purged with water vapour. The spectra were collected every 5 min for 2 hours between 4000 − 400 cm^{-1} with spectral resolution of 4 cm^{-1} and averaged over 100 scans.

5.3.1.2.3 PS treated with Iridium (IV) Hexachloride

The oxidation of PS surface with mild oxidising agent such as iridium (IV) hexachloride was also investigated and the resulting FTIR spectrum is given in Figure 5.6. The small, sharp peaks seen at 3471 cm^{-1} and 3362 cm^{-1} are assigned to OH stretches. The peaks associated with C=O stretches are seen at 1738 cm^{-1}, 1700 cm^{-1} and 1602 cm^{-1}. This indicates that carboxylic acids, esters and ketone type compounds are formed after treatment. A peak characteristic of C−O stretch is seen in the 1200 −1000 cm^{-1} range. Although very small its presence is reproducible.

In comparison, the spectrum obtained in this case (Fig.5.6) differs to the spectra obtained in Fig.5.3a and Fig 5.3b in the OH, C=O, C−C, in plane and out of plane C−H stretches regions. In particular, the broad OH stretches observed in the carbonyl and hydroxyl regions in spectrum (a) and spectrum (b) are not seen in spectrum (c), instead discrete, sharp peaks are observed. An additional peak attributed to C−O stretch is seen here (Fig.5.6). This band is also observed in Fig.5.3b but not Fig.5.3a.

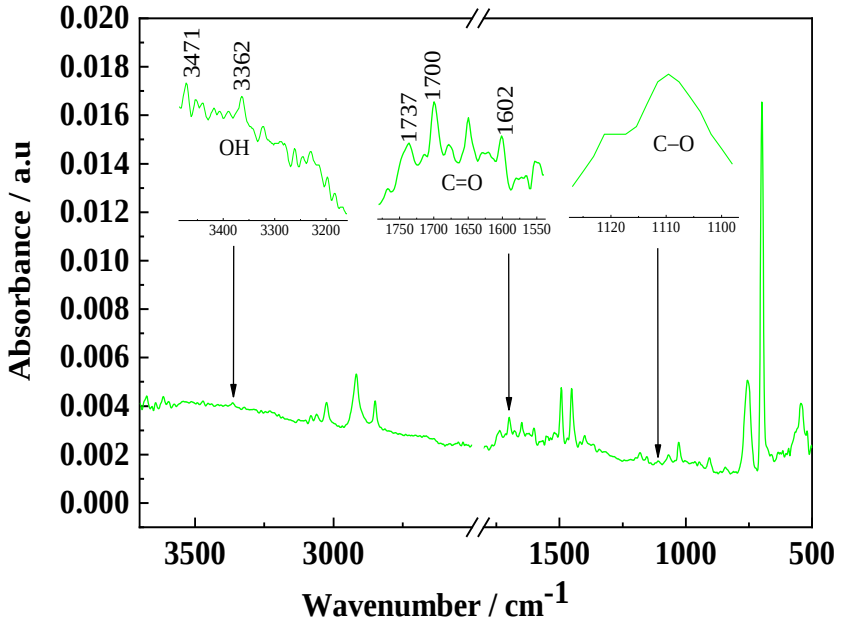

Figure 5.6: FTIR spectra of polystyrene treated with iridium (IV) hexachloride. The background was taken prior to sample deposition. The spectra were collected between 4000 − 400 cm^{-1} with spectral resolution of 4 cm^{-1} and each spectrum averaged over 100 scans.

The differences observed between the three spectra may be explained by the fact that all these three species have different reaction mechanisms by which they oxidised polystyrene. The Iridium (IV) species were expected to have a similar effect but this is not observed, and the reaction products appear different. This might be due to the fact that iridium (IV) tetrachloride with a standard potential (0.93 V) higher than the one of iridium (IV) hexachloride (0.68 V) have a stronger oxidizing effect and can react with water first to produce the hydroxyl radical which can then react with the polystyrene to form the polystyryl radical or initiate the other H-abstraction mechanism proposed for this compound.

In the PS treated with iridium hexachloride a small range of oxidation products are observed in the spectrum. This might be due to the fact that the iridium hexachloride as a mild oxidising agent doesn't oxidised the PS, but the defect sites present in the PS structure such as phenol and peroxides groups instead.

The oxidation of these groups leads to quinones and ethers as shown in earlier chapters. This oxidation reaction is very slow as shown by the limited amount of oxidation by this route compared to the reactions observed with PS treated with Iridium (IV) tetrachloride.

5.3.1.3 Analysis of the Oxidised Polystyrene films at different times

The as received polystyrene beads suspension was subjected to oxidative chemical treatments for different lengths of time (1h, 2h, 4h, 6h and 24h) using iridium (IV) hexachloride solutions. The oxidised PS samples were drop-coated onto the ATR prism and allowed to dry for 2 hours. A background spectrum was taken prior with no sample deposition. FTIR measurements were performed every 5min for 1 hour for each sample between 4000 − 400 cm^{-1} with spectral resolution of 4 cm^{-1} and the resulting spectra are presented in Figure 5.7.

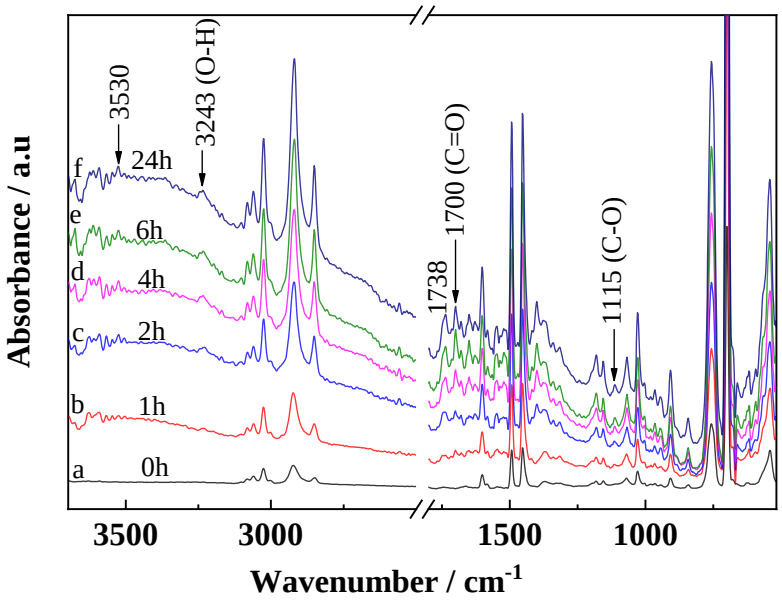

Figure 5.7: FTIR spectra of the polystyrene under study with and without iridium (IV) hexachloride treatment: (a) untreated polystyrene, (b) treated for 1 h, (c) treated for 2 h, (d) treated for 4 h, (e) treated for 6 h and (f) treated for 24 h. The background was taken with no sample deposition and each spectrum was averaged over 100 scans.

The carbonyl bands at 1738 cm^{-1} and 1700 cm^{-1} are assigned to ketones, carboxylic acids, aldehydes and ester type compounds. Esters, alcohols and carboxylic acids are also known to show an additional absorption band in the IR region between 1300 cm^{-1} and 1000 cm^{-1} due to vibrational stretching of the C–O bonds. The presence of the absorption

band at 1115 cm^{-1} may confirm then the formation of compounds with C−O bonds. As to the degree of oxidation of the samples, it is important to indicate that the intensity of absorbance of carbonyl (C=O) and hydroxyl (OH) groups increased with the treatment time.

The spectra in Fig.5.7 were recorded within 30 min of preparation. This was because problems with reproducibility had been noted if the samples were left suspended in water for a long time (i.e. overnight) before analysis. The C−O and OH bands were not seen in the spectrum of PS treated with Ir (IV) hexachloride for 4 h after subsequent overnight storage as shown in Fig. 5.8. This may be due to the fact that the oxidised PS already undergoes further chemical reactions when left suspended in water for longer time. These further reactions appear to involve the loss of C−O and OH bonding and need to be explained further.

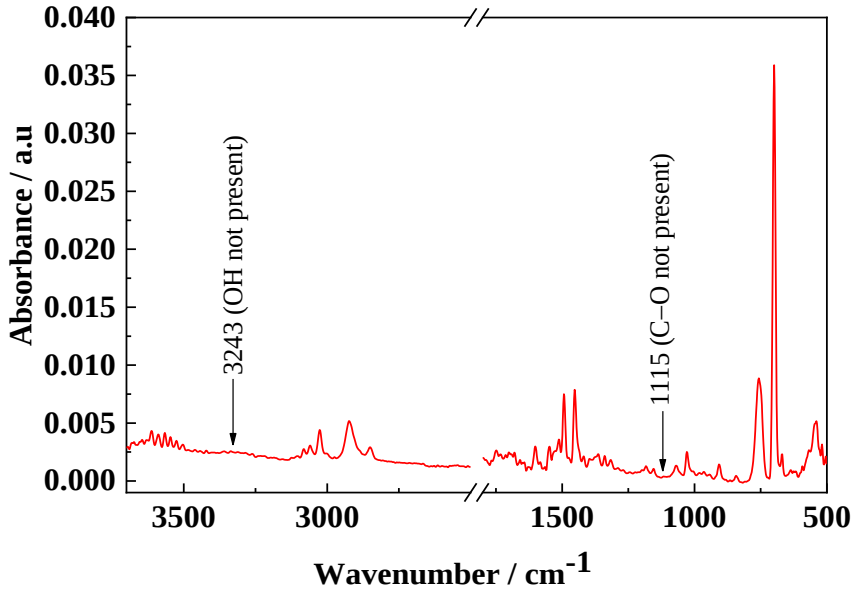

Figure 5.8: FTIR spectrum of PS treated with Ir (IV) hexachloride for 4 h analysed within 15 hours of preparation. The spectrum was collected between 4000 − 400 cm^{-1} with spectral resolution of 4 cm^{-1}. The background was taken with no sample deposition and the spectrum was averaged over 100 scans.

In comparison to the non – treated PS, the spectra of the treated PS showed the presence of hydroxyl (-OH) absorption bands at 3243 cm^{-1}, carbonyl peaks at 1738 cm^{-1}, 1700 cm^{-1} and C−O band at 1115 cm^{-1} [11]. By analogy with past finding in polystyrene oxidation, the increasing hydroxyl band at 3243 cm^{-1} is generally related to both alcohol and carboxylic acid type compounds [11], [12]. Based on the resulting spectral data

obtained, two possible reaction mechanisms can be proposed: the first is shown in scheme 5.5. In this mechanism, we considered that the polystyrene undergoes hydrolysis, leading to the formation of carboxylic acid (compound iii) and aldehyde (compound iv). Alternatively, the Ir (IV) hexachloride can oxidise any of the phenol groups present at the surface of PS leading the formation of compounds 7 and 8 as shown in scheme 5.6.

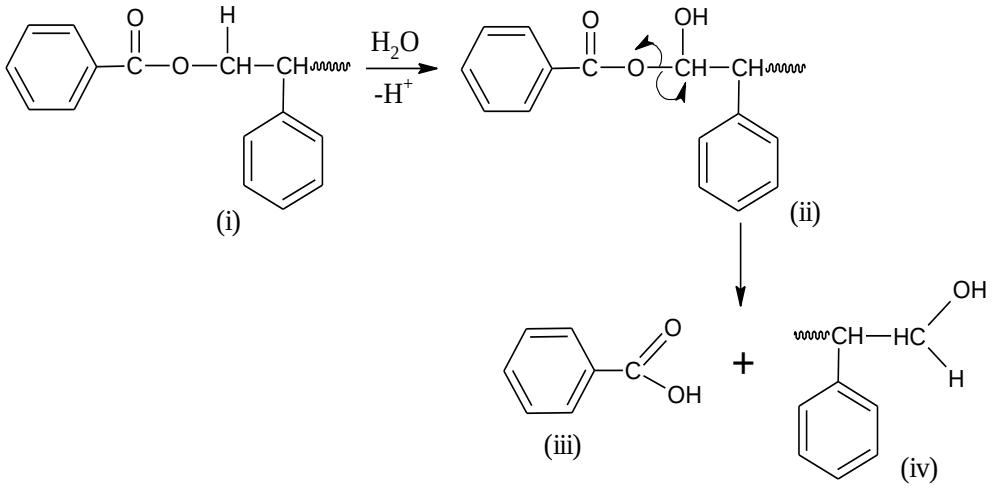

Scheme 5.5

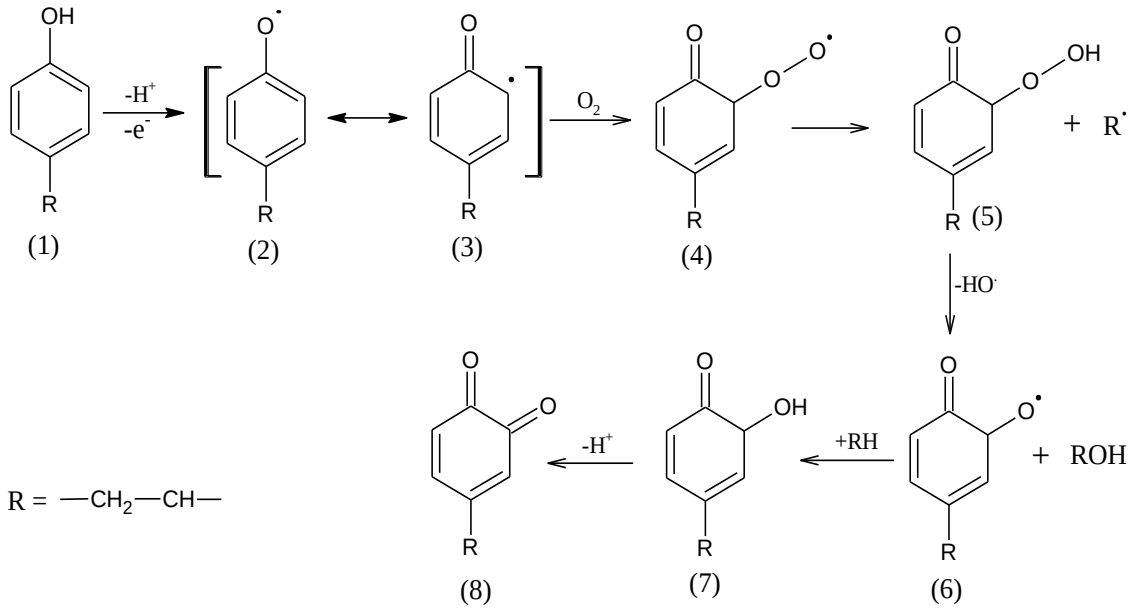

Scheme 5.6 Proposed Oxidation Mechanism for PS treated with Iridium (IV) hexachloride.

5.3.1.4 In Situ FTIR Studies of non-oxidised and oxidised PS in Water

The effect of water absorption on the physical structural organisation of the polystyrene was investigated using FTIR spectroscopy by exposing the non-oxidised and oxidised PS (pre-oxidised by treatment with Ir (IV) hexachloride) film to de-ionised water for 2 hours. The spectra were collected for both samples every 5 min for 2 hours (Fig. 5.9). In Figure 5.9a, the broad positive band centred at 3424 cm^{-1} is attributed to the OH vibration stretch of water. The absorption peaks associated with the aromatic CH stretches are seen at 3061 and 3026 cm^{-1}. The two peaks at 2920 and 2853 cm^{-1} are related to the asymmetric and symmetric stretching vibration of the methylene (CH_2) in the PS chain. The positive broad band centred at 1650 cm^{-1} is attributed to the OH bending of water. The peak at 1492 cm^{-1} and 1452 cm^{-1} correspond to the aromatic CC stretching vibration but the later peak can also be associated with the -CH_2 deformation. The peaks at 1072 and 1025 cm^{-1} are associated with the in-plane C−H bending in the ring and the out of plane C−H bending are observed at 777, 710 and 694 cm^{-1}. The intensity of all these bands excepting the band associated with water decrease with time. In the spectra of the oxidised PS (Fig.5.9 b), the broad band centred at 3424 cm^{-1} is associated with the OH vibration of water with contribution of OH from carboxylic acid (iii), aldehyde (iv) and compounds 5 and 7. The two peaks observed at 2920 cm^{-1} and 2904 cm^{-1} are more likely to be associated with the C−H of the methylene (-CH_2), the C=O vibration stretch of carboxylic acid (iii) and ketone (8) are seen at 1705 cm^{-1} and 1663 cm^{-1}. The positive band centred at 1653 cm^{-1} is associated with the OH bending of water. The broad negative absorption bands centred at 1398, 1237 and 1064 cm^{-1} are more likely to be related to the OH bending stretch, OH and C−O vibration stretches of compound 7, (iii) and (iv) respectively. The decrease in intensity of these bands is more significant on the oxidised PS in comparison to the non-oxidised PS. Hence it seems that degree of prior oxidation of the polystyrene influences the spectral characteristics observed when immersed in water. In the work of others, it was suggested that these observed changes are due to structural rearrangement of the polystyrene surface in response to the adsorption of water [3], [13]. It has been shown that PS surfaces are highly dynamic and reorganise in response to changes in hydrophobicity/ hydrophilicity of the interface conditions. The oxygen-containing polar groups which are present on the PS surface migrate from the bulk to the surface when exposed to water. Conversely in a hydrophobic environment (e.g. in argon or nitrogen atmosphere), the polar groups move from the surface to the

bulk of the polymer. In reference to this, the loss of intensity of the peaks associated with the hydrophobic parts PS (e.g. phenyl rings) and increase in intensity of these oxygen-containing polar groups are associated with the reorganisation of the PS surface upon exposure to water.

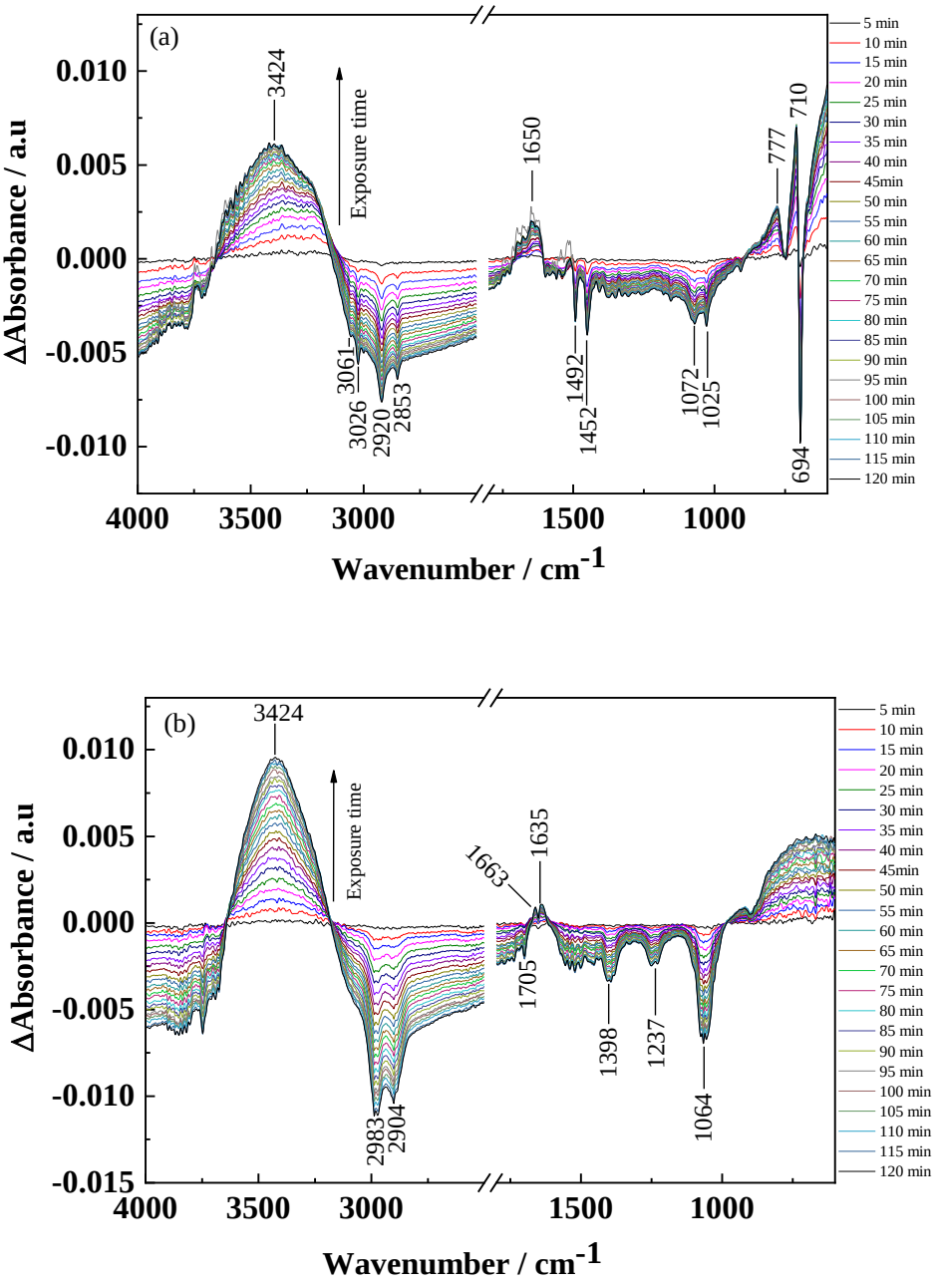

Figure 5.9: FTIR difference spectra of PS film: (a) non-treated and (b) treated with Ir (IV) hexachloride upon exposure to de-ionised water. The adherent films were used as background before water addition respectively. The spectra were collected every 5 min for 2 hours and averaged over 100 scans.

Comparison of the intensity of the very broad OH stretch absorption band in the 3600 − 3100 cm^{-1} range centred at 3424 cm^{-1} between the two samples shows that the OH band increases more with time in water for the oxidised PS. This effect was illustrated by plotting the increasing absorbance intensities at 3424 cm^{-1} related to OH stretches against water exposure time and the result is presented in Figure 5.10. The trends of the plots show greater increase in the number of -OH groups on the oxidised PS matrix than the non-oxidised one.

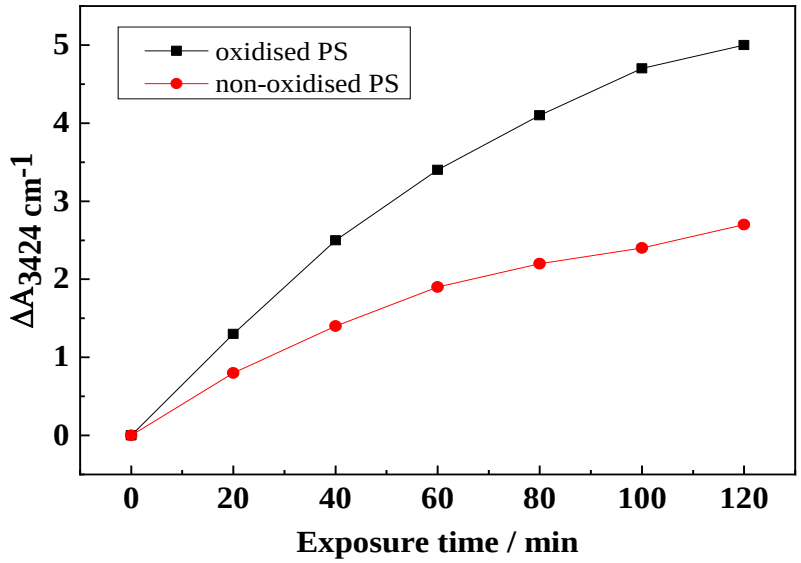

Figure 5.10: Increasing absorption intensities at 3424 cm^{-1} vs exposure time for the non-oxidised and oxidised polystyrene films upon exposure to water.

5.3.1.5 Effect of Oxidizing Agents on the non-oxidised Polystyrene Surface In Situ with and without the Presence of Oxygen

The chemical oxidation of PS was also monitored in situ using FTIR spectroscopy technique. In these experiments, 5 µL of non-oxidised PS suspension was drop-coated onto the ATR prism which was left to dry for 1 hour to form an adherent film.1 mL of water was then added to the sample compartment and the solvated PS film allowed to equilibrate for 5 min before collecting the background spectrum. 100 µL of 5 mM of the oxidising agents (iridium (IV) hexachloride, iridium (IV) tetrachloride and potassium ferricyanide) solution was added to the sample compartment and left for 10 min before collecting the spectra every 5 min for 1 hours between 4000 − 400 cm^{-1} with a spectral resolution of 4 cm^{-1}.

For some experiments the difference spectra were collected overtime under argon and this was carried out in order to investigate the effect of oxygen on the oxidation reaction mechanism of polystyrene. The analysis of the results obtained shows differences in the spectra collected under oxygen and under argon only for the experiments where Iridium (IV) tetrachloride was used as oxidising agent and therefore only these spectra are presented here (Figure 5.11). The spectra obtained for the other oxidising agents are presented in the appendix for future reference. In Figure 5.11(a) is presented the resulting spectra obtained under oxygen and the broad absorption band observed in the 3600 − 3200 cm^{-1} range is attributed to vibration stretches of free OH of alcohols (compound 7), carboxylic acids (compound iii), aldehyde (compound iv) as well as OH from water and –OOH of compound 5. The band assigned to C=O vibration stretch of compound iii (scheme 5.5), compounds 7 and 8 (scheme 5.6) is observed in the 1800 −1600 cm^{-1} range. This band seems to be related to the negative bands observed in the 1580 −1400 cm^{-1} range centred at 1500 and 1456 cm^{-1} which are characteristic of the C=C stretch in the phenyl ring. The intensity of this band decreases with the increasing intensity of the C=O band, indicating a loss of C=C bond in relation to the formation of carbonyl compound. Changes can also be observed within the range of appearance of bands corresponding to the stretching vibration of C−O. These assigned are consistent with the oxidation mechanism proposed in scheme 5.5 and 5.6. In the spectra obtained under argon (Figure 5.11b), a broad band in the 1800 − 1600 cm^{-1} range centred at 1650 cm^{-1} is seen. This broad band incorporates small bands at 1700 cm^{-1} and 1680 cm^{-1} which is consistent with C=O vibration stretch of carboxylic acid and aldehyde. Several positive bands associated with C=C vibration stretches are observed in the 1600 − 1400 cm^{-1} region. In comparison to the spectra obtained in Figure 11a, the loss of C=C and C−O stretches are not observed. Additionally, the band associated with the C=O vibration stretch (Fig.11b) shows different peaks associated with different oxidation products. This suggests that under argon (oxygen free environment) compound (iii) and (iv) (scheme 5.5) are also formed. In scheme 5.6, under argon, the intermediate hydroperoxide compound (compound 5) is not formed, the oxidation proceeds as shown below in scheme 5.7 instead. In this mechanism product (3) might react with the $HO^{\bullet}$ generated from the reaction of the iridium and water and this leads to the formation of compound (4) and then compound 5 through one electron and proton transfer reaction.

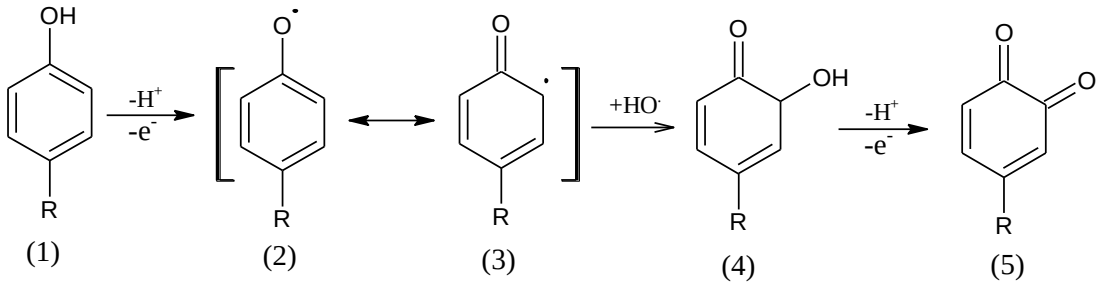

Scheme 5.7 Proposed Oxidation Mechanism for PS in water on addition of iridium (IV) tetrachloride in deoxygenated solution

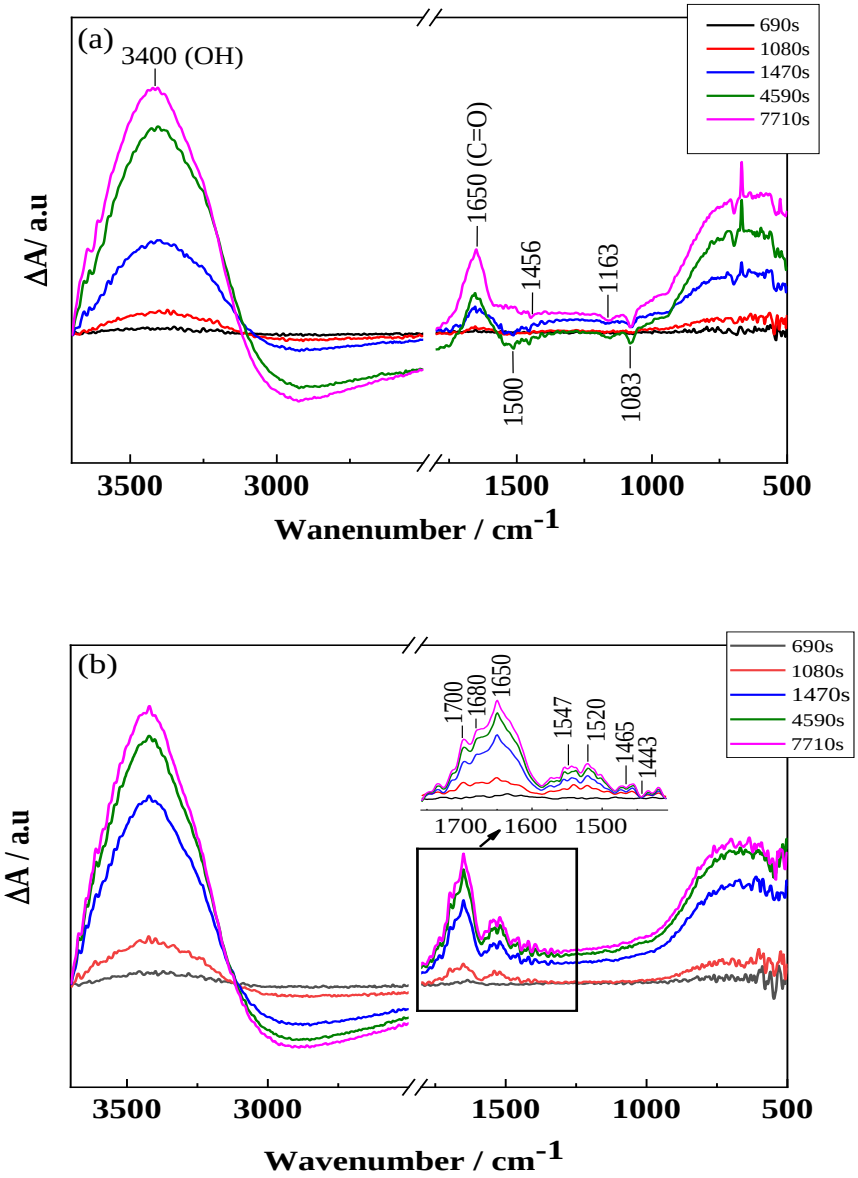

Figure 5.11: FTIR difference spectra of non-oxidised PS film on addition of Iridium (IV) tetrachloride solution in water: (a) not purged with argon and (b) purged with argon. The spectra were averaged over 100 scans.

5.4 Conclusion

In this work the non-oxidised polystyrene was first characterised using FTIR spectroscopy and the bands assigned accordingly. These bands assignments agreed with the data published in the literature.

The changes to polystyrene structure after chemical treatments using three different oxidising agents (iridium (IV) tetrachloride, iridium (IV) hexachloride and hydrogen peroxides) were monitored and the resulting spectra (in Fig.5.3 and Fig.5.6) obtained show the formation of carbonyl and hydroxyl group. These groups were also observed when the samples were analysed using XPS (cf appendix for data). This indicates that all three species can induce changes to the polystyrene structure. Although they all have different reaction mechanisms by which they oxidised polystyrene, as indicated by the differences observed between their spectra.

The degree of oxidation of PS oxidised at different times using iridium (IV) hexachloride solution was also evaluated and the results in section 5.3.1.3 (Fig.5.7) show that the intensity of absorbance of the carbonyl and hydroxyl groups increases with the oxidation time, indicating that the concentration of these groups on the polystyrene depend on the treatment time. However, problems with reproducibility was noted when the samples were left suspended in water for long time (e.g. overnight). This effect may be due to the fact that the oxidised PS already undergoes further chemical reactions when left suspended in water for longer time. These further reactions appear to involve the loss of C−O and OH bonding and need to be investigated further in future works.

The effect of water absorption on the physical structural organisation of the polystyrene was also investigated using FTIR spectroscopy. The results show greater changes for the oxidised polystyrene than the non-oxidised PS. This may be related to structural rearrangement and swelling effect in the polymer in response to the adsorption of water.

The changes to PS structure on addition of oxidising agents such as iridium (IV) hexachloride, iridium (IV) tetrachloride and potassium ferricyanide in water was also investigated in situ deoxygenated and non-deoxygenated solution. Carbonyl and hydroxyl bands were observed in the spectra obtained in experiments where iridium (IV) tetrachloride was used as oxidising agent under both conditions. These results indicate that polystyrene can be oxidised in situ by oxidation agent such as iridium (IV) tetrachloride and the oxidation products can be detected by in situ FTIR technique.

References for Chapter 5

[1] H. Kaczmarek, M. Świątek, and A. Kamińska, "Modification of Polystyrene and Poly(vinyl chloride) for the Purpose of Obtaining Packaging Materials Degradable in the Natural Environment," *Polym. Degrad. Stab.*, vol. 83, no. 1, pp. 35–45, Jan. 2004.

[2] D. J. Hourston, "Degradation of Plastics and Polymers," *Polym. Mater.*, vol. 2, pp. 2369–2376, 2010.

[3] T. S. Varley, M. Rosillo-lopez, S. Sehmi, N. Hollingsworth, and K. B. Holt, "Surface Redox Chemistry and Mechanochemistry of Insulating Polystyrene Nanospheres," *Phys. Chem. Chem. Phys.*, vol. 17, no. 3, pp. 1837–1846, 2015.

[4] C. Y. Liang and S. Krimm, "Infrared Spectra of High Polymers," *J. Mol. Spectrosc.*, vol. 3, no. 1958, pp. 554–574, 1959.

[5] B. Stuart, *Infrared Specroscopy: Fundamentals and Applications*, 1st ed. Chichester: John Wiley & sons, Ltd, 2004.

[6] C. Stihi, "Atr-Ftir Spectrometry Characterisation of Polymeric Materials," *Rom. reports Phys.*, vol. 66, no. 3, pp. 765–777, 2014.

[7] B. Stuart, *Infrared Spectroscopy : Fundamentals and Applications*, 1st ed. Chichester: John Wiley & Sons, Ltd, 2014.

[8] M. Gattrell and D. W. Kirk, "A Fourier Transform Infrared Spectroscopy Study of the Passive Film Produced During Aqueous Acidic Phenol Electro-Oxidation," *J. Electrochem. Soc.*, vol. 139, no. 10, pp. 2736–2744, 1992.

[9] A. Torikai, T. Takeuchi, and K. Fueki, "Photodegradation of Polystyrene and Polystyrene Containing Benzophenone," *Polym. Photochem.*, vol. 3, pp. 307–320, 1983.

[10] B. Dickens and J. Marchal, "Oxidation of Polystyrene in Solution," *Polymer Degradation and Stability*, vol. 6, no. 4. pp. 211–241, 1984.

[11] O. Watanabe, M. Tabata, J. Sohma, and A. Lund, "Chemical Degradation of Polystyrene Induced by Chlorinated Nitrosobenzene," *Polym. Degrad. Stab.*, vol. 7, pp. 13–24, 1984.

[12] J. L. Gardette, B. Mailhot, and J. Lemaire, "Photooxidation Mechanisms of Styrenic Polymers," *Polym. Degrad. Stab.*, vol. 48, no. 3, pp. 457–470, Jan. 1995.

[13] M. Inutsuka, H. Tanoue, N. L. Yamada, K. Ito, and H. Yokoyama, "Dynamic Contact Angle on a Reconstructive Polymer Surface by Segregation," *RSC Adv.*, vol. 7, no. 28, pp. 17202–17207, 2017.

[14] M. Nowakowska, J. Kowal, and B. Waligora, "Photo-Oxidation of Polystyrene Film: 2. Photo-Oxidation of Polystyrene Film with Light Absorbed by the Polystyrene-Oxygen Complex," *Polymer (Guildf).*, vol. 19, no. 11, pp. 1317–1319, Nov. 1978.

[15] S. Wang, J. Chang, and R. C. Tsiangq, "Infrared Studies of Thermal Oxidative Degradation of Polystyrene-Block-Polybutadiene-Block-Polystyrene Thermoplastic Elastomers," *Polym. Degrad. Stab.*, vol. 52, pp. 51–57, 1995.

[16] J. Kubica and B. Waligóra, "The Effect of Carbonyl Compounds on Photo-Oxidation in Polystyrene Films," *Eur. Polym. J.*, vol. 13, no. 4, pp. 325–329, Jan. 1977.

[17] J. Gardette and M. Benedicte, "Polystyrene Photooxidation. 1. Identification of the IR-Absorbing Photoproducts formed at short and long wavelenghts," *Macromolecules*, vol. 25, no. 16, pp. 4119–4126, 1992.

[18] G. Gryn'ova, J. L. Hodgson, and M. L. Coote, "Revising the Mechanism of Polymer Autooxidation," *Org. Biomol. Chem.*, vol. 9, no. 2, pp. 480–490, 2011.

[19] B. Dickens and J. Marchal, "Oxidation of Polystyrene in Solution," *Polym. Degrad. Stab.*, vol. 6, no. 4, pp. 211–241, 1984.

[20] B. G. Achhammer, M. J. Reiney, and F. W. Reinhart, "Study of Degradation of Polystyrene, using Infrared Spectrophotometry," *J. Res. Natl. Bur. Stand. (1934).*, vol. 47, no. 2, p. 116, Aug. 1951.

[21] N. Allen, "Photooxidation of Styrene–Ethylene–Butadiene–Styrene (SEBS) Block Copolymer," *J. Photochem. Photobiol. A Chem.*, vol. 162, no. 1, pp. 41–51, Feb. 2004.

[22] F. Vilaplana, A. Ribes-Greus, and S. Karlsson, "Degradation of Recycled High-Impact Polystyrene. Simulation by Reprocessing and Thermo-Oxidation," *Polym. Degrad. Stab.*, vol. 91, pp. 2163–2170, 2006.

[23] G. Botelho, A. Queirós, A. Machado, P. Frangiosa, and J. Ferreira, "Enhancement of The Thermooxidative Degradability of Polystyrene by Chemical Modification," *Polym. Degrad. Stab.*, vol. 86, pp. 493–497, 2004.

[24] P. U. Singare, R. S. Lokhande, and R. S. Madyal, "Thermal Degradation Studies of Polystyrene Sulfonic and Polyacrylic Carboxylic Cationites," *Russ. J. Gen. Chem.*, vol. 80, no. 3, pp. 527–532, 2010.

[25] F. Kanwal, S. M. Waraich, and T. Jamil, "FT-IR Analysis of Recycled Polystyrene for Food Packaging," *J.chem.Soc.Pak*, vol. 29, no. 3, pp. 239–242, 2007.

[26] O. Motta *et al.*, "Utilization of Chemically Oxidized Polystyrene as Co-Substrate by Filamentous Fungi," *Int. J. Hyg. Environ. Health*, vol. 212, no. 1, pp. 61–66, 2009.

[27] L. F. A. Pinto, B. E. Goi, C. C. Schmitt, and M. G. Neumann, "Photodegradation of Polystyrene Films Containing UV-Visible sensitizers," *J. Res. Updat. Polym. Sci.*, vol. 2, no. 1, pp. 39–47, 2013.

[28] M. A. Grayson, C. J. Wolf, R. L. Levy, D. B. Miller, and M. Douglas, "The Mechanical Degradation of Polystyrene Determination of Residual Volatile Compounds," *J. Polym. Sci.*, vol. 14, pp. 1601–1609, 1976.

[29] W. Urbaniak-Domagala, "The Use of the Spectrometric Technique FTIR-ATR to Examine the Polymers Surface," *Adv. Apects Spectrosc.*, pp. 86–104, 2012.

[30] C. Engineer, J. Parikh, and A. Raval, "Review on Hydrolytic Degradation Behavior of Biodegradable Polymers from Controlled Drug Delivery System," *Trends Biomater. Artif. Organs*, vol. 25, no. 2, pp. 79–85, 2011.

[31] C. Direksilp and P. Threepopnatkul, "Performance Improvement of PS from Expanded Polystyrene Off-Grade," *Energy Procedia*, vol. 56, pp. 135–141, 2014.

[32] B. Enko, S. M. Borisov, J. Regensburger, W. Ba, G. Gescheidt, and I. Klimant, "Singlet Oxygen-Induced Photodegradation of the Polymers and Dyes in Optical Sensing Materials and the Effect of Stabilizers on These Processes," *J. Phys. Chem.*, vol. 117, pp. 8873–8882, 2013.

[33] A. Naima, "Biodegradability of Synthetic Plastics Polystyrene and Styrofoam by Fungal Isolates," Qaid-i-Azam University, Islamabad, 2011.

[34] I. A. Mudunkotuwa, A. Al Minshid, and V. H. Grassian, "ATR-FTIR Spectroscopy as a Tool to Probe Surface Adsorption on Nanoparticles at the Liquid-Solid Interface in Environmentally and Biologically Relevant Media.," *Analyst*, vol. 139, pp. 870–81, 2014.

[35] N. S. Allen *et al.*, "Influence of Ozone on Styrene–Ethylene–Butylene–Styrene (SEBS) Copolymer," *Polym. Degrad. Stab.*, vol. 79, no. 2, pp. 297–307, Jan. 2003.

[36] B. Ranby and J. Lucki, "New Aspects of Photodegradation and Photooxidation of Polystyrene," *Pure Appl. Chem.*, vol. 52, no. 2, pp. 295–303, 1980.

[37] L. Fernandes, H. Gaspar, and G. Bernardo, "Inhibition of Thermal Degradation of Polystyrene by C60 and PCBM: A Comparative Study," *Polym. Test.*, vol. 40, pp. 63–69, Dec. 2014.

[38] L. Cole, *Polystyrene: Synthesis, Characteristics and Applications*. Nova Science Publishers, Inc. New York, 2014.

[39] K. Chen and S. Vyazovkin, "Mechanistic Differences in Degradation of Polystyrene and Polystyrene-Clay Nanocomposite: Thermal and Thermo-Oxidative Degradation," *Macromol. Chem. Phys.*, vol. 207, pp. 587–595, 2006.

[40] G. Chen, S. Liu, S. Chen, and Z. Qi, "FTIR Spectra, Thermal Properties, and Dispersibility of a Polystyrene/Montmorillonite Nanocomposite," *Macromol. Chem. Phys.*, vol. 202, pp. 1189–1193, 2001.

[41] S. Al-Malaika, "Oxidative Degradation and Stabilisation of Polymers," *Int. Mater. Rev.*, vol. 48, no. 3, pp. 165–185, Jun. 2003.

[42] J. Lucki and B. Ranby, "Thermally Polymerised PS Anionically Polymerised PS," *Polym. Degrad. Stab.*, vol. 1, no. 1, pp. 1–16, 1979.

[43] J. F. Rabolt, A. D. English, and C. G. Zimba, "A Spectroscopy Study of Syndiotacic Polystyrene," *Macromolecules*, vol. 22, no. 6, pp. 2867–2869, 1989.

[44] G. Guerra, P. Musto, F. E. Karasz, and W. J. MacKnight, "Fourier Transform Infrared Spectroscopy of the Polymorphic Forms of Syndiotactic Polystyrene," *Makromoil . Chem*, vol. 191, pp. 2111–2119, 1990.

[45] J. Peeling and T. D. Clark, "An ESCA Study of the Photo-oxidation of the Surface of Polystyrene Film," *Polym. Degrad. Stab.*, vol. 3, pp. 97–105, 1980.

[46] T. Murakami, S. Kuroda, and Z. Osawa, "Dynamics of Polymeric Solid Surfaces Treated with Oxygen Plasma: Effect of Aging Media after Plasma Treatment," *J. Colloid Interface Sci.*, vol. 202, no. 202, pp. 37–44, 1998.

[47] J. L. Gejo *et al.*, "Vacuum-Ultraviolet Photochemically Initiated Modification of Polystyrene Surfaces: Morphological Changes and Mechanistic Investigations.," *R. Soc. Chem. Own. Soc.*, vol. 5, no. 10, pp. 948–54, Oct. 2006.

[48] B. Mailhot, S. Morlat, and J. L. Gardette, "Photooxidation of Blends of Polystyrene and Poly(vinyl methyl ether): FTIR and AFM Studies," *Polymer (Guildf).*, vol. 41, pp. 1981–1988, 2000.

[49] N. Grassie and N. A. Weir, "The Photooxidation of Polymers.," *J. Appl. Polym. Sci.*, vol. 9, pp. 999–1003, 1965.

[50] I. C. Mcneill, L. P. Razumovskii, V. M. Gol'dberg, and G. E. Zaikov, "The Thermo-Oxidative Degradation of Polystyrene," *Polym. Degrad. Stab.*, vol. 45, pp. 47–55, 1994.

[51] S. Stack, O. O'Donoghue, and C. Birkinshaw, "The Thermal Stability and Thermal Degradation of Blends of Syndiotactic Polystyrene and Polyphenylene Ecosther," *Polym. Degrad. Stab.*, vol. 79, pp. 29–36, 2003.

[52] Z. Chen, "Investigating Buried Polymer Interfaces using Sum Frequency Generation Vibrational Spectroscopy.," *Prog. Polym. Sci.*, vol. 35, no. 11, pp. 1376–1402, Nov. 2010.

[53] S. I. Kuzina and A. I. Mikhailov, "Chain and Photochain Mechanisms of Photooxidation of Polymers," *High Energy Chem.*, vol. 44, no. 1, pp. 37–51, Jan. 2010.

[54] D. Nagle, J, M. Celina, L. Rintoul, and M. Fredericks, "Infrared Microscopic Study of the Thermo-Oxidative Degradation of Hydroxy-Terminated Polybutadiene/Isophore diisocyanate Polyurethane," *Polym. Degrad. Stab.*, vol. 92, no. 8, pp. 1446–1454, 2007.

[55] F. Vilaplana, "High-Impact Polystyrene During the First Use and Subsequent Recycling," stockholm, 2007.

[56] W. R. Waldman and M. A. De Paoli, "Photodegradation of Polypropylene/Polystyrene Blends: Styrene–Butadiene–Styrene Compatibilisation Effect," *Polym. Degrad. Stab.*, vol. 93, no. 1, pp. 273–280, Jan. 2008.

[57] D. Olmos, E. V. Martín, and J. González-Benito, "New Molecular-Scale Information on Polystyrene Dynamics in PS and PS–BaTiO3 Composites from FTIR Spectroscopy," *Phys. Chem. Chem. Phys.*, vol. 16, pp. 24339–24349, 2014.

Chapter 6

Final Conclusions and Future works

The aim of this thesis was to investigate the changes in chemical structure to polystyrene upon treatment with oxidising agents and to monitor the oxidation in situ on addition of these agents using FTIR spectroscopy technique in order to get more insight into the oxidation mechanism of PS which is not well understood especially in chemical oxidation. The following sections outline the major findings and future works.

6.1 Electrochemical oxidation of TBP, Phenol and o,m,p-cresols

Chapter 3 investigated the electrochemistry of phenolic compounds such as TBP, unsubstituted phenol and cresols at EPPG electrode using cyclic voltammetry technique. The electrochemical oxidation of TBP studied using different electrode material (EPPG, GC and BD) showed that its oxidation involves a one electron per proton transfer that lead to the formation of 2,4,6-tri-tert-butylphenoxy radical. Additionally, enhanced electron-transfer kinetics was observed at the EPPG in comparison to the GC and BDD electrodes and this was attributed to the presence of the edge sites which are highly reactive and allow strong adsorption tendency and chemical modifications.

The electrochemical oxidation of phenol was also investigated and the results revealed a reversible reaction occurring in the oxidation process. The oxidation current was found to be significantly decreasing on the second and subsequent scan and this was attributed to the fouling of the electrode due to the deposition of the polymeric oxidation product at the surface of the electrode. The rate of formation of quinone formation was calculated according to the charge associated with the oxidation and reduction peaks and this was found to be equal to approximately ca.10%. This indicated that only the tenth of the initial phenol is converted onto quinones species. The number of electrons that could possibly be transferred during oxidation of the unsubstituted phenol was evaluated (between 2 and 3 electrons) and an oxidation mechanism proposed after investigating the effect of pH

and scan rate on the electrochemical response. The oxidation involves initially a one electron transfer, leading to the phenoxy radical then to polymeric, dimer link through O−O and quinone products. The rate of formation of these oxidation products depends greatly to the experimental conditions such as pH, concentration and scan rate. Furthermore, the study of the electrochemical oxidation of ortho-, meta- and para cresols under the same experimental conditions as the unsubstituted phenol and TBP reveals that o-cresol shows a peak assigned to quinoid species reduction on the reverse scan, no such peak was observed for meta- and para-cresols. Similarly to the unsubstituted phenol, the number of electrons which might be involved in the oxidation reaction of ortho, meta and para-cresol, was evaluated to be approximately between 1 and 2 electrons for ortho-cresol and between 2 and 3 electrons for meta- and para-cresols. This suggested that different reaction mechanisms take place depending on the substitution position of the methyl group on the phenyl ring. While ortho-cresol was found to give polymeric, dimer link through O−O and quinone products, polymeric and dimer link through O−O oxidation products were assigned to m-cresol. Only dimer link through O−O oxidation product was assigned to p-cresol. The possibility of polymeric and quinoid oxidation products formation for p-cresol was not considered due to the presence of the methyl groups in the para-position and to the fact that the molecule being too sterically crowded.

These oxidation mechanisms described above for all these phenolic compounds were proposed after interpretation of the results obtained. These mechanisms are consistent with the results obtained.

This electrochemical study contributes to the knowledge of understanding substituted phenols redox chemistry using CV techniques which can be very useful in the treatment of wastewater containing phenols. The oxidation potential determined for these phenolic compounds having similar structure to the proposed defects sites in the polystyrene structure has allowed us to know at what potential polystyrene is more susceptible to undergo oxidation and to understand the oxidation of polystyrene especially when treated with mild oxidising agents.

6.2 In Situ Spectroelectrochemical Study of TBP, Phenol and o,m,p-cresols.

Chapter 4 explores the electrochemical oxidation of the unsubstituted phenols, TBP and cresols using a combined technique of chronoamperometry and in situ ATR-FTIR spectroscopy. The assignments of the IR peaks obtained were consistent with the oxidation products proposed of the phenolic compounds in chapter 3. Prior to this the effect of SWCNT on the EPPG electrode surface was investigated and this revealed that the SWCNT increases the spectral intensity of the sulfate and water bands. This was probably due to the swelling of the SWCNT material and filled the existing gap between the surface of the EPPG electrode and the ATR prism upon immersion in the electrolyte. Only concentrations of 2.5 mM for TBP and 10 mM for phenols and cresols were needed to obtain high resolution spectra of these compounds in this work and this not possible in the works published by other authors. However, two limitations of the technique was identifies with the first being the presence of ethanol which shows strong IR bands in the infrared spectra that were taken into account on the peaks assignments. The second is that the existing gap between the EPPG electrode surface and the ATR prism. Even assuming that this gap (~ 17μm) was filled due to SWCNT modification, the exact electrode-prism separation is not known and the consequence of this is that we don't know where we are actually probing and this needs to be investigated further in future research.

6.3 Chemical Oxidation of Polystyrene Studied with In Situ Infrared Spectroscopy

Finally, Chapter 5 investigated the changes to polystyrene structure after chemical treatments using oxidising agents such as iridium (IV) tetrachloride, iridium (IV) hexachloride and hydrogen peroxides. Carbonyl and hydroxyl groups were observed on the surface of the polystyrene and this is indicative of oxidation. These oxygen containing groups were also observed in the in situ study of the PS in water on addition of Iridium (IV) tetrachloride in oxygen and oxygen free environment. This shows that polystyrene can be oxidised in situ on addition of strong oxidation agent such as Iridium (IV) tetrachloride regardless of the presence or not of oxygen.

In general, it can be concluded from this work that the understanding of the oxidation mechanism of molecular having similar structure as the defect sites in the polystyrene structure can help in enhancing degradation in polystyrene by adding these compounds in the polystyrene structure.

6.4 Future Works

Although, this technique has allowed to successfully study the chemical oxidation of polystyrene and to propose some reaction mechanisms, the exact oxidation products are not known and this can be overcome by characterising the surface of the oxidised polystyrene using other technique such as Raman and spin radical trap experiments. Another useful future study can be to monitor the changes to polystyrene structure while carrying oxidation by applying an electrode potential of 0.75 V rather than adding an oxidising agent using the combined of chronoamperometry and in situ ATR-FTIR spectroscopy. This will allow us to determine whether electron transfer is a key step in the oxidation process or whether other mechanisms should be considered (e.g. generation of reactive species). In this method, the PS modified EPPG electrode will be used along with a counter and reference electrodes on a standard three electrodes cell immersed in 0.3 M phosphate buffer solution (PBS). FTIR measurements will be performed with an applied potential of 0.75 V. Finally, FTIR experiments can be design in order to accurately estimate the existing gap between the ATR-prism and the electrode surface. This gap was estimated to be 17µm but its exact value it is not known and this can affect greatly the measurements.

Appendix

Appendix 1

Additional Figures for chapter 4

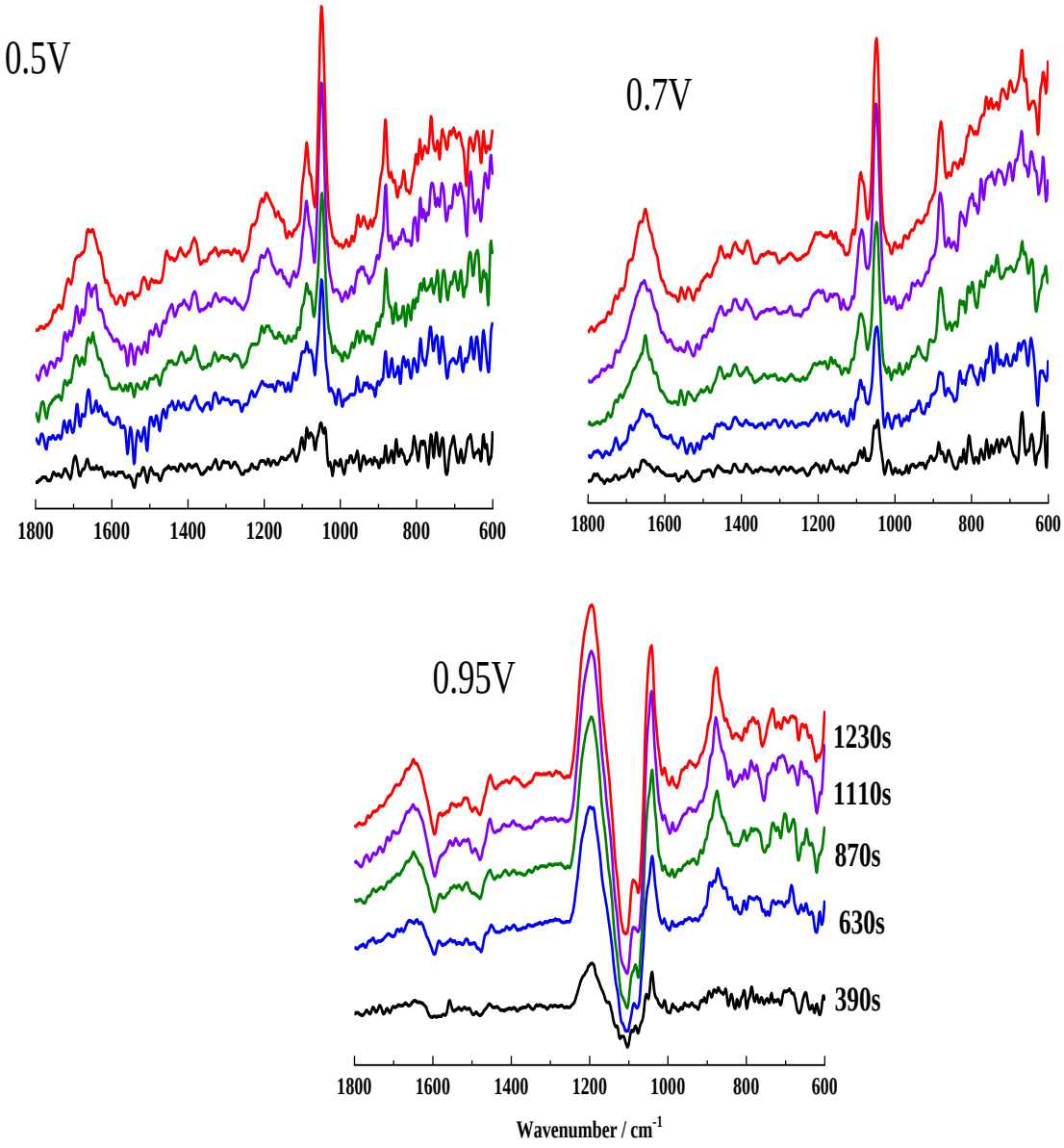

Figure 1.1: FTIR in situ different spectra collected for phenol at EPPG coated with SWCNT in EtOH / Na2SO4.10H2O at applied potentials of: 0.2 V, 0.7 V and 0.95 V. The background was taken 5 mins after sample deposition and the spectra were collected between 4000 − 500 cm^{-1} with a resolution of 4 cm^{-1} and averaged over 500 scans.

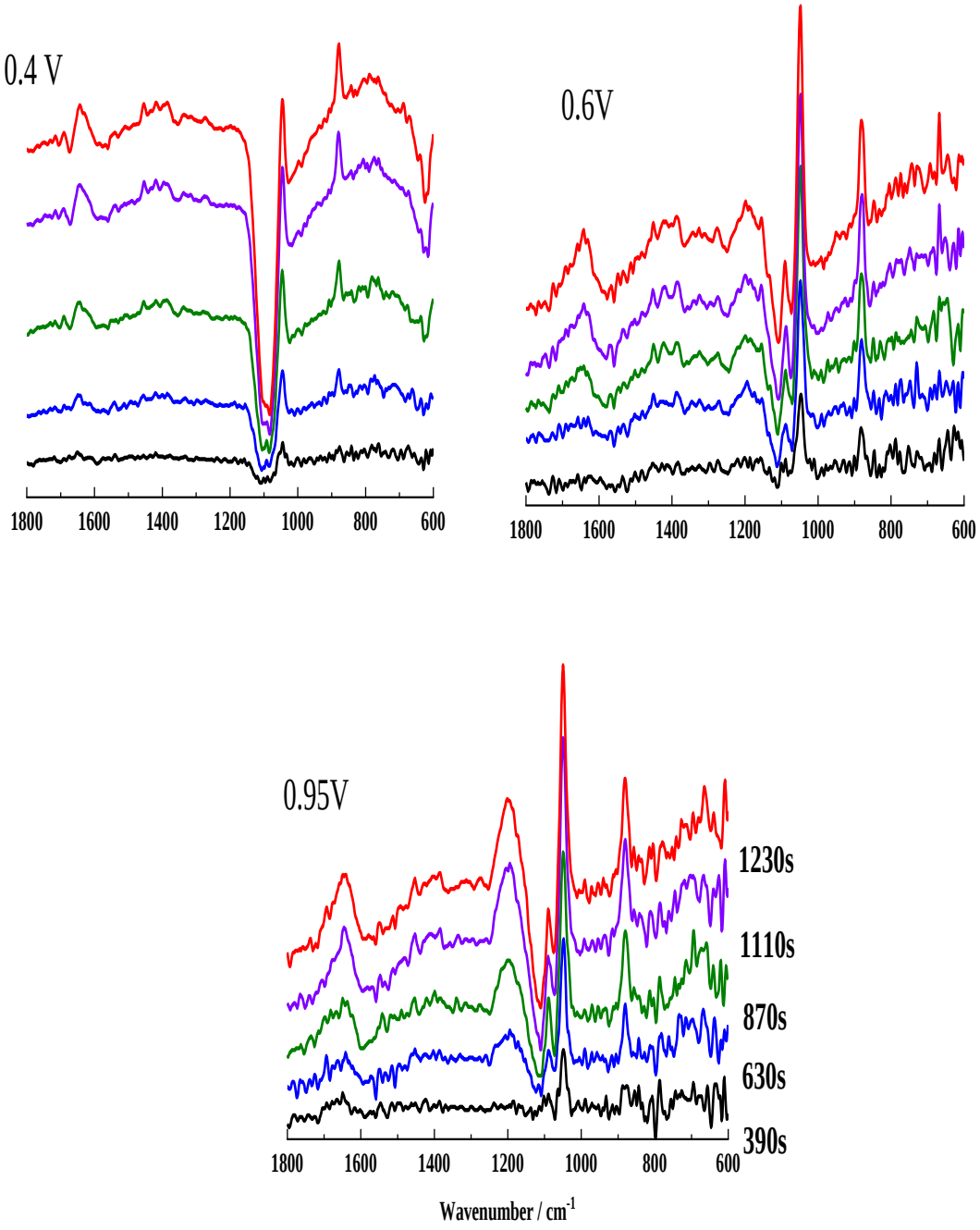

Figure 1.2: FTIR in situ different spectra collected for o-cresol at EPPG coated with SWCNT in EtOH / Na2SO4.10H2O at applied potentials of: 0.2 V, 0.6 V and 0.95 V. The background was taken 5 mins after sample deposition and the spectra were collected between 4000 − 500 cm^{-1} with a resolution of 4 cm^{-1} and averaged over 500 scans.

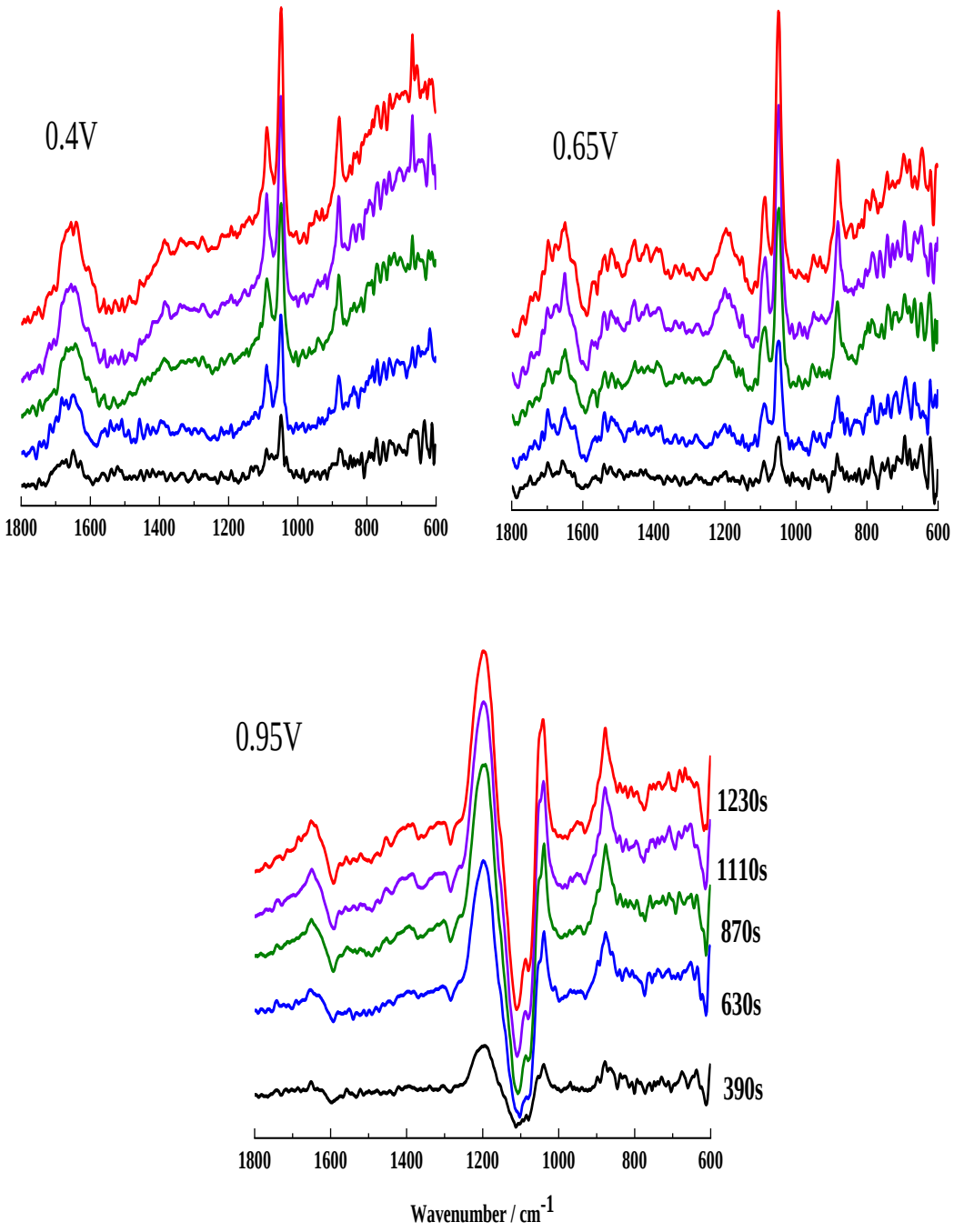

Figure 1.3: FTIR in situ different spectra collected for m-cresol at EPPG coated with SWCNT in EtOH / Na2SO4.10H2O at applied potentials of: 0.2 V, 0.65 V and 0.95 V. The background was taken 5 mins after sample deposition and the spectra were collected between 4000 − 500 cm^{-1} with a resolution of 4 cm^{-1} and averaged over 500 scans.

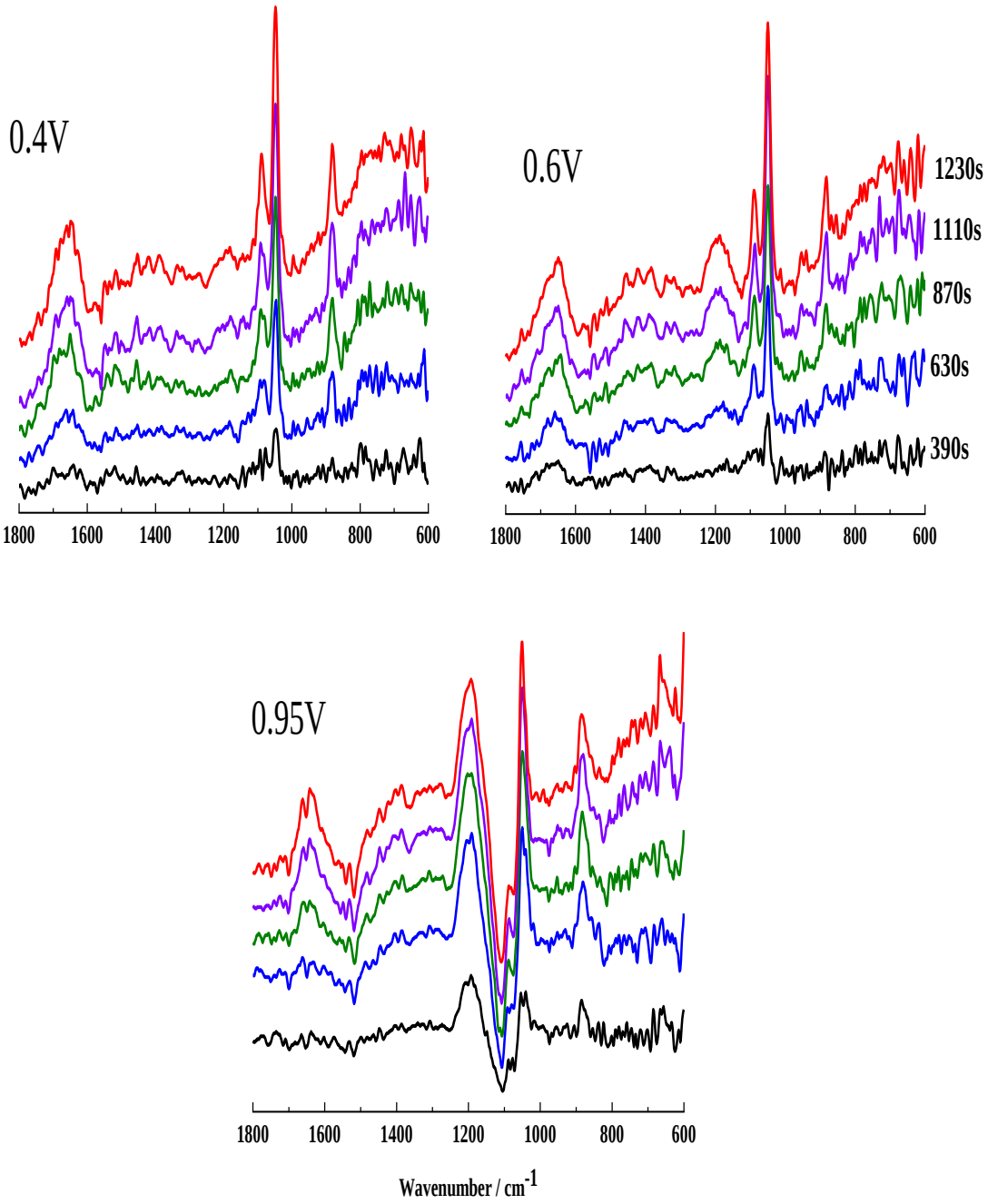

Figure 1.4: FTIR in situ different spectra collected for m-cresol at EPPG coated with SWCNT in EtOH / Na2SO4.10H2O at applied potentials of: 0.2 V, 0.65 V and 0.95 V. The background was taken 5 mins after sample deposition and the spectra were collected between 4000 − 500 cm^{-1} with a resolution of 4 cm^{-1} and averaged over 500 scans.

Appendix 2

Additional Figures for chapter 5

A. XPS Data of PS non treated and treated with Iridium (IV) tetrachloride

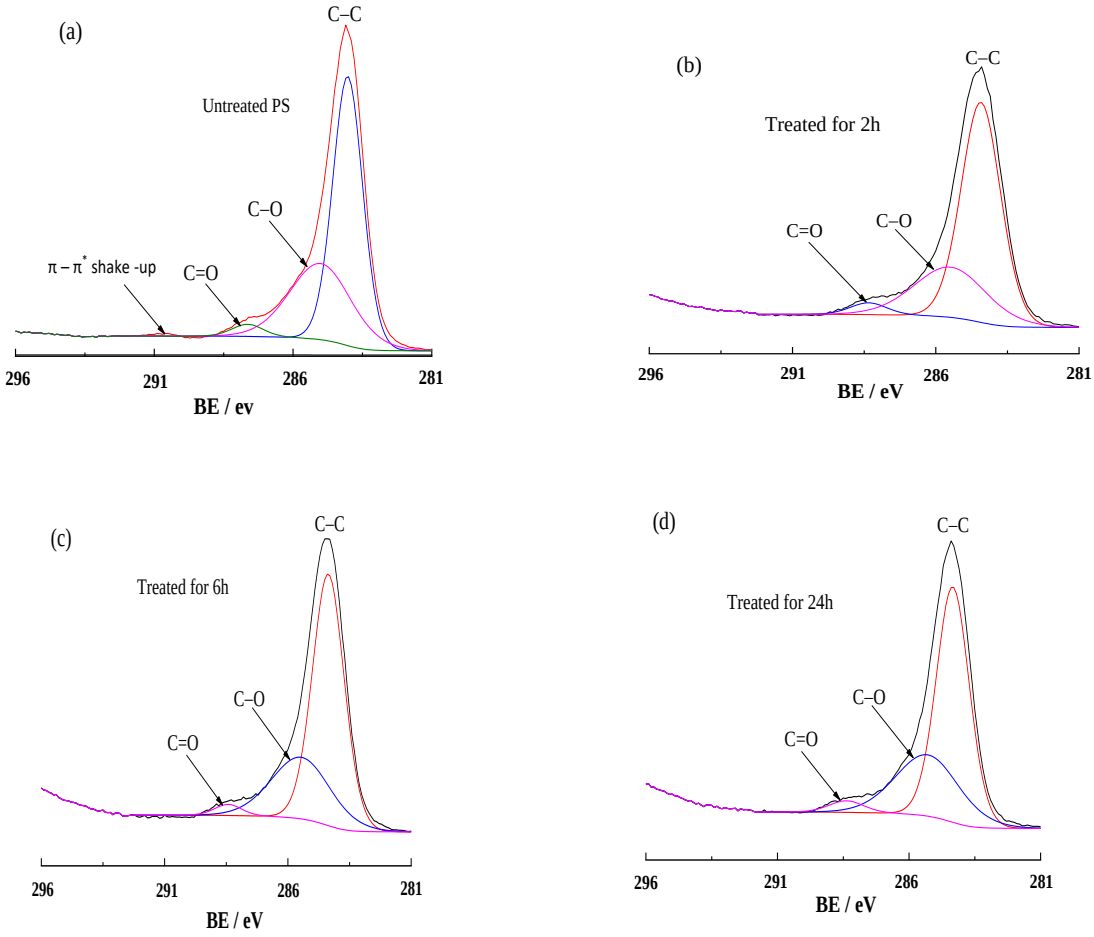

Figure A: Carbon 1s XPS spectra of PS: (a) untreated; (b) treated for 2 h; (c) treated for 6 h; (d) treated for 24 h.

B. In situ data of PS oxidising with addition of different oxidation agent in water purged and not purged with argon.

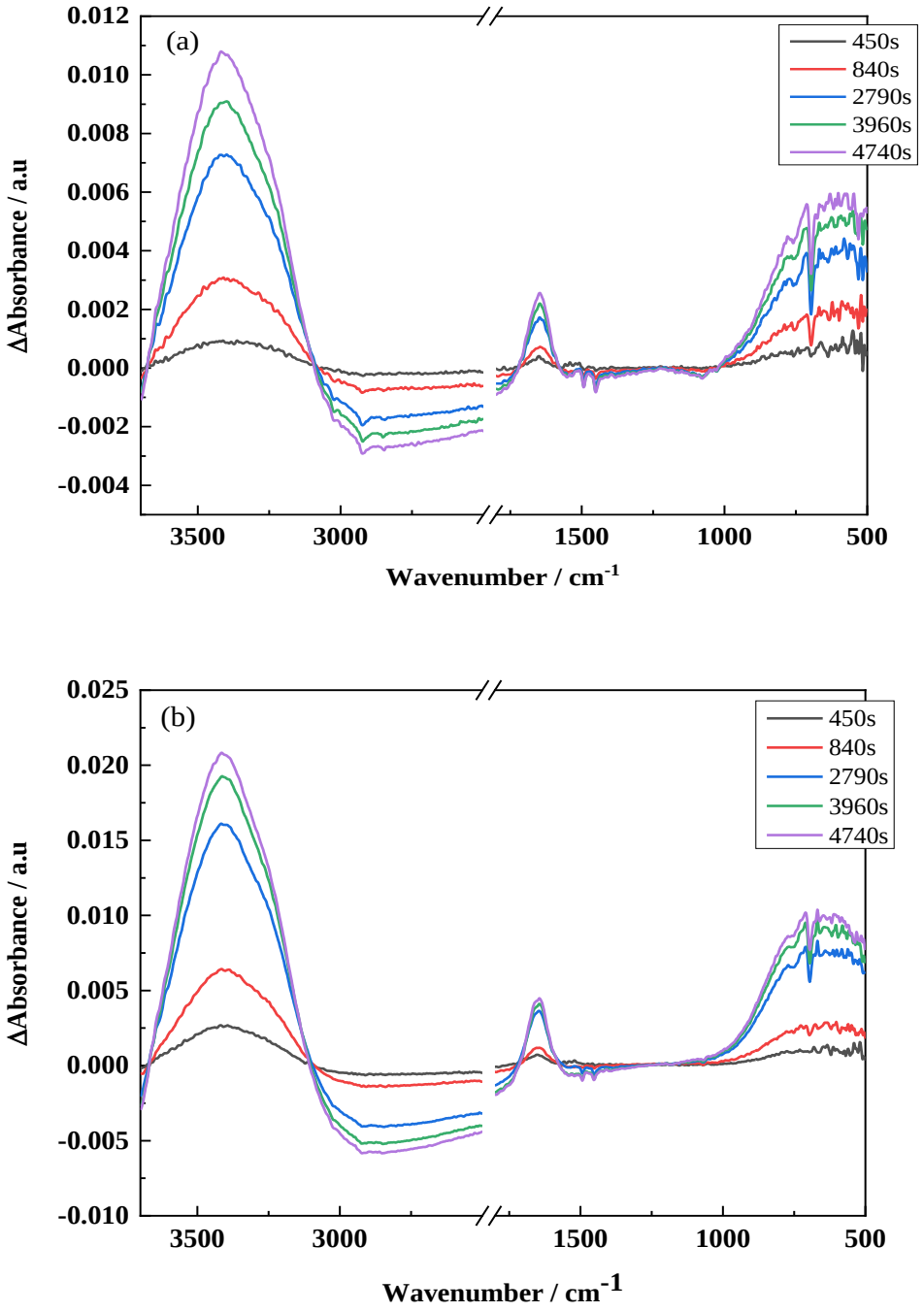

Figure B1: FTIR difference spectra of non-treated PS film in water with no addition of oxidizing agent: (a) not purged with argon and (b) purged with argon.

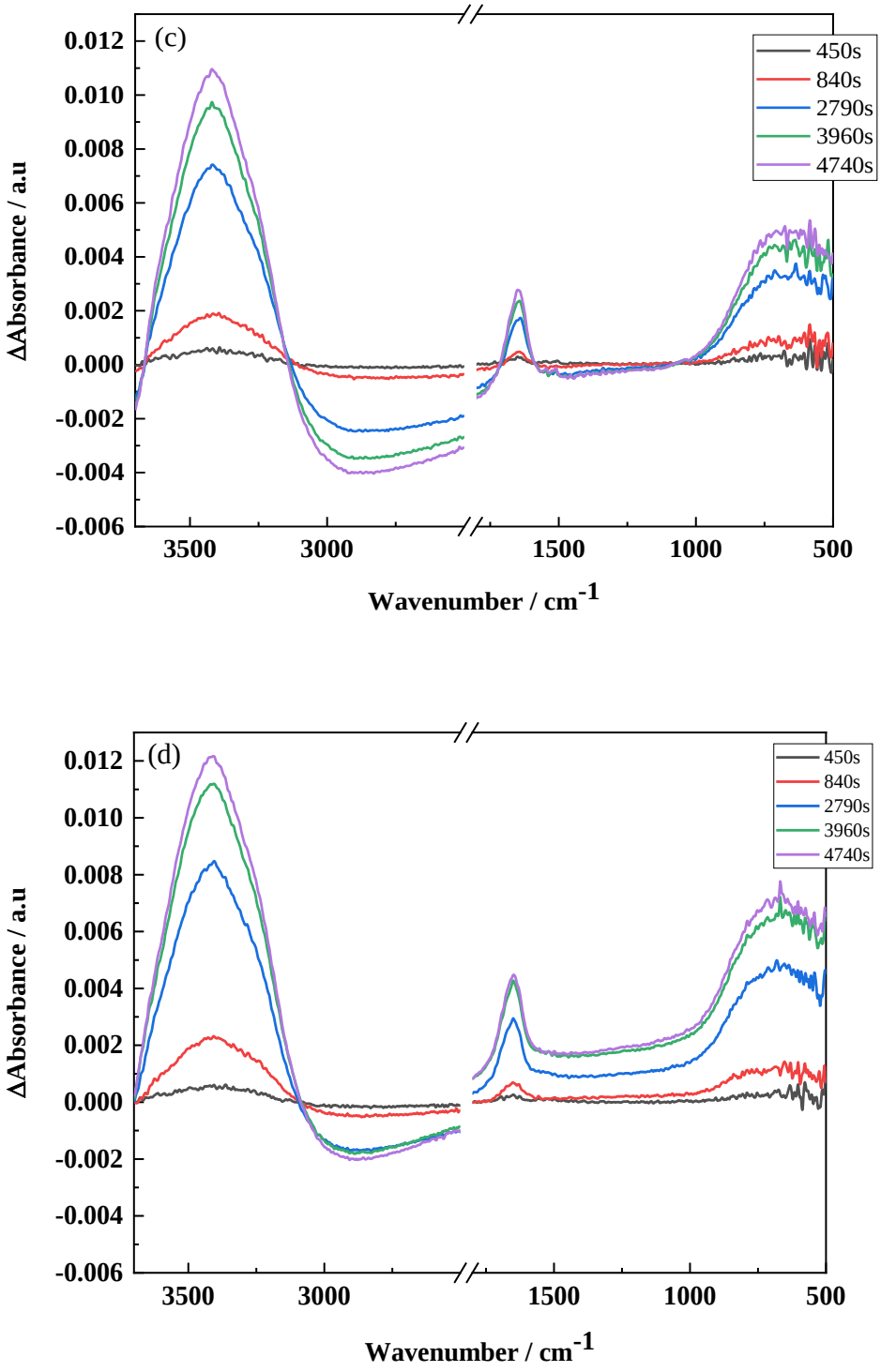

Figure B2: FTIR difference spectra of non-treated PS film in water with addition of 100 µL iridium (IV) hexachloride: (c) not purged with argon and (d) purged with argon. The background spectrum was collected 5 mins after water addition.

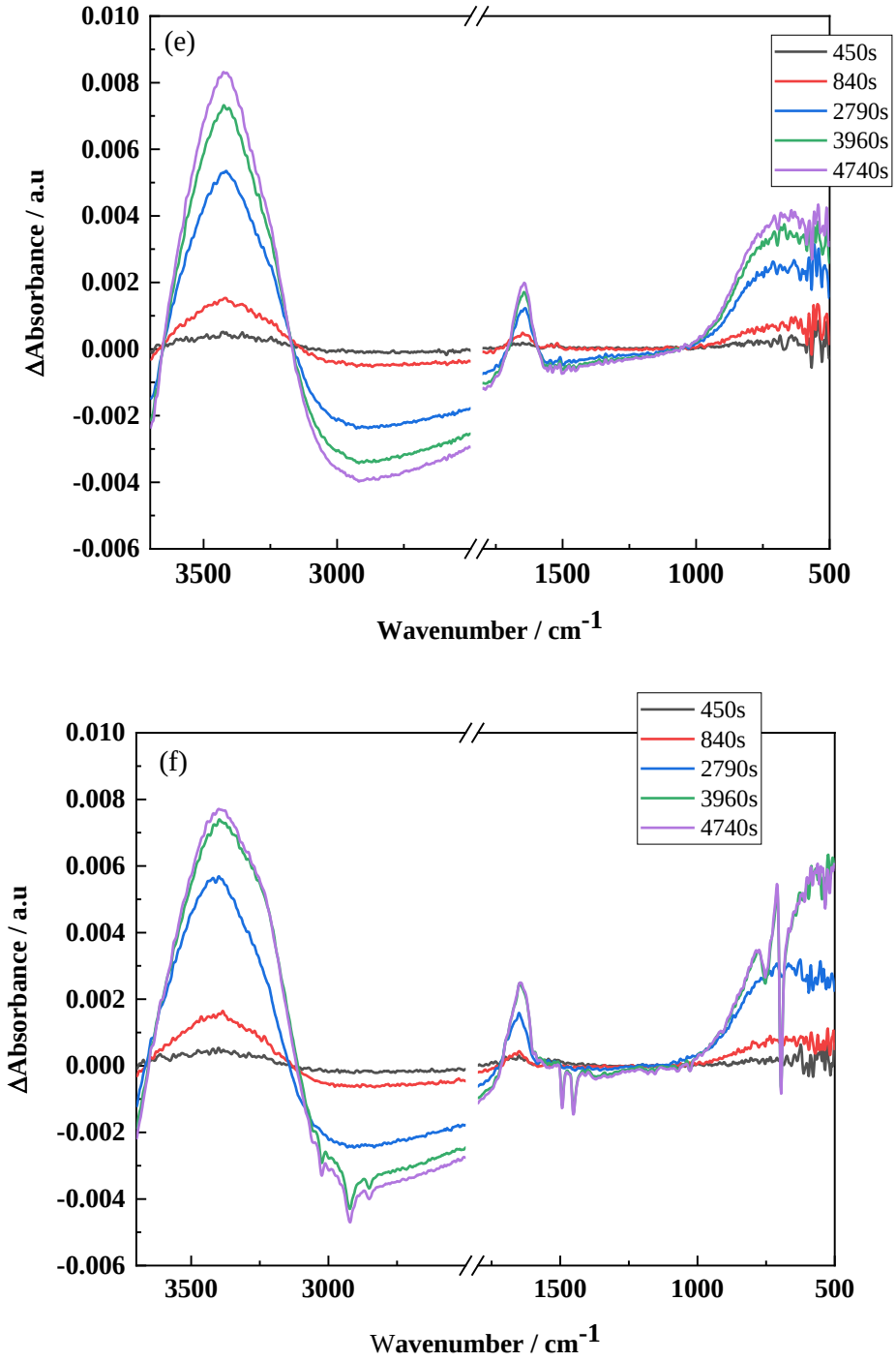

Figure B3: FTIR difference spectra of non-treated PS film in water with addition of 100 µL potassium ferricyanide: (e) not purged with argon and (f) purged with argon. The background spectrum was collected 5 mins after water addition.

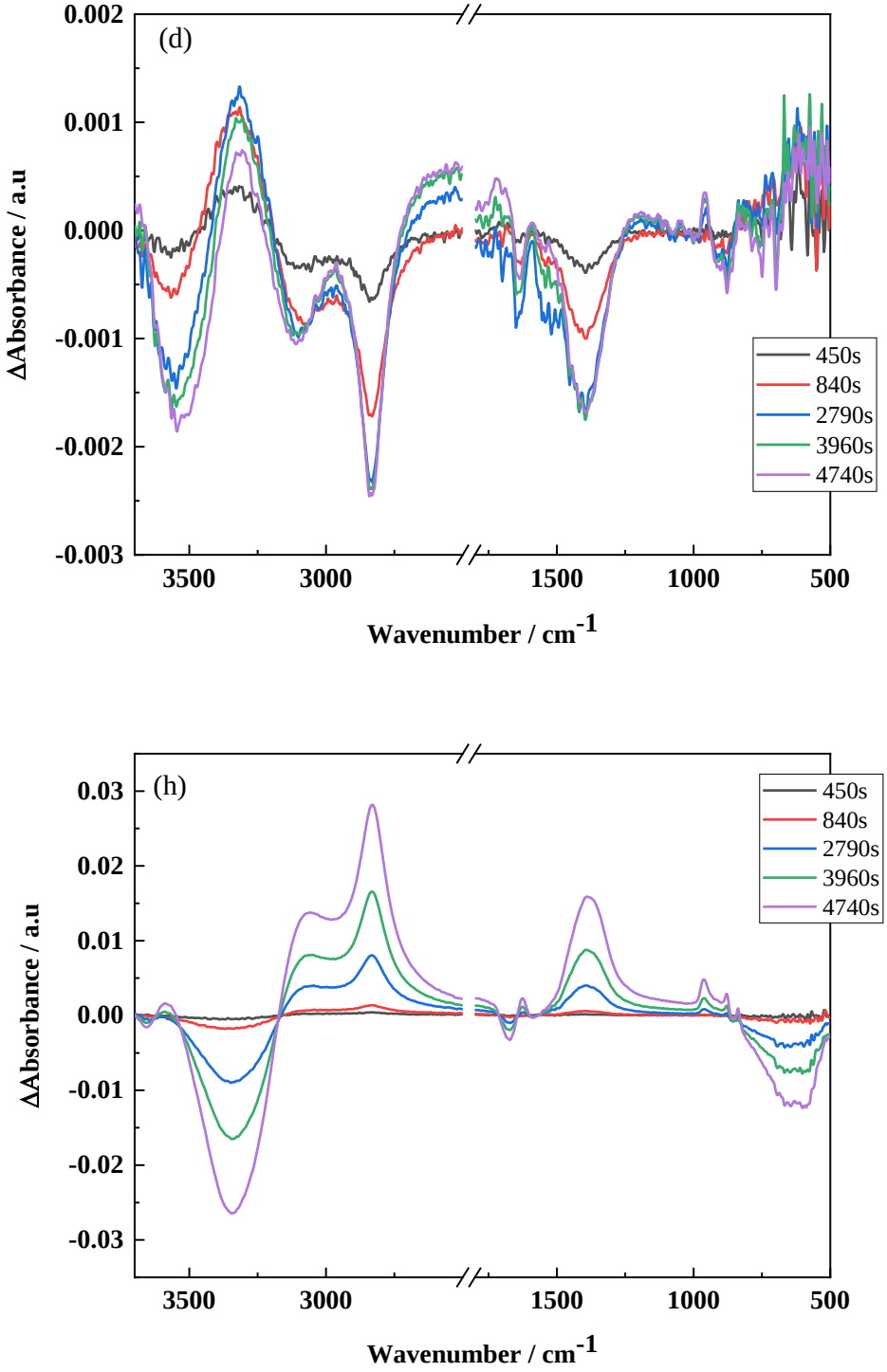

Figure B4: FTIR difference spectra of non-treated PS film in water with addition of 100 µL potassium ferricyanide: (g) not purged with argon and (h) purged with argon. The background spectrum was collected 5 mins after water addition.

C. Behaviour of non- treated PS surface in different electrolyte

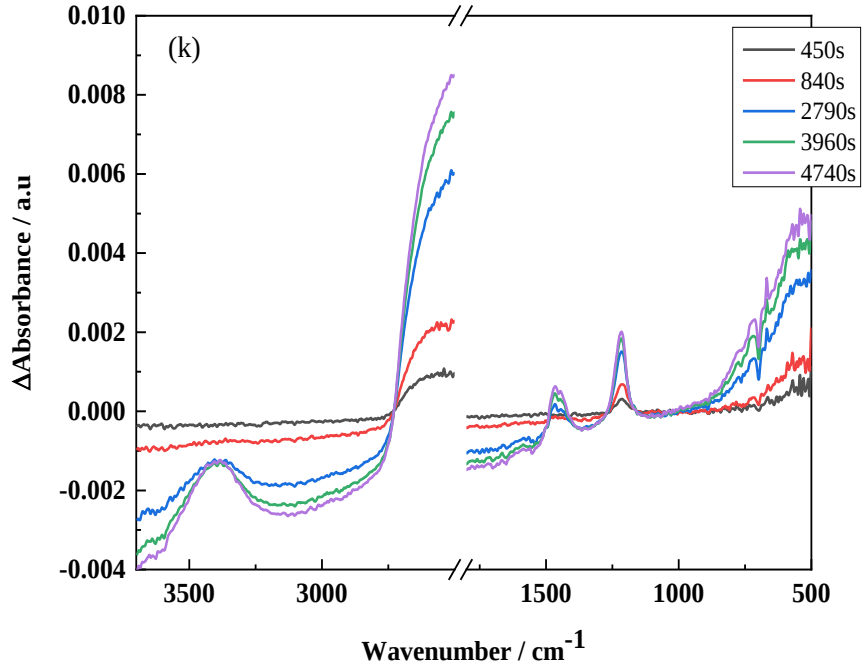

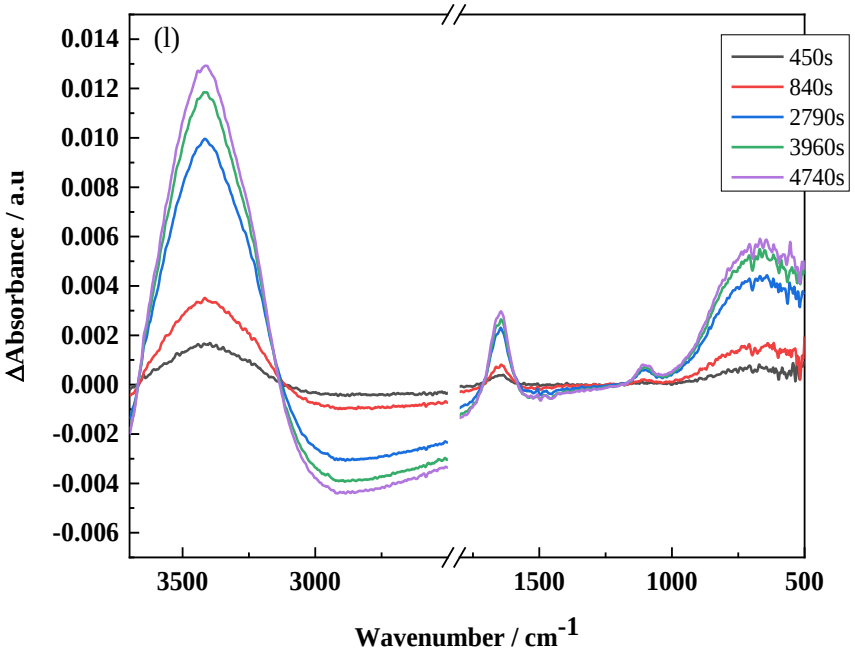

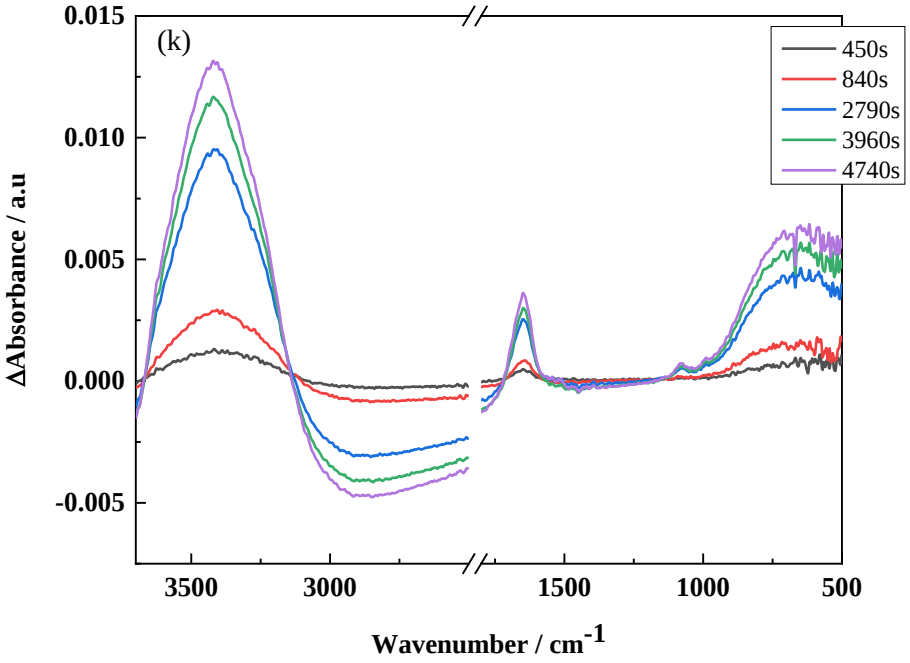

Figure C: FTIR difference spectra of non-oxidised PS film non -purged with argon in solution of: (i) D_2O; (j) $Na_2SO_4.10H_2O$; (k) PBS (pH_7. The spectra were collected between 4000 − 400 cm^{-1} with a spectral resolution of 4 cm^{-1} and averaged over 100 scans. The background spectra were collected after 5mins of electrolyte addition.